

Copyright

by

Natalia Zuniga Garcia

2017

The Thesis Committee for Natalia Zuniga Garcia
Certifies that this is the approved version of the following thesis:

Predicting Friction with Improved Texture Characterization

APPROVED BY
SUPERVISING COMMITTEE:

Supervisor:

Jorge A. Prozzi

Andre D. Smit

Predicting Friction with Improved Texture Characterization

by

Natalia Zuniga Garcia, B.S.C.E.

Thesis

Presented to the Faculty of the Graduate School of
The University of Texas at Austin
in Partial Fulfillment
of the Requirements
for the Degree of

Master of Science in Engineering

The University of Texas at Austin

May 2017

Dedication

To my parents, my brother, and to the memory of my grandmother.

Acknowledgements

I would like to express my gratitude to my advisor Dr. Jorge Alberto Prozzi for his guidance and valuable support through my graduate studies. His advice and encouragement were essential to the development of this thesis and my professional formation. I will always be thankful for the opportunity he gave me to work with him and to be part of his research group.

I would like to thank Dr. Andre de Fortier Smit for his constant advice and support during my Master studies, and for his help with the development of the present work. His guidance and willingness to meet and listen to all my questions through these years made it possible to accomplish my goals.

I also would like to acknowledge the following people for their support during the field testing: Joaquin Hernandez, Andres Sanchez, Hossein Roshani and Andre de Fortier Smit. This thesis work would not be possible without their help. Special thanks to Joaquin Hernandez for his help with the field testing arrangement and organization.

I also want to thank my friends in the U.S. and Costa Rica. They made this journey easier. Additionally, I want to express my gratitude to my parents Wagner and Marielos, and to my brother Wagner, whose love and support help to reach any of the goals I set.

Finally, I want to acknowledge the support and sponsorship of the “Accelerating Innovation in Partnered Pavement Preservation Center” of the University of Texas at Austin, sponsored by the Texas Department of Transportation (TxDOT), and the Center for Highway Pavement Preservation (CHPP), sponsored by the U.S. Secretary of Transportation under the University Transportation Center (UTC) Program.

Abstract

Predicting Friction with Improved Texture Characterization

Natalia Zuniga Garcia, M.S.E.

The University of Texas at Austin, 2017

Supervisor: Jorge A. Prozzi

Current methodologies to measure road friction present several disadvantages that make them impractical for field data collection over large highway networks. Thus, it is important to study different ways to estimate surface friction characteristics based on other properties that are easier to measure. The main objective of this study was to analyze surface texture characteristics and to observe their influence on friction. A Line Laser Scanner (LLS) was implemented to make an improved characterization of the road texture which includes macro- and micro-texture description using different texture parameters.

Field measurements of friction and texture were collected around Texas using different tests methods. The friction characterization tests included the British Pendulum test (BPT), the Dynamic Friction test (DFT), and the Micro GripTester. Thirty-six different pavement sections were evaluated, including different surface types such as hot-mix asphalt (HMA), surface treatment, and concrete sidewalk.

Among the principal conclusions, it was found that there is not a unique relationship between texture and friction. The relationship between texture and friction is strong but it is different for each type of surface, thus, cross-sectional analysis cannot be utilized to

quantify the relationship. Additionally, the prediction of friction measures obtained using the BPT and the DFT significantly improved when including information of both macro- and micro-texture into the prediction model. Therefore, a measure of micro-texture should be included into friction models based on texture. Finally, among the study of different texture parameters, the mean profile depth (MPD) was the most significant parameter for macro- and for micro-texture to explain the distinct friction measures.

Table of Contents

List of Tables	xi
List of Figures	xii
Chapter 1: Introduction	1
Background	1
Main Objectives	3
Scope and Methodology	3
Description of Content	4
Chapter 2: Literature Review	5
Texture	5
Pavement Texture Components	6
Measuring Texture of Pavement Surfaces	9
Roughness level	9
Macro-texture level	9
Micro-texture level.....	13
Texture Characterization.....	15
Spatial Parameters.....	16
Spectral Parameters.....	20
Friction and Skid Resistance.....	22
Slip Speed Effect.....	23
Friction Mechanisms.....	25
Measuring Skid Resistance of Pavements	26
Stationary Testing Methods	27
Pulled Device Methods	29
Skid Resistance Measures Harmonization.....	31
Relationship between Pavement Texture and Surface Friction	33
Macro-Texture and Micro-Texture Testing Using Laser Sensors	34
Incorporating Surface Micro-texture in the Prediction of Skid Resistance	35

Chapter 3: Characterization and Processing of Texture Data	37
Line Laser Scanner (LLS) Characterization	37
Laser Scanner	37
Translation Stage (TS)	40
Line Laser Scanner (LLS) Setup.....	40
Laser Scanner Setup.....	43
Translation Stage (TS) Setup	45
Comparison with Other Laser Systems.....	45
Data Processing.....	46
Processing Invalid and Erroneous Data	46
Filtering Macro- and Micro-Texture Profiles	50
Characterization of Pavement Texture.....	55
Chapter 4: Friction and Texture Data Collection	57
Experiment Design.....	57
Test Sections	59
Data Collection Procedure	63
Chapter 5: Analysis of Friction and Texture Measurements	67
Friction	67
Texture	71
Sand Patch Test and Circular Track Meter (CTM)	71
Line Laser Scanner (LLS).....	73
Friction as a Function of Texture	74
Chapter 6: Summary, Conclusions and Recommendations	89
Summary	89
Important Findings Conclusions	91
Recommendations	93
Appendices	94
Appendix A. Butterworth Filters Python Code.....	94
Appendix B. Samples Description	95

Appendix C. Friction Models Using Different Texture Parameters	100
References	107

List of Tables

Table 2.1:	Texture components.....	7
Table 2.2:	Texture parameters used for pavement texture characterization.	18
Table 3.1:	Laser specifications (Keyence, 2015).....	38
Table 3.2:	Linear translator specifications.....	40
Table 3.3:	Comparison of laser systems used to characterize pavement texture	46
Table 4.1:	Test sections.....	60
Table 4.2:	Summary of samples per surface type.	61
Table 4.3:	Asphalt surface type description	63
Table 4.4:	Texture and friction tests and parameters.....	64
Table 5.1:	Friction Models Using Mean Profile Depth (MPD) as a Texture Parameter	84
Table 5.2:	Friction models for different texture parameters.	86
Table 5.2:	Friction models for different texture parameters (Cont.).....	87
Table 5.3:	Proposed friction models as a function of texture and HMA-type ..	88

List of Figures

Figure 2.1: Texture profile basic terminology.....	6
Figure 2.2: Texture components (Sandburg, 1998).	8
Figure 2.3: Texture wavelength influence on tire/pavement interactions (Henry, 2000).	8
Figure 2.4: (a) Sand Patch test equipment, and (b) field data collection.....	10
Figure 2.5: Mean profile depth (MPD) procedure (ASTM E 1845, 2009).	11
Figure 2.6: (a) Circular Track Meter (CTM), and (b) CTM segments.....	12
Figure 2.7: (a) Laser Texture Scanner (LTS), and (b) 3D plot of a measured surface.	13
Figure 2.8: Aggregate Imaging System (AIMS) equipment (Mahmoud et al., 2010).	15
Figure 2.9: Positive and negative texture (McGhee and Flintsch, 2003).	17
Figure 2.10: Texture profiles with (a) different skewness values, and (b) different kurtosis values (ASME B46, 2010).	19
Figure 2.11: Friction coefficient and slip speed curve (Hall et al., 2009).	23
Figure 2.12: Effect of texture on tire/pavement friction at different sliding speeds (Ueckerman and Wang, 2014; Flinstch et al., 2002 cited by Hall et al., 2009).	24
Figure 2.13: Key mechanism of tire/pavement friction (Hall et al., 2009).....	26
Figure 2.14: (a) British Pendulum Tester (BPT), and (b) field operation.....	28
Figure 2.15: (a) Dynamic Friction Tester (DFT) and (b) field operation.	29
Figure 2.16: (a) GripTester, and (b) field operation.	31
Figure 2.17: (a) Micro GripTester, and (b) field operation.....	31

Figure 2.18: Relationship between (a) BPN and macro-texture MPD and, (b) BPN and micro-texture MPD (Serigos et al., 2014).....	35
Figure 3.1: Axis convention and direction of movement.....	39
Figure 3.2: Linear translation stage (TS).....	40
Figure 3.3: (a) Line Laser Scanner (LLS), and (b) field data collection.....	41
Figure 3.4: Longitudinal profiles and sampling rate.....	42
Figure 3.5: (a) 3D plot of original 800 transverse readings, and (b) 3D plot of 700 readings after trimming.....	47
Figure 3.6: (a) Dropouts in series, and (b) processed profile example.....	48
Figure 3.7: Example of negative values (a) 3D plot of original profiles, (b) histogram of original profiles, (c) 3D plot of processed profiles, and (b) histogram of processed profiles.....	49
Figure 3.8: Example of reflective pavement surface (a) 3D plot of original profiles, (b) histogram of original profiles, (c) 3D plot of processed profiles, and (b) histogram of processed profiles.....	50
Figure 3.9: (a) Macro-texture low-pass filter, (b) average PSD of macro-texture filtered profiles, (c) micro-texture band-pass filter, and (d) average PSD of micro-texture filtered profiles.....	52
Figure 3.10: Original profile and filtered profiles.....	53
Figure 3.11: (a) Micro-texture noise in valleys, and (b) Micro-texture processed profile	54
Figure 3.12: Micro-texture for the active area.....	55
Figure 3.13: Final profiles.....	56
Figure 4.1: Surface combination of macro- and micro-texture.....	58
Figure 4.2: Location of test sections.....	59

Figure 4.3: Typical gradation curves per asphalt surface type (based on TxDOT, 2014)	62
Figure 4.4: Field test sampling method.....	65
Figure 4.5: Location of the Line Laser Scanner (LLS).	66
Figure 5.1: Dynamic Friction Test (DFT) results.....	68
Figure 5.2: British Pendulum Test (BPT) and Dynamic Friction Test (DFT) results.	69
Figure 5.3: Micro GripTester and Dynamic Friction Test (DFT) results.....	70
Figure 5.4: Micro GripTester and British Pendulum Test (BPT) results.	71
Figure 5.5: Mean texture depth (MTD) as a function of the mean profile depth (MPD_{CTM}).	72
Figure 5.6: (a) Standard deviation of the mean profile depth (MPD_{CTM}), and (b) standard deviation of the root mean square (RMS_{CTM})	73
Figure 5.7: (a) Mean profile depth (MPD) from the CTM and from the LLS, and (b) root mean square (RMS) from the CTM and from the LLS.....	73
Figure 5.8: (a) British pendulum number (BPN) as a function of the mean profile depth (MPD_{LLS}), and its (b) description per surface type.....	75
Figure 5.9: (a) British pendulum number (BPN) as a function of the mean profile depth for the micro-texture component ($MPD\mu$), and its (b) description per surface type.	75
Figure 5.10: BPN as a function of MPD_{LLS} per flexible pavement type (a) limits, and (b) proposed pavement types groups.	77
Figure 5.11: BPN as a function of $MPD\mu$ per flexible pavement type (a) limits, and (b) proposed pavement types groups.	78
Figure 5.12: Representation of the (a) Model 1, and (b) Model 2.....	80

Chapter 1: Introduction

This chapter introduces the work presented in this thesis. The background section presents the main justifications for the research performed. Additionally, the main technical objectives are described as well as the methodology used to reach these aims and the scope of the work. Finally, a brief description of the rest of the chapters and contents are presented.

BACKGROUND

According to the Federal Highway Administration (FHWA), in 2015, there were 18,695 fatalities as a result of roadway departure crashes in the United States (US), which was 53.3% of all the traffic fatalities in the US. Poor road conditions, especially wet pavement surface, have been identified as a major contributing factor in roadway departure crashes. Research conducted by the National Transportation Safety Board (NTSB) and FHWA in 1980 indicates that about 70% of wet pavement crashes can be prevented or minimized by improving pavement friction. Pavement surfaces should be designed, constructed, and maintained to provide durable and adequate skid resistance properties for drivers.

The texture of the pavement surface and the surface texture of the aggregate play a leading role in providing high skid resistance to a pavement surface. Surface texture is the primary pavement property affecting the skid resistance. Micro-texture and macro-texture are the two key pavement surface characteristics necessary for the development of a good skid resistance. Pavement surface texture is influenced by many factors, such as aggregate type and size, mixture gradation, and texture orientation among others. Micro-texture refers to the small-scale texture of the pavement aggregate component, which controls contact

between the tire rubber and the pavement surface. Macro-texture relates to the large-scale texture of the pavement due to the aggregate particle arrangement, which controls the flow of water from under the tire and, hence, the potential loss of skid resistance with increased speed under wet conditions.

The effect of the aggregate texture (micro-texture) and the effect of the pavement surface macro-texture on the skid resistance of a highway surface are well recognized. However, there is a lack of fundamental understanding and quantification of the individual effect that each of these properties, micro- and macro-texture, have on the final skid properties of the road. Most research studies in this regard have been based on theory, assumptions and sound engineering judgment. The individual effects have not been quantified and their contribution to skid under different conditions of moisture, speed and highway conditions are not well understood. Recent developments in optics and computers allowed the collection of high definition 3-D images of the surface of the highway pavement. In particular, it is now possible to quantify micro-texture in the field in an effective and efficient manner. This can be done with the use of laser-based technology that allows measurements below 0.5 mm (500 μm).

The subject of this thesis is the investigation of surface texture, focused on the influence of texture on the friction of the road pavement, separating the effects of macro- and micro-texture.

MAIN OBJECTIVES

The goal of this thesis was to study the effect of different texture components and their parametric description on the skid resistance of a pavement surface. The main technical objectives were to:

- Develop a methodological framework to collect and process surface texture measurements using a high-resolution Line Laser Scanner (LLS), developed by the University of Texas at Austin (UT Austin).
- Characterize highway pavement macro- and micro-texture using the LLS, to model and estimate friction.
- Analyze the influence of macro- and micro-texture in the development of surface skid resistance.

SCOPE AND METHODOLOGY

Field measurements of friction and texture on different surfaces were collected on Texas highway network using various technologies. A high-resolution LLS was used to characterize surface macro- and micro-texture. Signal processing techniques were used to separate the effect of the different texture components, i.e. macro- and micro-texture. Distinct surface texture parameters were evaluated. These parameters were then compared to determine the better predictors of friction. The effect of each of the surface texture component on the friction was also analyzed and quantified.

The present study is limited to the prediction of friction based on texture information. Friction measures were collected using different tests performed mainly at low speed such as the British Pendulum test, the Dynamic Friction Test (DFT), and Micro GripTest.

DESCRIPTION OF CONTENT

This thesis is divided into six chapters. The present chapter introduced the research problem, the main objectives and the methodology used to achieve the objectives. Chapter 2 presents a literature review regarding texture and friction properties, characterization and measuring techniques. Chapter 3 describes the development of characterization and processing of the texture data using the LLS. Chapter 4 consists of the description of the friction and texture data collection process. Chapter 5 presents the analysis of the measurements of texture and the effect on friction prediction. Finally, Chapter 6 provides a summary and the main findings and conclusions obtained in the study, along with recommendations for future work.

Chapter 2: Literature Review

Pavement surfaces should be designed, constructed, and maintained with durable and adequate friction and texture properties to achieve a good pavement performance and provide a safe ride. This chapter provides definitions for texture and friction, as well as the description of most common methods used to measure and test these surface properties.

TEXTURE

Pavement texture is the result of the deviations of the surface layer from a true planar surface (ASTM E867, 2012). Pavement texture is the most important feature of the road surface that ultimately determines most tire/pavement interactions, including friction, noise, splash-and-spray, rolling resistance, and tire wear (Henry, 2000).

A profile is a general description of the surface obtained using a sensor device, such as a needle or a laser. It is usually a two-dimensional sample of the surface texture described by two coordinates: distance (longitudinal or transversal), and height. However, new technologies are now allowing 3-D measurements of texture. This profile is considered as a stationary, random function of the distance along the surface (Sandberg, 1998). Using Fourier analysis, this function can be mathematically represented as a series of sinusoidal components of various spatial frequencies or texture wavelengths.

The texture wavelength is the spatial period of a wave, as shown in Figure 2.1. Typically, the wavelength is given in longitude units (m or mm) and uses a *lambda* (λ) as a symbol. The spatial frequency (f) is defined as the inverse of the wavelength; it is given in units of cycle/m. The texture amplitude is defined as the peak-to-peak height difference, as shown in Figure 2.1.

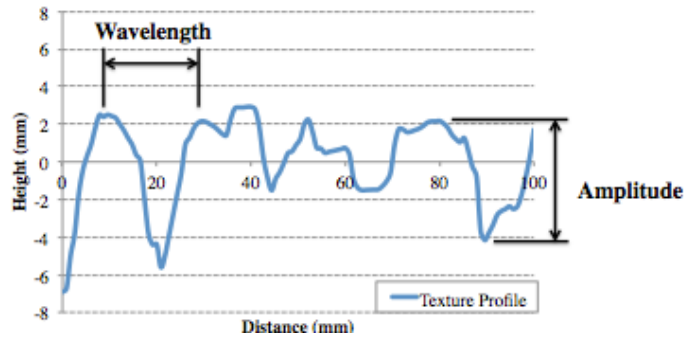


Figure 2.1: Texture profile basic terminology.

Pavement Texture Components

The World Road Association, previously Permanent International Association of Road Congresses (PIARC), presented the first proposal for texture geometric-classification during the XVII World Road Congress (PIARC, 1983). This first classification includes three different orders of surface irregularities based on pavement surface features: first order (micro-texture), second order (macro-texture), and third order (mega-texture).

PIARC refined the first classification in order “*to convert the study of pavement surface qualities with respect to phenomena affecting the road user into a study of the geometric characteristics of pavement surfaces – more precisely the amplitudes and wavelengths of their irregularities*” (PIARC, 1987). This classification includes a range of wavelength and amplitudes for each texture component, as presented in Table 2.1. Later, standard specifications such as American Society of Testing Materials (ASTM E867), International Organization for Standardization (ISO 13473-1), and German Institute for Standardization (DIN on ISO 13473-1), accepted and incorporated these definitions. The ISO 13473-1 refined the terms by incorporating typical amplitudes (Sandberg, 1998), as shown in Table 2.1.

Micro-texture refers to the small-scale texture of the aggregate surface, which controls the contact between the tire rubber and the pavement surface. Micro-texture is a function of aggregate particle mineralogy and petrology, the aggregate source (natural or manufactured), and is affected by the environmental effects and the action of traffic (Hall et al., 2009; AASHTO, 2008).

Table 2.1: Texture components.

<i>Component</i>	<i>Wavelength</i>	<i>Amplitude (PIARC, 1987)</i>	<i>Typical Amplitude ISO 13472-1 (Sandberg, 1998)</i>
Mega-texture	50 to 500 mm	1 to 50 mm	0.1 to 50 mm
Macro-texture	0.5 to 50 mm	0.2 to 10 mm	0.1 to 20 mm
Micro-texture	0 to 0.5 mm	0 to 0.2 mm	0.0001 to 0.5 mm

Macro-texture refers to the large-scale texture of the pavement surface due to the aggregate particle arrangement. In asphalt pavements, the mixture properties (aggregate shape, size, and gradation), which define the type of mixture and control the macro-texture. In concrete pavements, the method of finishing, such as dragging, tinning, grooving width and spacing, and direction of the texturing, controls the macro-texture (Hall et al., 2009).

Mega-texture has wavelengths in the same order of size as the tire/pavement interface. Examples of mega-texture include ruts, potholes, and major joints and cracks. It affects vibration in the tire walls, and it is therefore strongly associated with noise and rolling resistance (PIARC, 1983; Hall et al., 2009; AASHTO, 2008).

A fourth level can also be considered: roughness or unevenness, with longer wavelengths than mega-texture ($\lambda > 500$ mm). Roughness refers to the irregularities in the pavement surface that affect the ride quality, smoothness, and serviceability. Figure 2.2 shows the different component based on a reference length.

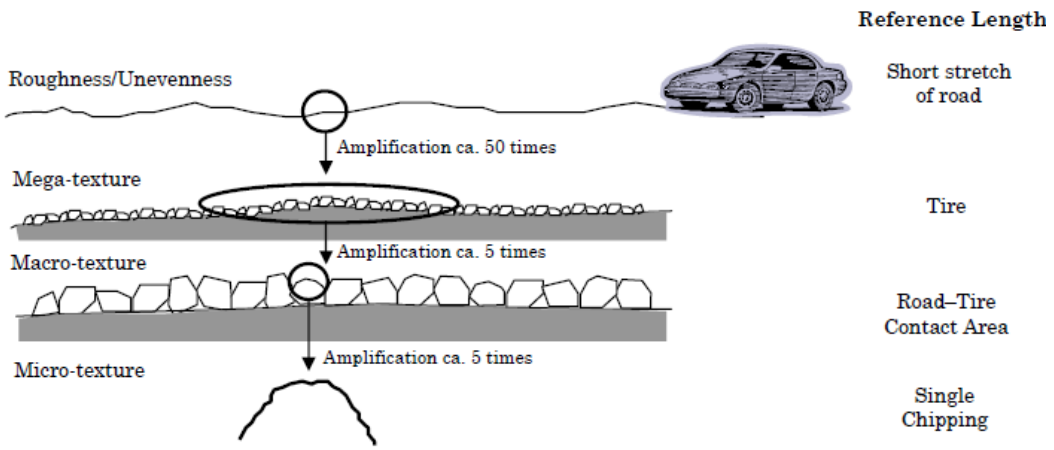


Figure 2.2: Texture components (Sandburg, 1998).

It is widely recognized that pavement surface texture influences many different tire/pavement interactions. Figure 2.3 shows the ranges of texture wavelengths affecting various vehicle-road interactions including friction, interior and exterior noise, splash and spray, rolling resistance, and tire wear (Henry, 2000). As can be seen, friction is primarily affected by micro-texture and macro-texture.

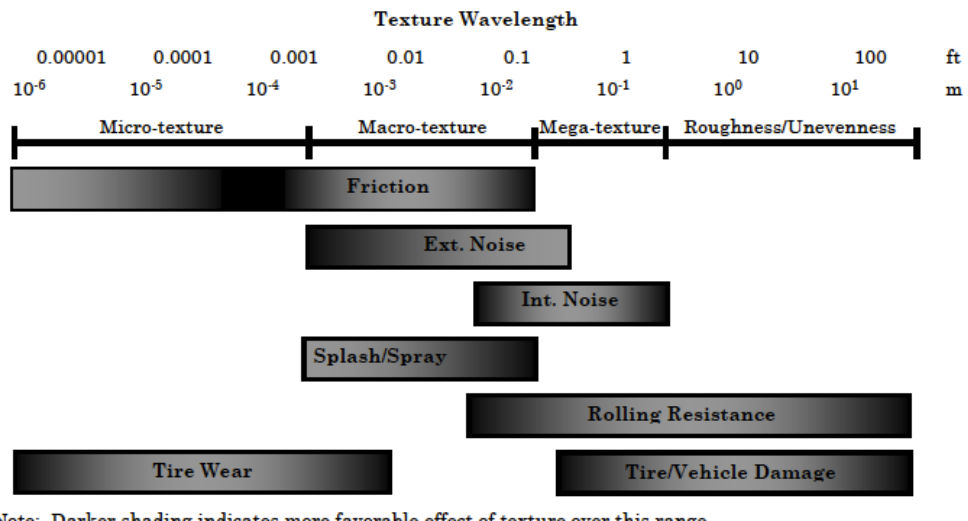


Figure 2.3: Texture wavelength influence on tire/pavement interactions (Henry, 2000).

Measuring Texture of Pavement Surfaces

The information about the highway pavement texture can be used by transportation agencies for different purposes, such as routine surveys, accident analysis, construction, rehabilitation, and pavement management. Different equipment and techniques are used depending on the texture component being measured.

Roughness level

At a roughness or unevenness level, a topological survey or a profilometer can be used to describe the pavement texture by obtaining the International Roughness Index (IRI). The IRI was developed by the World Bank in 1986 (Sayers et al., 1986), it summarizes the longitudinal surface profile in the traveled wheel path, and constitutes a standardized roughness measurement. It is commonly expressed in inches per mile (in/mi) or meters per kilometer (m/km). The IRI contains pavement surface profile information within a wavelength range of 1.3 and 30 m (Sayers et al., 1986), thus is highly related with rolling resistance and tire or vehicle damage (see Figure 2.3). The IRI can be used as a measure of road pavement performance in term of riding quality and serviceability.

Macro-texture level

The macro-texture can be described by indirect measures using volumetric techniques, such as the Sand Patch, the Grease Patch or the Outflow Meter. The Sand Patch test (ASTM E965, 2015) is known as the classical macro-texture measure technique. The method requires the use of solid glass spheres or Ottawa natural silica sand. The sand is spread on a pavement in a circular motion with a spreading tool (as shown in Figure 2.4). The area of the roughly circular patch of sand is calculated by measuring the average of four equally spaced diameters. The known volume of sand divided by the area of the circle is reported as the Mean Texture Depth (MTD), as presented in Equation 2.1. A variation

of the volumetric method used by NASA is the Grease Patch method in which the material used is grease (Henry, 2000). The Outflow Meter (ASTM E2380, 2015) is a transparent vertical cylinder that is located on the top of the pavement surface, it is filled with water and the time for the water level to fall by a fixed amount is measured and reported as the outflow time (OFT). The OFT is highly correlated with the MTD for non-porous pavements (Henry, 2000).

$$MTD = \frac{4V}{\pi D^2} \quad (2.1)$$

Where,

V = material sample volume (mm^3)

D = average diameter covered by the material (mm)



Figure 2.4: (a) Sand Patch test equipment, and (b) field data collection.

Advances in technology allow now the direct measure of the texture profiles using non-contact lasers, such as the Circular Track Meter (CTM) and the Laser Texture Scanner 9300 (LTS). The information collected can be used to compute various profile statistics such as the Mean Profile Depth (MPD). The MPD is estimated by diving the texture profile into segments of 100 mm in length. After that, a slope suppression is applied to each

segment by subtracting a linear regression; this provides a zero-mean profile segment. The segment is then divided into two halves, and the height of the highest peak within each half is determined. The average of these two peaks is referred to as the mean segment depth, as shown in Figure 2.5. The average value of the mean segment depth of the measured profiles is the MPD (ASTM E 1845, 2009). Therefore, while MPD is a one-dimensional measurement, MTD is a two-dimensional measurement.

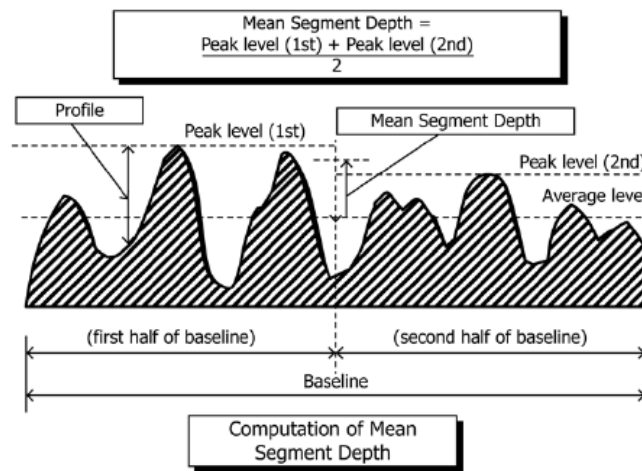


Figure 2.5: Mean profile depth (MPD) procedure (ASTM E 1845, 2009).

The Circular Track Meter (CTM) is a device used to measure MPD. It uses a laser displacement sensor that is mounted on an arm that rotates clockwise at a fixed elevation from the measured surface. The device is controlled by a notebook computer that saves the processed data and reports the MPD, and the Root Mean Square (RMS), presented in Equation 2.2. The device measures a profile of a circle 284 mm in diameter and 892 mm in circumference (as shown in Figure 2.6). The profile is divided into eight segments of 111.5 mm. The MPD is determined for each of the segments of the circle and the MPD reported is the average of the eight segments (ASTM 2157, 2015). The CTM is a reliable

and robust equipment for field operations. However, it measures texture along a circumference so it has its limitations for measuring longitudinal or traverse texture separately, which is very important for concrete pavement.

$$RMS = \sqrt{\frac{1}{N} \sum_{i=1}^N h_i^2} \quad (2.2)$$

Where,

N = number of coordinates

h_i = height value for coordinate i (mm)

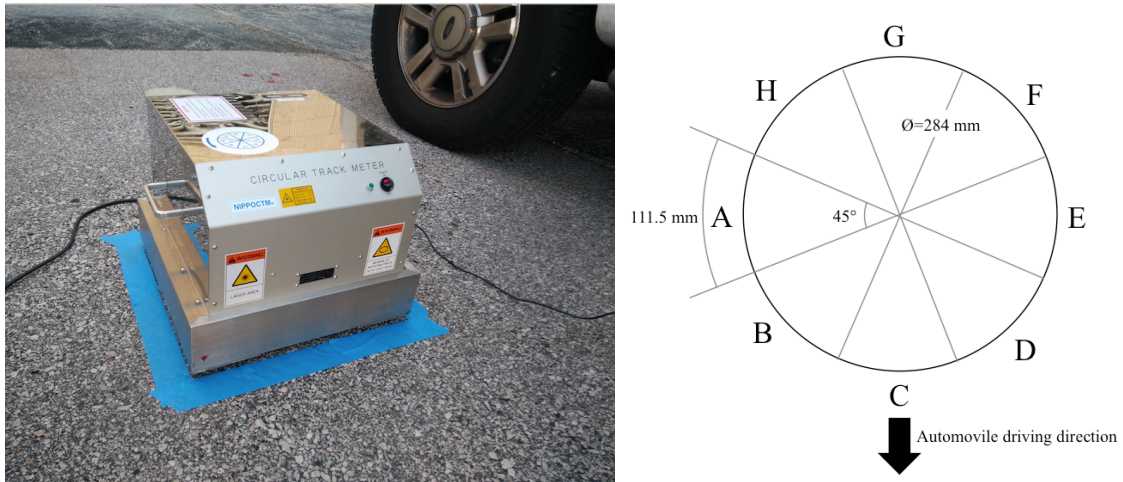


Figure 2.6: (a) Circular Track Meter (CTM), and (b) CTM segments.

The Laser Texture Scanner (LTS) model 9300, shown in Figure 2.7, is a non-contact laser device capable of measuring texture profiles with wavelengths down to 0.05 mm ($50 \mu\text{m}$), including macro-texture and the first decade of micro-texture. It computes the MPD, RMS, texture profile index (TPI), and estimated texture depth (ETD), which is an estimation of MTD based on MPD using an empirical equation (Equation 2.3). This device can scan a maximum area of 100 by 75 mm. The main disadvantage of the LTS is that, at the highest resolution, it takes approximately two hours to scan the 100 by 75 mm

area, making it impractical for field studies (Serigos et al., 2014). The device is also not as reliable as the CTM and the researchers have experienced many operational problems.

$$ETD = 0.2 + 0.8 \cdot MPD \quad (2.3)$$

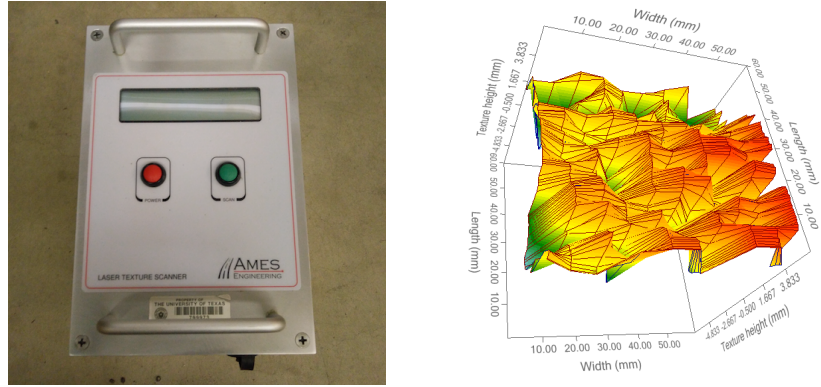


Figure 2.7: (a) Laser Texture Scanner (LTS), and (b) 3D plot of a measured surface.

The methods described previously, provide a spot measure of the pavement texture, and require traffic control. There are other methods capable of measuring the macro-texture continuously at traffic speed, such as the Laser Crack Measurement System (LCMS), the Rugolaser, and the VTexture from the Texas Department of Transportation (TxDOT). These techniques are capable of measuring MPD continuously and detect surface irregularities such as distresses and rutting. However, none of these methods can collect micro-texture information.

Micro-texture level

Currently, there are not standard methods to measure micro-texture. Research on the measurement of micro-texture is mainly based on the use of laser scanners and image

analysis techniques. Although, due to the high correlation of micro-texture and low-speed friction, low-friction test measures are commonly used as a surrogate of micro-texture.

Methods like the LTS and the Aggregate Imaging System (AIMS) are used to describe micro-texture. The LTS equipment is capable of reaching micro-texture wavelengths, as explained previously. However, its main purpose is measuring macro-texture, and the method does not provide any indication of micro-texture descriptions. The analysis must be done separately, based on the profile collected.

The Aggregate Imaging System (AIMS) (Masad, 2005) uses a simple setup that consists of one camera and two different types of lighting schemes to capture images of aggregates at different resolutions; from which aggregate shape properties are calculated using image analysis techniques (Masad, 2005). The system, shown in Figure 2.8, is designed to analyze the form, angularity, and texture of coarse aggregates and the angularity and form of fine aggregates. It also has the capability to characterize the surface of asphalt cores for micro- and macro-texture parameters. The captured images are analyzed using several different techniques. The aggregate texture is analyzed using the Wavelet method (Energy Signature), angularity is analyzed using the gradient method and radius method (Angularity Index), and the three-dimensional form is analyzed using the Sphericity and Shape factors.



Figure 2.8: Aggregate Imaging System (AIMS) equipment (Mahmoud et al., 2010).

Texture Characterization

The use of summary statistics or parameters is the base of pavement texture characterization. For roughness and macro-texture description, there are several well-defined and widely used parameters. The most common are the International Roughness Index (IRI) for roughness and the MPD and MTD for macro-texture, described in the previous section. Although the MPD and MTD are widely used, these parameters are too simplistic and do not describe the distribution of the profile, which is critical for assessing friction characteristics. For example, pavements with similar MPDs could have very different texture. In the pavement engineering literature, there are no standardized methods for micro-texture characterization; however, different parameters are described to characterize micro-texture, including those used to describe macro-texture.

With the development of new technologies for digitalizing surfaces, a series of experimental characterization procedures have been developed. Recent characterization is focused on the study of several different spatial parameters, and the incorporation of spectral analysis (scale-independent evaluation) to describe texture. Texture

characterization is scale-dependent when the same parameters must be defined separately at each scale (Rajaei et al., 2017). For example, obtaining a value of MPD for macro-texture component, and a value of MPD for micro-texture component. Spectral parameters are considered scale-independent parameters since they are estimated along multi-scale measures, including a wide range of texture wavelengths. Spectral techniques are used to avoid the complexity of defining the same parameters at different scales.

Spatial Parameters

Spatial texture parameters are divided into four groups: amplitude, hybrid, spacing, and functional parameters. Amplitude or height parameters involve the statistical distribution of height values along the Z-axis, the RMS is an example of this category. Spacing parameters include the spatial periodicity of the data. Additionally, the hybrid property is a combination of amplitude and spacing. The functional parameters give information about the surface structure, based on the material bearing ratio curve. The bearing ratio curve is the integral of the amplitude distribution function (ADF), which is the function that gives the probability of a texture profile having a certain height, Z, at any position X. It is a cumulative probability distribution.

Table 2.2 summarizes some of the parameters used for characterization of pavement texture. The root mean square (RMS) value is used when a more accurate measurement of surface roughness is required. RMS value has been implemented in highway texture description research (Madeiros et al., 2016; Serigos et al., 2014; Gunaratne et al., 2000; Li et al., 2011) because it can be used along with the MPD to identify surfaces with positive or negative texture (Figure 2.9), which cannot be deduced from measurements of only MPD or MTD. The RMS is a statistic that measures how much the measured profile deviates from the best fit of the data. For instance, based on the profiles

in Figure 2.9, both have the same RMS since its profile variation is identical. However, the positive texture profile will have an MPD larger than the negative texture profile. Thus, when comparing both RMS and MPD, it is possible to know if the pavement texture is positive or negative.

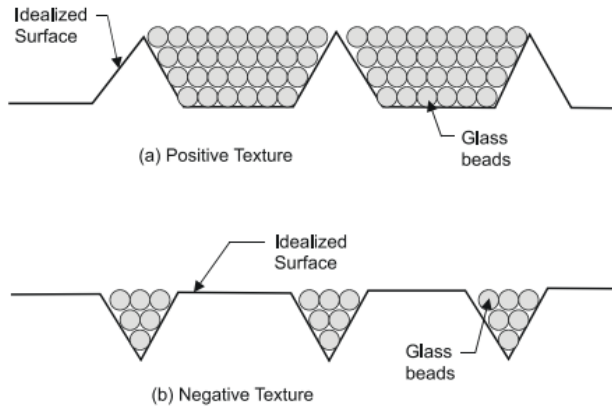


Figure 2.9: Positive and negative texture (McGhee and Flintsch, 2003).

Additionally, values of Skewness (R_{sk}) and Kurtosis (R_{ku}), offer a good description of the surfaces regarding the height distribution (Table 2.2). Skewness represents the degree of symmetry of the profile heights about the mean plane. The sign of skewness indicates the predominance of peaks (positive skewness), or valleys (negative skewness), (Figure 2.10 a). Kurtosis indicates the presence of extremely high peaks or depth valleys (skewness higher than 3), or the lack of them (skewness lower than 3) (Figure 2.10 b). If the profile heights follow a normal distribution, the value of skewness is 0, and the value of kurtosis is 3.

Table 2.2: Texture parameters used for pavement texture characterization.

Amplitude	Mean Profile Depth (MPD)	$MPD = \frac{1}{2} [\max(h_1, \dots, h_{N/2}) + \max(h_{N/2+1}, \dots, h_N)]$
	Height Average (R_a)	$R_a = \frac{1}{N} \sum_{i=1}^N h_i $
	Maximum Height (R_z)	$R_z = \max(h_i) - \min(h_i), i = 1..N$
	Root Mean Square (RMS)	$RMS = \sqrt{\frac{1}{N} \sum_{i=1}^N h_i^2}$
	Skewness (R_{sk})	$R_{sk} = \frac{1}{RMS^3} \sqrt{\frac{1}{N} \sum_{i=1}^N h_i^3}$
	Kurtosis (R_{ku})	$R_{ku} = \frac{1}{RMS^4} \sqrt{\frac{1}{N} \sum_{i=1}^N h_i^4}$
Hybrid	Two Points Slope Variance (SV_{2pts})	$SV_{2pts} = \sqrt{\frac{1}{N} \sum_{i=1}^N \left(\frac{h_{i+1} + h_i}{\Delta x} \right)^2}$
	Six Points Slope Variance (SV_{6pts})	$SV_{6pts} = \sqrt{\frac{1}{N} \sum_{i=1}^N \left(\frac{h_{i+3} - 9*h_{i+2} + 45*h_{i+1} - 45*h_{i-1} + 9*h_{i-2} - h_{i-3}}{60*\Delta x} \right)^2}$
Where, h_i = height value for coordinate "i" N = number of coordinates within the baseline Δx = horizontal distance between coordinates		

Li et al. (2011) and Serigos et al. (2014) used two hybrid parameters to describe pavement surface texture (Table 2.2). The first one is the two points slope variance points (SV_{2pts}), it measures the slopes between two consecutive points as the difference in height between two consecutive coordinates, divided by the horizontal distance between them. The second parameter, six points slope variance (SV_{6pts}), calculates the slopes using a weighted sum of the height values of six coordinates divided by the horizontal distance between them (Table 2.2).

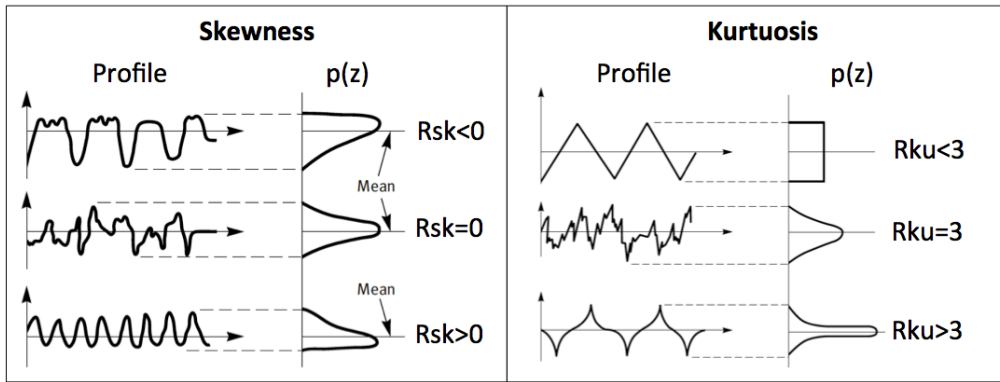


Figure 2.10: Texture profiles with (a) different skewness values, and (b) different kurtosis values (ASME B46, 2010).

Spatial parameters can be obtained in two dimensions (2D) from a linear profile, or in three dimensions (3D) from a surface profile. 2D parameters are predominant in pavement texture characterization since the data collected mainly consist of linear profiles. However, some researchers have recently started to use 3D parameters (Madeiros et al., 2016; Li et al., 2017).

Spatial parameters can be described as scale-dependent parameters. For this reason, they can be applied to both macro-texture and micro-texture components; this provides an independent characterization. At a macro-texture level, generally, the analyzed segments have a baseline distance of 100 mm, as established for the estimation of MPD (ASTM E 1845, 2009). This baseline corresponds to two times the maximum wavelength. For micro-texture description, there are not current specifications of baseline. Li et al. (2011) found that a baseline of 12.75 mm will provide stable values of MPD, RMS, and $SV_{2\text{pts}}$. However, Serigos et al. (2014) found that baselines shorter than 10 mm enhance the prediction of surface friction and recommended a baseline of 1 mm when characterizing micro-texture to predict skid resistance. Additionally, Serigos et al. (2014) found that data obtained from

the median of the baseline-segments made texture parameters better predictors of the friction than data obtained from the average value.

When using spatial parameters to characterize texture and assess its influence on tire/pavement interactions, it is important to highlight that the measured profile is not an accurate outline of the actual tire/pavement contact profile. Due to the stiffness of the tire, the contact area does not include all the points of the measured profiles. In the case of micro-texture, the polishing effect of the traffic may result in lower micro-texture at the contact area. Serigos et al. (2014) found that accounting for the contact area at the tire/pavement interaction, for micro-texture characterization, significantly improved the prediction of friction.

Spectral Parameters

Spectral parameters refer to parameters obtained in the domain of spatial frequencies (or texture wavelengths) rather than the spatial domain. Several researchers have used Fourier analysis to examine the surface texture profiles since it can capture relevant texture level distributions. As mentioned previously, it is possible to decompose a texture profile in sinusoidal wavelengths using Fourier analysis.

A common approach is to determine parameters from the texture spectrum, which is obtained when a surface profile has been analyzed by filtering techniques to determine the magnitude of its spectral components at different spatial frequencies. The technical specification ISO 1373-4 (ISO, 2008) describes the procedure to obtain the texture spectrum expressed in octave or one-third octave bandwidth. An octave bandwidth is a frequency band where the highest frequency is twice the lowest frequency. The parameter used in this approach is the texture profile level ($L_{tx,\lambda}$), which is a logarithmic transformation of an amplitude representation of a texture profile, having a center

wavelength of λ , its units are decibels (dB). The texture spectrum approach is used mainly to assess the influence of texture on tire/pavement noise (Sandberg and Descornet, 1980), but it has been used to assess friction too (Miller et al., 2011).

Other researchers have based their analysis on the Power Spectral Density (PSD), which is a description of how the energy or “power” of a pavement texture profile, is distributed over the different frequencies. Serigos et al. (2014) characterized surfaces macro- and micro-texture using the slope and the intercept of the linearized PSD, i.e. Log (PSD) vs. Log (spatial frequencies), obtained using the LTS.

Several studies have used fractal and multi-fractal theory to characterize texture (Miao et al., 2014; Villani et al., 2014; Panagouli et al., 1997). This theory assumes that the texture irregularities follow the same (or approximately similar) pattern at different scales. In this case, pavement texture is considered a self-affine surface, which means that to appreciate the similarity of the texture patterns at different scales (for instance, macro- or micro-texture), the patterns need to be scaled by different amounts (known as fractal dimension) in the coordinate axis. The fractal dimension (D_f) and the Hurst exponent (H) are the most widely used parameters. The fractal dimension is estimated from the slope (β) obtained in the linearized PSD using empirical models, such as the ones shown in Equation 2.4 to 2.6 (Rajaei, 2017). The Hurst exponent is obtained using the fractal dimension, as shown in Equation 2.7.

$$D_f = 4 - \frac{1}{2} |\beta| \quad (2.4)$$

$$D_f = \frac{6+\beta}{2} \quad (2.5)$$

$$D_f = \frac{7+\beta}{2} \quad (2.6)$$

$$H = 3 - D_f \quad (2.7)$$

FRICITION AND SKID RESISTANCE

Pavement friction is the force that resists the relative motion between a vehicle tire and a pavement surface (Hall et al., 2009). As the tire rolls or slides over the pavement surface, the resistive force is generated. This resistive force is characterized by a non-dimensional friction coefficient μ that is the ratio of the tangential friction force (F) and the vertical load or perpendicular force (F_w), as shown in Equation 2.8.

$$\mu = F/F_w \quad (2.8)$$

Where,

F = tractive force applied to the tire at the tire/pavement contact

μ = coefficient of friction

F_w = dynamic vertical load on the tire

Skid resistance is the ability of the traveled surface to prevent the loss of tire traction (AASHTO, 2008). The skid resistance is commonly estimated as the coefficient of friction multiplied by 100 and reported as skid number (SN). In paved surfaces, the SN is used to report the results of a pavement friction test conducted by the locked-wheel method (ASTM E 274, 2015). SN is determined from the force required to slide the locked test tire at a stated speed, divided by the effective wheel load and multiplied by 100. While texture is a property of the pavement surface, skid resistance is a characteristic that depends on the texture and many other variables.

The friction force is developed mainly in response to acceleration, braking or steering (Flintsch et al., 2012). There are two types of friction that are commonly measured: the side forced friction and the longitudinal friction. The side forced friction “*relates to the lateral or side force friction that occurs as a vehicle changes direction or compensates for pavement cross-slope and/or cross-wind effects*” (AASHTO, 2008). The longitudinal friction is developed along the driving direction and has two extreme modes of operations:

free-rolling or no braking, and constant break. The speed between tire circumference and the pavement, known as slip speed, is zero in the free-rolling mode. While for the constant break mode it increases from zero to potential maximum of the speed of the vehicle (Flintsch et al., 2012). Conditions in between are also possible and they are referred as variable slip and it is measured in percentage.

Slip Speed Effect

The coefficient of friction between a tire and the pavement changes with varying slip speed (Henry, 2000). The coefficient of friction increases rapidly with increasing slip to a peak value (peak friction), that usually occurs between 10 and 30 percent slip (critical slip), as shown in Figure 2.11. The friction then decreases to a value known as the coefficient of sliding friction, which occurs when the wheel stops rotating and the tire skids over the surface (Hall et al., 2009; Flintsch et al., 2012). The anti-lock braking systems (ABS) is a vehicle safety system that detects the onset of wheel slip and momentarily release and then re-apply the brakes to make sure the peak friction is not exceeded (Flintsch et al., 2012).

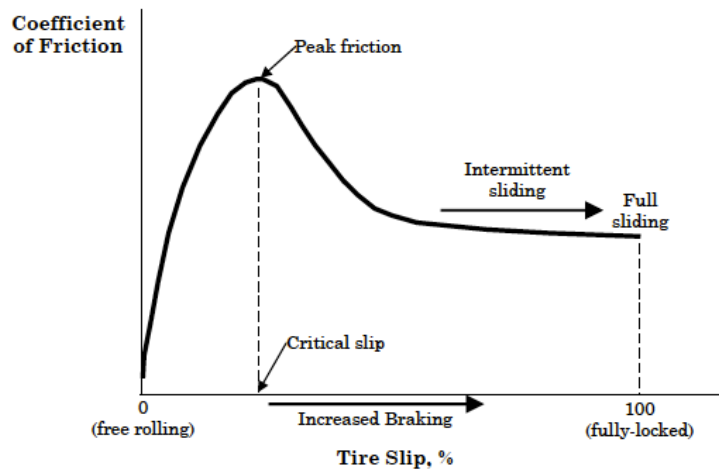


Figure 2.11: Friction coefficient and slip speed curve (Hall et al., 2009).

The difference between the peak and sliding coefficients of friction may equal up to 50 percent of the sliding value, and is much greater on wet pavements than on dry pavements (Hall et al., 2009). Flintsch et al. (2012) mentioned that this difference depends not only on vehicle speed and tire properties, but also on the characteristics of the road surface, particularly its state of micro-texture, the form and magnitude of the macro-texture, and the amount of water and other contaminants on the pavement.

Ueckerman and Wang (2014) stated that micro-texture governs the peak friction, while macro-texture governs the decreasing value, as shown in Figure 2.12 (a). Figure 2.12 (b) shows the relative influences of micro-texture, macro-texture, and speed on pavement friction. As can be seen, micro-texture influences the magnitude of tire friction, while macro-texture impacts the friction-speed gradient. At low speeds, micro-texture dominates the wet and dry friction level. At higher speeds, the presence of high macro-texture facilitates the drainage of water so that the adhesive component of friction afforded by micro-texture is re-established by being above the water (Hall et al., 2009).

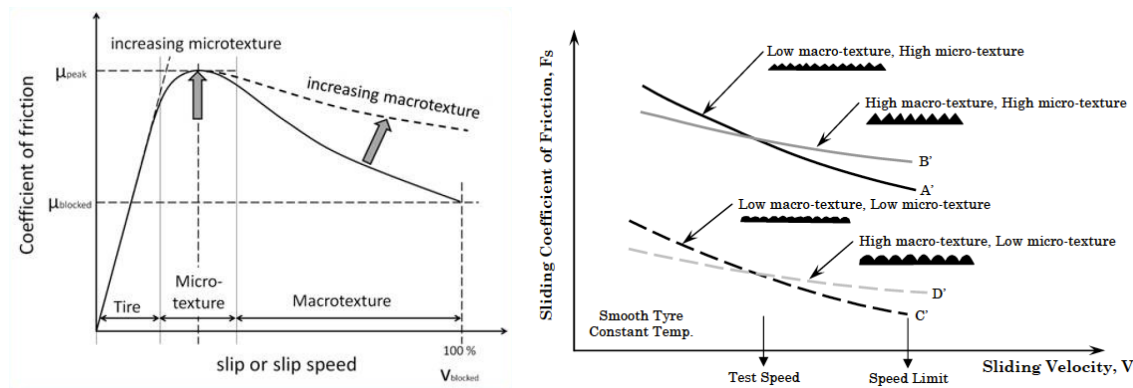


Figure 2.12: Effect of texture on tire/pavement friction at different sliding speeds (Ueckerman and Wang, 2014; Flinstch et al., 2002 cited by Hall et al., 2009).

Friction Mechanisms

Pavement friction is the result of a complex interplay between two principal frictional force components: adhesion and hysteresis (AASHTO, 2008; Henry, 2000; Hall et al., 2009). Although there are other components of pavement friction, such as tire rubber shear, they are relatively insignificant when compared to the adhesion and hysteresis force components (AASHTO, 2008). Thus, friction can be viewed as the sum of the adhesion and hysteresis.

Adhesion is the friction that results from the small-scale bonding/interlocking of the vehicle tire rubber and the pavement surface (Figure 2.13). It is a function of the interface shear strength and contact area (AASHTO, 2008; Hall et al., 2009). The hysteresis component of frictional forces results from the energy loss due to enveloping of the tire around the texture. Because adhesion force is developed at the tire/pavement interface, it is most responsive to the micro-level asperities (micro-texture) of the aggregate particles. In contrast, the hysteresis force developed within the tire is most responsive to the macro-level asperities (macro-texture) formed in the pavement surface. Thus, in principle, adhesion governs the overall friction on smooth-textured and dry pavements, while hysteresis is the dominant component on wet and rough-textured pavements (AASHTO, 2008; Henry, 2000; Hall et al., 2009).

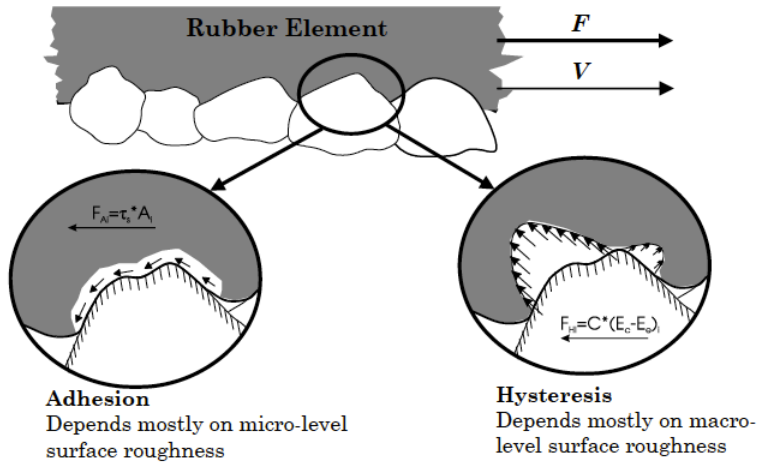


Figure 2.13: Key mechanism of tire/pavement friction (Hall et al., 2009).

Measuring Skid Resistance of Pavements

Several different friction-measuring devices have been developed based on the main principle of a rubber sliding over the road surface and measuring the reaction force. The three major operating principles of frictional measurement equipment are (Kogbara et al., 2016): slider, longitudinal friction coefficient (LFC), and side force coefficient (SFC).

Slider principle covers devices used for stationary testing; therefore, they are mainly used in the laboratory. It entails the use of sliders attached either to the foot of a pendulum arm or to a rotating head, which slows down on contact with the road surface. The rate of deceleration is used to derive a value representing the skid resistance of the road (Flintsch et al., 2012).

In general, the LFC and SFC principle devices are used for friction measurements in the field. The LFC principle consists of the application of a braking force to a test wheel so that it rotates more slowly than the forward speed of the vehicle. Thus, the test wheel slips over the surface and frictional forces are developed. The LFC is represented as the ratio of vertical and drag forces. LFC principle-based devices are divided into three modes

depending on the percentage of slip: locked-wheel, fixed-slip, and variable-slip. The SFC-principle devices are side-force friction testers that use an instrumented measuring wheel set at an angle, known as slip or yaw angle, to the direction of travel of the vehicle. The slip angle induces friction between the tire and road as it makes the tire slip over the road surface. The SFC is expressed as the ratio of the vertical and sideway forces (Flintsch et al., 2012; Kogbara et al., 2016).

Stationary Testing Methods

Stationary testing methods are mainly implemented through slide-principle devices; they are mostly used in laboratory. In general, these devices are relatively inexpensive and require lane closure if used in field (AASHTO, 2008). The most commonly used devices are the British Pendulum Test (BPT) (ASTM E 303, 1998) and the Dynamic Friction Test (DFT) (ASTM E 1911, 2009).

The BPT is manually operated and provides a spot measurement of the surface friction. It measures the friction coefficient at a skidding speed of approximately 10 km/h (Henry, 2000), therefore evaluates the skid resistance at low speed. The procedure entails the use of a pendulum-type tester with a standard rubber slider, as shown in Figure 2.14. The pendulum is raised to a locked position, then released, thus allowing the slider to contact the test surface. A drag pointer indicates the British Pendulum Number (BPN). The greater the friction between the slider and the test surface, the more the swing is retarded, and the larger the BPN reading. Due to the high influence of micro-texture on low-speed friction, the BPN values have been used as a surrogate of micro-texture description.

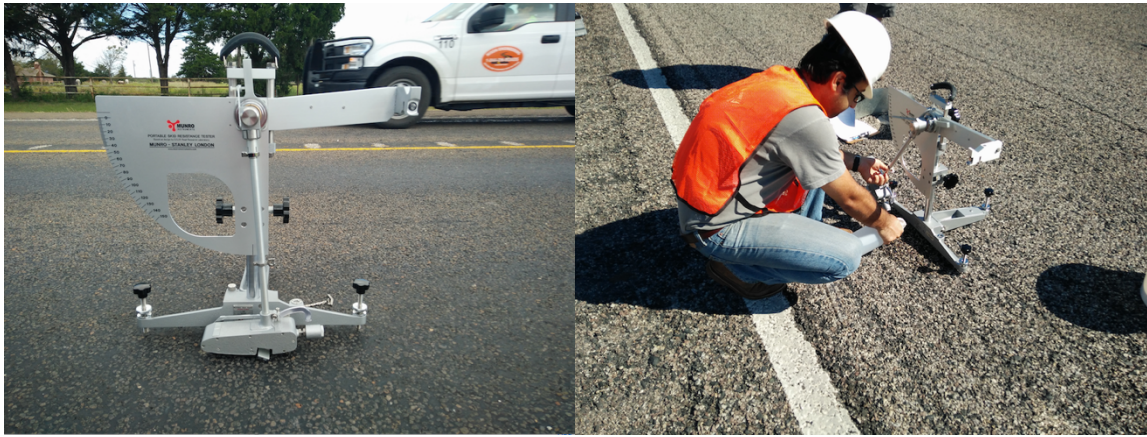


Figure 2.14: (a) British Pendulum Tester (BPT), and (b) field operation.

The DFT is a modular system that is controlled electronically to measure friction by the rotating principle. It measures the torque necessary to rotate three rubber sliders in a circular path at different speeds. Water is introduced in front of the sliders during the tests by using a water tank as shown in Figure 2.15. Results are typically recorded at 20, 40, 60, and 80 km/h (12, 24, 36, and 48 mph), and the speed versus friction relationship can be obtained (AASHTO, 2008). Based on measurements at the annual National Aeronautics and Space Administration (NASA) Friction Workshops (1993–1999), the values of DFT friction when the slip speed is 20 km/h are highly correlated with BPN (Wambold et al., 1998; cited by Henry, 2000).

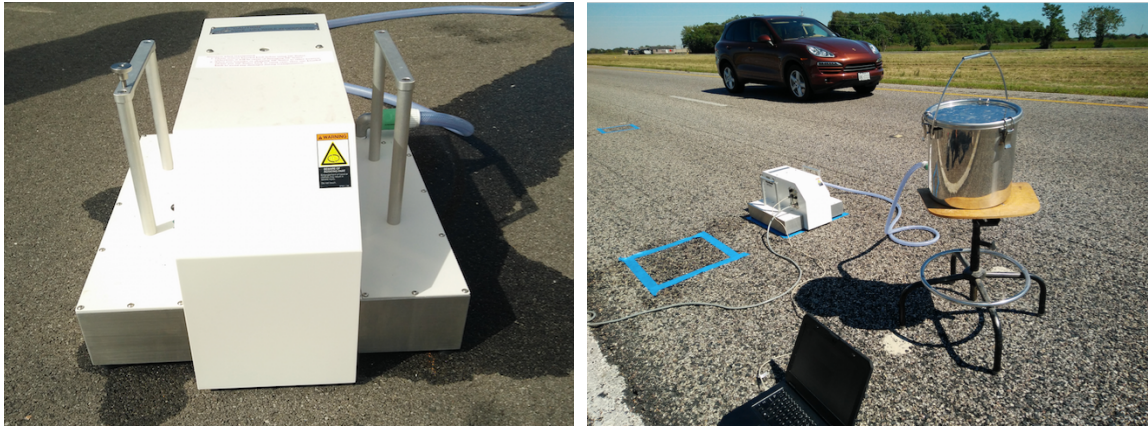


Figure 2.15: (a) Dynamic Friction Tester (DFT) and (b) field operation.

Pulled Device Methods

Pulled devices methods utilize one or two full-scale test tires to measure pavement friction properties in one of four modes: side-force (SFC principle), locked-wheel, fixed-slip, or variable-slip (LFC principle) (Hall et al., 2009).

The locked-wheel test (ASTM E 274, 2015) is the most commonly used method for measure pavement friction at high-speed in the United Stated (Henry, 2000; Hall et al., 2009). This method is meant to test the frictional properties of the surface under emergency braking conditions for a vehicle without ABS, using LFC principle. Unlike the side-force and fixed-slip modes, the locked-wheel method tests at a slip speed equal to the vehicle speed, which means that the wheel is locked and unable to rotate (Henry, 2000).

The results of the locked-wheel test are reported as skid number (SN), as mentioned previously. The skid device is installed on a trailer, which is towed behind the measuring vehicle at a typical speed of 64 km/h (40 mph). The device uses a locked wheel with either a ribbed tire (ASTM E 501, 2015) or a smooth tire (ASTM E 524, 2015). The smooth tire is more sensitive to pavement macro-texture, and the ribbed tire is more sensitive to micro-texture changes in the pavement (Hall et al., 2009). TxDOT implemented changes to its

skid testing procedure in 1999. These changes included the use of smooth tire test wheel instead of the previously used ribbed tire wheel, and the use of test speed of 80 km/h (50 mph) instead of the previously used 64 km/h (40 mph) (Jayawickrama and Madhira, 2008). Although, in the US the most commonly used tire in this test is the ribbed tire wheel (Henry, 2000).

Outside the US, side-force and fixed-slip modes are the most common, and the test tires are, in general, smooth tread tires (Henry, 2000). The side-force mode devices use the SFC principle. The most commonly used are the Mu-Meter (ASTM E 670, 2015) and the Sideway-Force Coefficient Routine Investigation Machine (SCRIM), both originated in the United Kingdom. The side-force testers are sensitive to micro-texture since the slip speed used, and the slip or yaw angle is small and insensitive to macro-texture variations (Hall et al., 2009; Henry, 2000). The Mu-Meter is the only side force device that has been used in the US, primarily at airports, with limited use on highways (Henry, 2000). Recently FWHA acquired a SCRIM but its use has been limited so far.

The fixed-slip methods measure friction experienced by vehicles with ABS braking system. Fixed-slip devices maintain a constant slip, typically between 10 and 20 percent, as a vertical load is applied to the test tire (Henry, 2000). The devices are based on the LFC principle. Examples of the fixed-slip tester are the GripTester (Figure 2.16), and the Micro GripTester (Figure 2.17). They are Continuous Friction Measuring Equipment (CMFE) capable of measuring continuously and dynamically the longitudinal skid resistance coefficient of the pavement, expressed as Grip Number (GN). They have a single measuring wheel, fitted with a special smooth tread tire that is mounted on an axle instrumented to measure both the horizontal drag force and the vertical load force (Thomas, 2008). The GripTester is towed behind a vehicle and uses measurement speeds of 5 to 100

km/h (Kogbara et al., 2016). The Micro GripTester is performed manually at a recommended speed of 2.5 km/h. A study prepared by the University of Ulster in Northern Ireland for the Micro GripTester manufacturer showed that the GN presents a high correlation with measures of the BPT (Woodward, 2010).

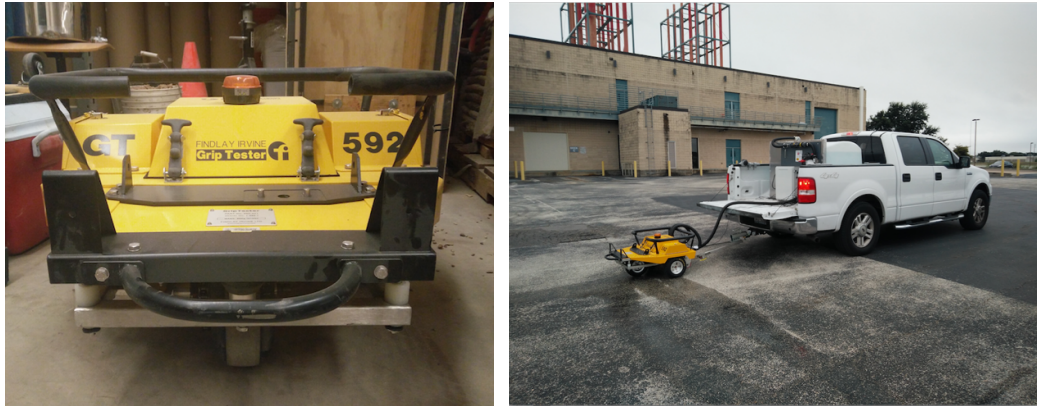


Figure 2.16: (a) GripTester, and (b) field operation.



Figure 2.17: (a) Micro GripTester, and (b) field operation.

Skid Resistance Measures Harmonization

Harmonization is defined as the adjustment of the outputs of different devices used for the measurement of a specific phenomenon so that all devices report the same value

(ASTM E 2100, 2015). There have been several studies done to harmonize various friction measurement equipment. These include:

- The World Road Association (PIARC) International Experiment (Wambold et al., 1995).
- The European “Harmonization of European Routine and Research Measurement Equipment for Skid Resistance” (HERMES) Project (Descornet et al., 2006).
- NASA Wallop Tire/Runway Friction Workshops (Wambold and Henry, 2002).
- Virginia Tech Transportation Institute (VTTI) Pavement Surface Properties Consortium Rodeo Reports.
- The “Tyre and Road Surface Optimization for Skid resistance and Further Effects” (TYROSAFE) (Scharnigg et al., 2011).
- The “Rolling resistance, Skid resistance, and Noise Emission measurement standards for road surfaces” (ROSANNE) Project (Haider et al. 2014).

One of the most comprehensive efforts around the world was the International PIARC experiment, which compared and harmonize texture and skid resistance measurements. It was conducted at 54 sites across US and Europe, in the fall of 1992 (Henry, 2000). One of the main results of the PIARC experiment was the development of the International Friction Index (IFI). The process to calculate the IFI is standardized by the ASTM (ASTM E1960, 2015). The IFI, is composed of two parameters: a speed constant (Sp) based on macro-texture measurements (Equation 2.9), and a friction number at 60 km/h ($FR60$), Equation 2.10. The IFI ($F60$) can be obtained from Equation 2.11.

$$S_p = a + b \cdot TX \quad (2.9)$$

Where,

S_p = IFI speed number

a,b = calibration constants dependent on the method used to measure macro-texture (for MPD a = 14.2 and b = 89.7; for MTD a = -11.6 and b = 113.6)

TX = Macro-texture (MPD or MTD) measurement in mm.

$$FR(60) = FR(S) \cdot e^{\left(\frac{S-60}{S_p}\right)} \quad (2.10)$$

Where,

$FR(60)$ = adjusted value of friction measure $FR(S)$ at the speed S to the speed of 60 km/h

$FR(S)$ = friction value at selected slip speed S

S = selected slip speed

$$F(60) = A + B \cdot FR(60) + C \cdot TX \quad (2.11)$$

Where,

$F(60)$ = IFI friction number

A, B = calibration constants dependent on friction measuring device

C = calibration constant required for measurements using ribbed tire

RELATIONSHIP BETWEEN PAVEMENT TEXTURE AND SURFACE FRICTION

Monitoring and managing the skid resistance in pavement surfaces is important to improve safety by controlling and reducing the number of road accidents. Several studies indicate the influence of the skid resistance in the number of crashes (Hall et al., 2009). The test methods for friction evaluation, described in the previous section, present several disadvantages such as the use of water, which make impractical the continuous evaluation of the traffic network, and the requirement of road control, which is costly and unviable in some cases. For this reason, different models have been developed to try to predict friction based on the texture properties.

Empirical modeling is a common approach to describe the influence of pavement texture on surface friction (Rajaei, 2017). Due to the limitation on the measure of high frequency (very small wavelengths), many of the texture-friction relations have been implemented using only macro-texture, or a surrogate of micro-texture such as the BPN. Recent studies have tried to incorporate micro-texture to the skid resistance prediction, using non-contact technologies to characterize micro-texture (Li et al., 2010; Serigos et al., 2014).

Macro-Texture and Micro-Texture Testing Using Laser Sensors

Li et al. (2010) used the LTS to obtain macro- and micro-texture profiles. The authors correlated texture measures with the FN obtained from the locked wheel trailer, under dry and wet conditions. To characterize texture, they used MPD and SV_{2pts} for both texture components. The models of FN for wet and dry surface were obtained using linear regression, the prediction equations are shown in Equation 2.12 and 2.13, respectively. The authors found coefficient of determination of 1 for both equations, which indicates perfect correlation of the samples. However, they warned about the limited number of samples used for the models, which is not enough to ensure the accuracy and reliability of the models. Among the main conclusion, the authors found that for wet surfaces, the friction is more sensitive to SV_{2pts} than to the MPD, for the micro-texture measurement.

$$FN_{wet} = -11.425 + 38.133 \cdot MPD_{macro} - 731.263 \cdot MPD_{micro} + 69.714 \cdot SV_{2pts,micro} \quad (2.12)$$

$$FN_{dry} = 75.329 - 4.294 \cdot MPD_{macro} - 259.221 \cdot MPD_{micro} + 34.713 \cdot SV_{2pts,micro} \quad (2.13)$$

Where,

FN_{wet} = friction number for wet surface

FN_{dry} = friction number for dry surface

Incorporating Surface Micro-texture in the Prediction of Skid Resistance

Serigos et al. (2014) used the LTS and the BPN to obtain a model for friction prediction. The authors used profiles obtained from the LTS and obtained the micro-texture profiles using linear filters. They obtained several spatial parameters for both macro- and micro-texture, such as the MPD, R_z , RMS, $SV_{2\text{pts}}$, and $SV_{6\text{pts}}$. Additionally, they used spectral parameters, such as the slope and the intersection of the linearized PSD. Figure 2.18 shows the relation found between macro-texture MPD and micro-texture MPD with the BPN.

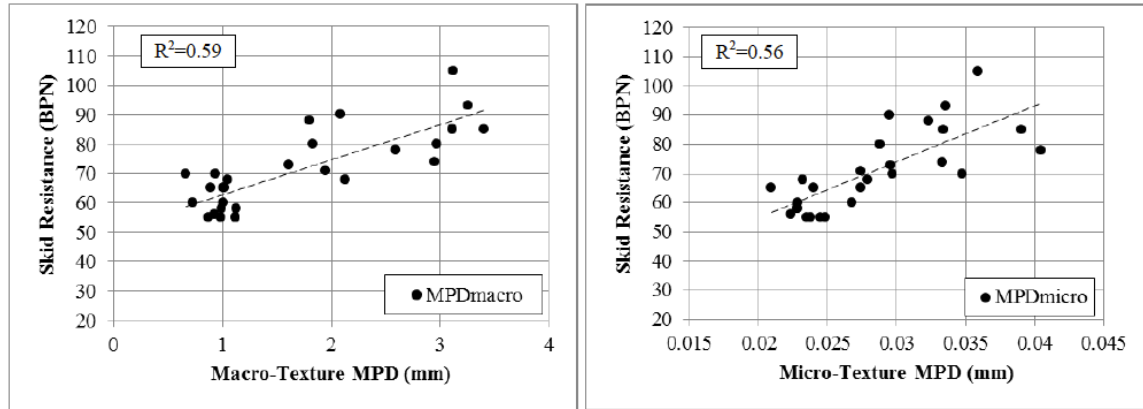


Figure 2.18: Relationship between (a) BPN and macro-texture MPD and, (b) BPN and micro-texture MPD (Serigos et al., 2014).

The authors found that the BPN was significantly affected by macro- and micro texture, and that incorporating micro-texture to the models that only used macro-texture, significantly improve the prediction of the BPN. Among the parameters used to incorporate texture characterization to the model, the main conclusions are:

- Slope variance parameters (hybrid) are better predictors of friction than amplitude parameters, where $SV_{6\text{pts}}$ showed better results than $SV_{2\text{pts}}$.
- Among the amplitude parameters, the MPD is the better predictor.

- The slope of the linearized PSD does not significantly affect the BPN, while the intercept does.

Chapter 3: Characterization and Processing of Texture Data

This chapter presents a description of the characterization and processing of the texture data obtained from the Line Laser Scanner (LLS), developed at the University of Texas at Austin (UT Austin). The chapter is divided into three main sections. The first section presents a description of the main characteristics of the laser system components. The second section is a description of the experimental setup and the LLS configurations used in this research. The third section describes the data processing performed to obtain the desired texture parameters.

LINE LASER SCANNER (LLS) CHARACTERIZATION

The LLS comprises a laser scanner and a translation stage (TS).

Laser Scanner

A surface profiling system was developed to characterize macro- and micro-texture. The system consists of a high-resolution 2D/3D laser scanner LJ-V7080 from Keyence. Table 3.1 presents the manufacturer's specifications for this laser head. The laser is based on diffusive reflection and uses a blue semiconductor light source with a wavelength of 405 nm. These conditions allow a minimum repeatability in the vertical or height axis (Z-axis, as shown in Figure 3.1) of $0.5 \mu\text{m}$, and a repeatability on the transverse axis (X-axis) of $10 \mu\text{m}$. The laser has a linearity of 0.1 % of full scale in the vertical axis. The maximum sampling frequency depends on the mode used. The frequency is 63 kHz for high-speed mode and 31 kHz for advanced function mode. Additionally, the maximum number of points that it can capture continuously is 800 in the transversal direction and 15,000 in the longitudinal direction (this limitation is imposed by the software, not by the hardware).

Table 3.1: Laser specifications (Keyence, 2015).

Characteristic		LJ-V7080
Mounting conditions		Diffuse Reflection
Reference distance		80 mm
Measurement Range	Z-axis (height)	± 23 mm (F.S.=46 mm)
	Near side	25 mm
	Reference distance	32 mm
	Far side	39 mm
Light Source		Blue semiconductor laser
	Wavelength	405 nm (visible beam)
	Laser class IEC60825-1 FDA(CDRH) Part 1040.10 ^{*11}	Class 2 Laser Product
	Output	4.8 mW
Spot shape (reference distance)		Approx. 48 mm x 48 μm
Repeatability	Z-axis (height)	0.5 μm
	X-axis (width)	10 μm
Linearity	Z-axis (height)	0.1 % F.S.
Profile data interval	X-axis (width)	50 μm
Sampling cycle (trigger interval)		Top speed: 16 μm (high-speed mode) Top speed: 32 μm (advanced function mode)
Temperature characteristics		0.01 % of F.S./°C
Environmental resistance	Enclosure rating	IP67 (IEC60529)
	Ambient operating illuminance	Incandescent lamp: 10,000 lux max
	Ambient temperature	0 to +45°C
	Operating Ambien humidity	20 to 85 % RH (No condensation)
	Vibration resistance	10 to 57 Hz, 1.5 mm double amplitude in X, Y, and Z directions, 3 hours respectively.
	Impact resistance	15 G/6 msec
Material		Aluminum
Weight		Approx. 400 g

The laser scanner LJ-V7080 is classified as Class 2 laser, which means that is considered to be safe regarding radiation exposure. However, it is recommended do not stare into the beam. It can be operated in ambient temperature from 0 to 45°C and relative humidity from 20 to 80 %. Additionally, it has a vibration resistance of 10 to 57 Hz and 1.5 mm double amplitude in X-, Y- and Z-axis. These conditions allow the use of the laser in both laboratory or field environments. The maximum illuminance resistance is 10,000 lux. The illuminance is the total of luminous flux on a surface per unit area. It is used as a

measure of the intensity of light that hit or passes through a surface. An illuminance of 10,000 lux corresponds to a full daylight with a non-direct sun. Under field environments, conditions such as direct sunlight can affect the measurement of the laser, since the illuminance can exceed the maximum resistance. Therefore, for all the measurements taken in this study, a box to provide shade was always used along with the laser to avoid the disturbance of the excess of illuminance and to keep the incident light as constant as possible.

The measurements obtained from the laser scanner correspond to discrete values of relative heights, in millimeters. The reference Z-axis distance is 80 mm; this means that the measurement of a point located at the height of 80 mm from the laser source is zero. Any point lower than 80 mm will be negative, any point higher will be positive, and both will be height measures relative to the reference height. The measurements can be exported to CVS format; this allows a further process of the information in common spreadsheet such as MS Excel.

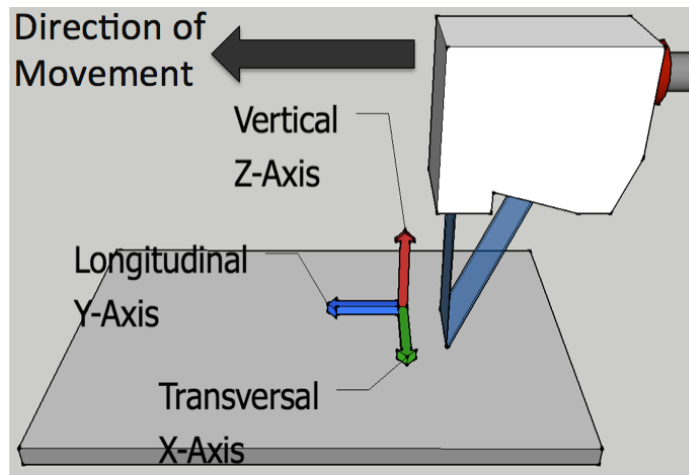


Figure 3.1: Axis convention and direction of movement.

Translation Stage (TS)

A linear translation stage (TS) controls the longitudinal movement (Y-axis) of the laser head, it is shown in Figure 3.2. Table 3.2 shows the relevant manufacturer's specifications. The TS has a maximum range of 150 mm with a bidirectional repeatability less than 2 μm . The maximum horizontal speed is 50 mm/s, with a minimum achievable incremental movement of 0.1 μm and a minimum repeatable incremental movement of 4 μm . The maximum vertical load capacity is 4 kg.

Table 3.2: Linear translator specifications.

Characteristic	LTS150
Travel Range	150 mm
Horizontal Velocity (Max)	50 mm/s
Vertical Velocity (Max)	3 mm/s
Minimum Achievable Incremental Movement	0.1 μm
Minimum Repeatable Incremental Movement	4 μm
Absolute On-Axis Accuracy	20 μm
Calibrated Accuracy	< $\pm 5.0 \mu\text{m}$
Bidirectional Repeatability	< $\pm 2 \mu\text{m}$
Backlash	2 μm
Horizontal Load Capacity (Max)	15 kg
Vertical Load Capacity (Max)	4 kg
Actuator Type	Stepper Motor



Figure 3.2: Linear translation stage (TS).

LINE LASER SCANNER (LLS) SETUP

The laser head was mounted onto a rigid aluminum plate that is attached to the TS. The TS is mounted onto a rigid frame that allows easy transportation of the entire setup in

the field and the laboratory. The equipment setup, shown in Figure 3.3, is controlled by a personal computer that allows changes to the laser's configuration, data storage, and TS configuration. The laser is mounted at the height of 82 mm from the frame base. The transverse coverage (X-axis) varies with the height from the base, as specified in Table 3.1. At 82 mm height, the total effective transverse coverage is 32.6 mm, approximately.



Figure 3.3: (a) Line Laser Scanner (LLS), and (b) field data collection.

The LLS is capable of collecting a maximum of 800 points in the transversal direction and a maximum of 15,000 points in the longitudinal direction. The transversal direction is time-independent since the 800 points are captured instantly. The longitudinal direction is time-dependent because the 15,000 points are captured during a period that depends on the sampling frequency. In this study, the analysis is focused on the longitudinal profiles, described in Figure 3.4. There are a total of 800 profiles with a maximum of 15,000 points per profile.

The sampling rate (ΔY) is given by the selected sampling frequency and the TS speed. The sampling frequency is the frequency for capturing the transversal axis measures (800 points time-independent measures). For instance, a frequency of 1 kHz will capture a set

of transversal axis measures each 0.001 second. Thus, at a sampling frequency of 1 kHz, the laser will capture the maximum number of 15,000 points (longitudinal axis) in 15 seconds. The speed selected in the TS will move the laser head along the longitudinal axis, as shown in Figure 3.4. For example, a speed of 8 mm/s will cover a total of 120 mm during 15 seconds. Thus, a combination of a sampling frequency of 1 kHz and TS speed of 8 mm/s corresponds to a sampling spacing of 8 μm . Equation 3.1 shows how to obtain the sampling spacing rate based on the sampling frequency and TS speed.

$$\Delta Y = \frac{v}{f_s} \quad (3.1)$$

Where,

ΔY = sampling rate for the longitudinal profile

f_s = sampling frequency of the laser

v = speed selected for the TS

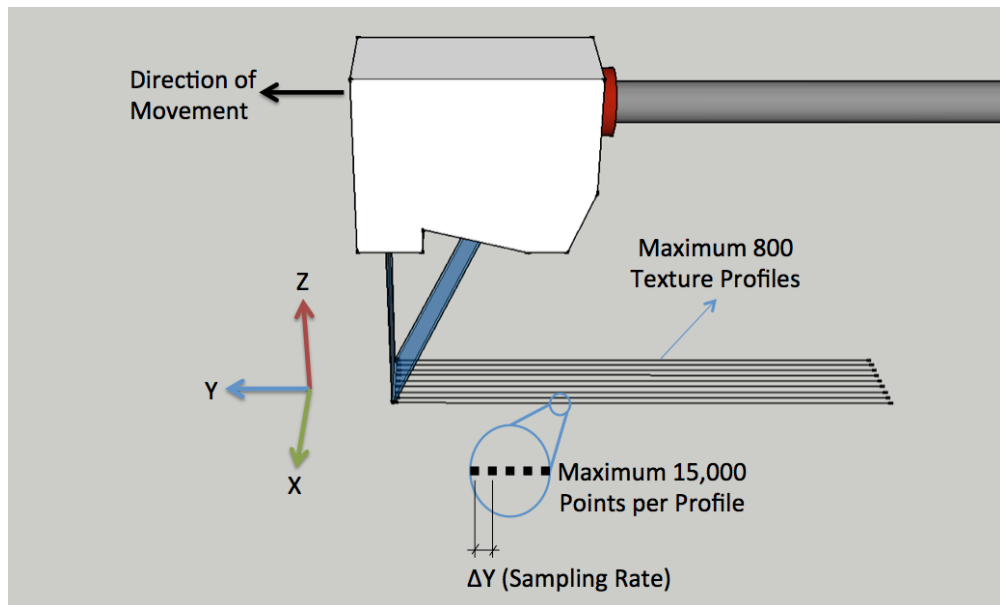


Figure 3.4: Longitudinal profiles and sampling rate.

One of the primary goals of this study was to characterize pavement surface macro- and micro-texture independently, and observe their effect on skid resistance. One of the

main advantages of the laser system developed as part of this study is its high resolution, which allows the capturing of both macro- and micro-texture components. As described previously, the LLS allows a minimum repeatability on the transverse axis of 10 μm (given by the laser scanner) and a longitudinal repeatability lower than 2 μm (given by the TS).

Based on the Nyquist sampling theorem presented in Equation 3.2, $\lambda/2$ is the minimum sample rate that permits a discrete sequence of samples to capture all the information of a signal (texture in this case) with a minimum wavelength of λ . For instance, with a sample rate of 8 μm , a texture of minimum wavelength of 16 μm can be reconstructed. For this reason, using the LLS, the texture characterization can cover macro-texture ($0.5 < \lambda < 50 \text{ mm}$) and the first decade of micro-texture ($50 < \lambda < 500 \mu\text{m}$), because the minimum sampling rate required is 25 μm which is higher than the minimum repeatability of the LLS.

$$\min \Delta Y = \frac{\lambda}{2} \quad (3.2)$$

Where,

ΔY = sampling rate for the longitudinal axis

λ = minimum wavelength of the texture component to reconstruct

Laser Scanner Setup

The laser head configurations can be managed using the manufacturer software LJ-Navigator 2. The main configurations used in the present study are described as follow:

- Sampling frequency: 1 kHz

A sampling frequency of 1 kHz was selected for the present study. This sampling frequency allowed the use of low speeds in the TS. The TS has a limitation of a maximum speed of 50 mm/s. Therefore, lower speeds are desired. Higher sampling frequencies will require that the TS use high speeds to capture the desired distance.

- Trigger mode: continuous sampling

A trigger corresponds to the time separation between measures of the points in the transversal axis. Two types of triggers modes are available: continuous and external trigger. The continuous trigger mode generates the trigger continuously at the set

sampling frequency. It is used when continuous sampling is required as in the present study. Continuous sampling allows a constant value of sampling rate (ΔY).

The external trigger generates the trigger at an arbitrary timing by an external input. Thus, the sampling rate is not constant using this mode. This mode is mainly used to other industrial applications of the laser.

- Batch measurement: on

Batch measurement mode is designed to handle collection and processing of multiple profiles. One batch has a maximum of 800 points in the transversal direction and a maximum of 15,000 points in the longitudinal direction. Thus, when “batch measurement” is on, it collects 800 profiles with 15,000 points each profile.

- Batch points: 15,000

The batch points are the number of points in the longitudinal axis. For the present study, the batch points are 15,000 (maximum allowed by the software). Thus, the measurement time using 1 kHz is 15 seconds.

- Operation Mode: high-speed

The laser head has two operational modes: advanced function and high-speed. Both modes use a processor that performs imaging, profile generation and buffering. However, the advanced function mode has an additional processor that handles measures performed on the transversal axis, and check to see whether the measures are within tolerance or not.

The advanced function mode limits measurement speed as more processing power is required for profile analysis. Thus, the measurement time presents variations for different types of surfaces. When using a sampling frequency of 1 kHz, experimental measurements presented increments of 5 to 10 seconds in the measurement time. Therefore, for the present study, the high-speed mode was selected since it presented constant measurement time of 15 seconds at 1 kHz of sampling frequency.

Translation Stage (TS) Setup

The translation stage (TS) controls the longitudinal displacement. The TS can be managed using the manufacturer software. The configurations used for TS are as follows:

- Acceleration and deceleration rate: 50 mm/s^2

The maximum acceleration and deceleration rate of 50 mm/s^2 was selected for this study. This allows the TS to reach the desired speed faster, without affecting the measurements due to differences in speed.

- Speed: 8.0 mm/s

The TS speed will depend on the sampling frequency of the laser head and the desired sampling rate, as presented in Equation 3.1. The sampling frequency is kept constant at 1 kHz . Therefore, the speed will depend on the desired sampling rates. For this study, the selected sampling rate is $8 \mu\text{m}$. Thus, the selected speed is 8 mm/s .

Comparison with Other Laser Systems

Currently, there are different systems used to characterize highway surface texture. The most commonly used are the Circular Track Meter (CTM) and the Laser Texture Scanner 9300 (LTS), described in Chapter 2. Table 3.3 shows a comparison of the main specifications of the CTM, LTS and the current setup used in the LLS.

The CTM has a sampling rate of $870 \mu\text{m}$. The minimum wavelength captured, based on the sampling theorem, is 1.74 mm . Thus, it can only cover macro-texture wavelengths, from 0.5 to 50 mm . The CTM is a reliable piece of equipment but it does not have the sampling rate desired for this study. The LTS has a sampling rate of $15 \mu\text{m}$; it can capture a minimum texture wavelength of $30 \mu\text{m}$. Therefore, it can be used to describe macro-texture and the first decade of micro-texture (with wavelengths from $50 \mu\text{m}$ to $500 \mu\text{m}$). The LTS has an improved sampling rate but the equipment is not as reliable. The LLS was set to a sampling rate of $8 \mu\text{m}$, and can also measure both macro-texture and the first

decade of micro-texture. Thus, the LLS has improved sampling rate and reliability as compared with the previous two devices.

The main advantage of the LSS is its vertical resolution of $0.5 \mu\text{m}$, compared to $15 \mu\text{m}$ from the LTS, and $3 \mu\text{m}$ from the CTM. Additionally, the duration for the data collection is 15 seconds, while for the LTS it can take up to 2 hours using its maximum resolution.

Table 3.3: Comparison of laser systems used to characterize pavement texture

Characteristic	CTM	LTS (Model 9300)	LLS
Sampling rate (ΔY)	$870 \mu\text{m}$	$15 \mu\text{m}$	$8 \mu\text{m}$
Maximum scan lines	1	800	800
Maximum samples per line	1,024	7,212	15,000
Vertical resolution	$3 \mu\text{m}$	$15 \mu\text{m}$	$0.5 \mu\text{m}$
Horizontal resolution	$50 \mu\text{m}$	Not indicated by the manufacturer	$Y\text{-axis} < 2 \mu\text{m}$ $X\text{-axis} = 10 \mu\text{m}$
Maximum scanned area	(circumference of 892 mm)	$107.95 \times 72.01 \text{ mm}$	$120 \times 3.26 \text{ mm}$
Duration	45 seconds approximately	45 seconds (10 scan lines) - 2 hours (800 scan lines)	15 seconds
Covered texture components	macro-texture	macro-texture and micro-texture (first decade)	macro-texture and micro-texture (first decade)

DATA PROCESSING

This section describes the data processing including the processing of invalid or erroneous data and the filtering procedure used to separate the various texture components. The data processing was performed using Python programming language.

Processing Invalid and Erroneous Data

In some cases, the data collected with the LLS presented a certain level of noise due to several reasons, such as reflective surfaces or shadowing effects or missing data due to the angle between the laser and the camera. These invalid or erroneous data show as

dropouts in the reading that can lead to erroneous results. For this reason, an important step of the processing of texture data was the evaluation and detection of these readings, and the adequate processing, to keep the larger number of data points possible.

In all cases, invalid profiles were found at the edges of the transverse coverage (X-axis). Figure 3.5 (a) illustrates this statement. These invalid profiles were easily recognized because all 15,000 points of the profile were invalid, it was only present on the edges, and the data showed a height value of -99.99. However, the number of invalid profiles is different in all the cases. To keep constant the size of the evaluated data, fifty profiles in each edge along the longitudinal axis were trimmed out and not considered for further analysis. This process ensured that the invalid profiles were not analyzed. Thus, the final evaluated data consisted of 700 profiles. Figure 3.5 (b) shows the final profiles after trimming out the readings close to the edges.

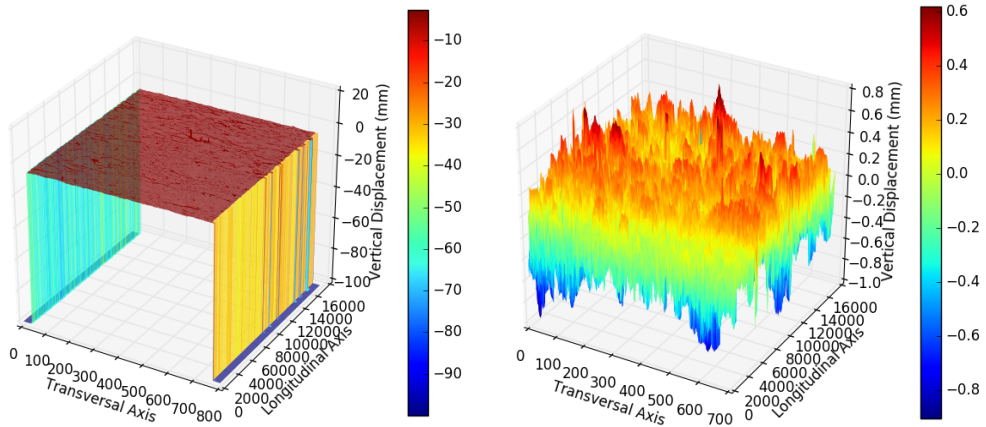


Figure 3.5: (a) 3D plot of original 800 transverse readings, and (b) 3D plot of 700 readings after trimming.

Dropouts in the data, also recognized as invalid, were present mainly in reflective surfaces, surfaces with high voids and areas not viewed by the camera. A maximum of 10 percent of dropouts per profile was allowed based on recommendations of standard procedures (ASTM E 1845, 2009). The profiles with less than 10% of dropouts were further processed to interpolate the missing values. When dropouts in series occur, as

illustrated in Figure 3.4 (a), the data were interpolated using Equation 3.3. Figure 4.7 (b) shows the final profiles after interpolation. In this study, none of the profiles presented a percentage of dropouts greater than 5%.

$$z_i = \frac{z_n - z_m}{n - m} (i - m) + z_m \quad (3.3)$$

Where,

i = sample number where the value is invalid

m = sample number of the nearest valid value before i

n = sample number of the nearest value after i

z_i = interpolated value for sample i

z_m = value for sample m

z_n = value for sample n

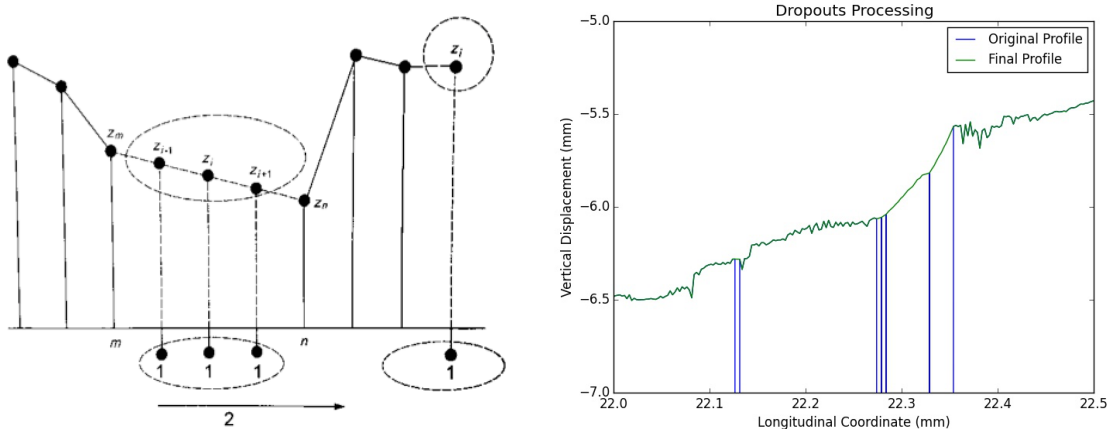


Figure 3.6: (a) Dropouts in series, and (b) processed profile example.

The procedure to detect dropout values includes evaluating of the profiles' height distribution. Figure 3.7 (a) shows an example of one of the profiles that presented mainly invalid negative values that can be detected by a simple algorithm. Figure 3.7 (b) shows the histogram of the height values for all profiles studied. As shown, the invalid data are concentrated around values of -100. Once these data are detected, the missing values are interpolated as explained previously. Finally, the processed profiles, presented in Figure 3.7 (c), show a more uniform height distribution, (Figure 3.7(d)).

Other types of observed dropouts include high reflective pavement surfaces that can lead to noisy data, mainly positive values, as shown in Figure 3.8 (a). In this case, the same procedure was followed. The height distribution, shown in Figure 3.8 (b), presents invalid data measurements above -4. These data were detected and processed as explained previously. The final profiles present a more uniform height distribution, as shown in Figure 3.8 (d).

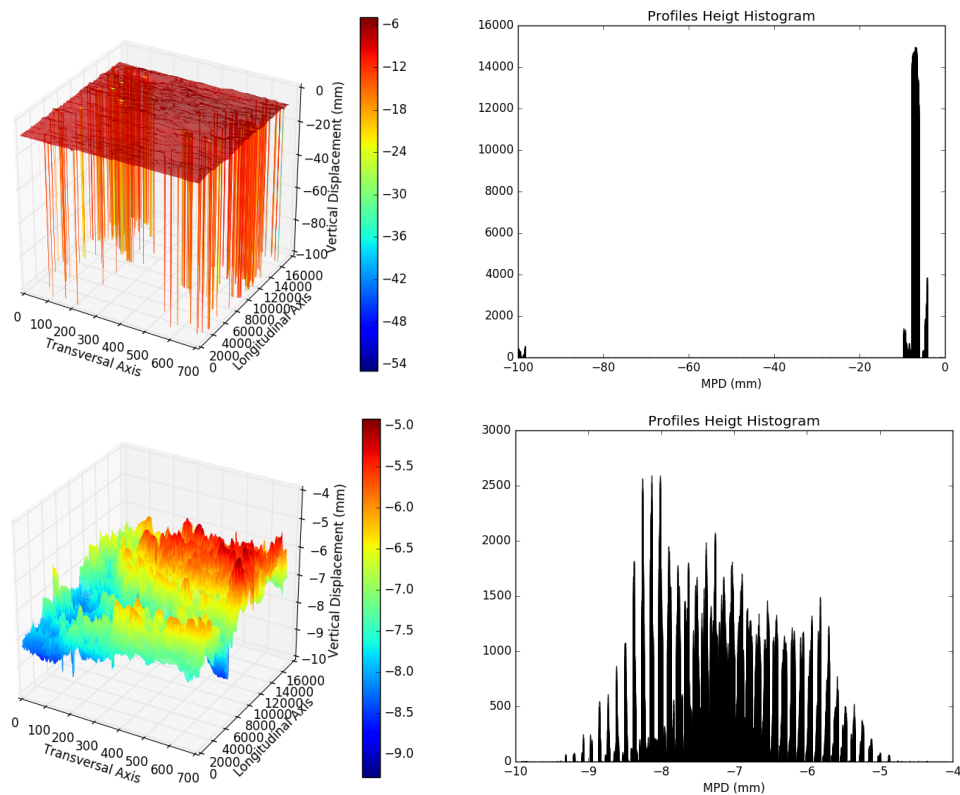


Figure 3.7: Example of negative values (a) 3D plot of original profiles, (b) histogram of original profiles, (c) 3D plot of processed profiles, and (b) histogram of processed profiles.

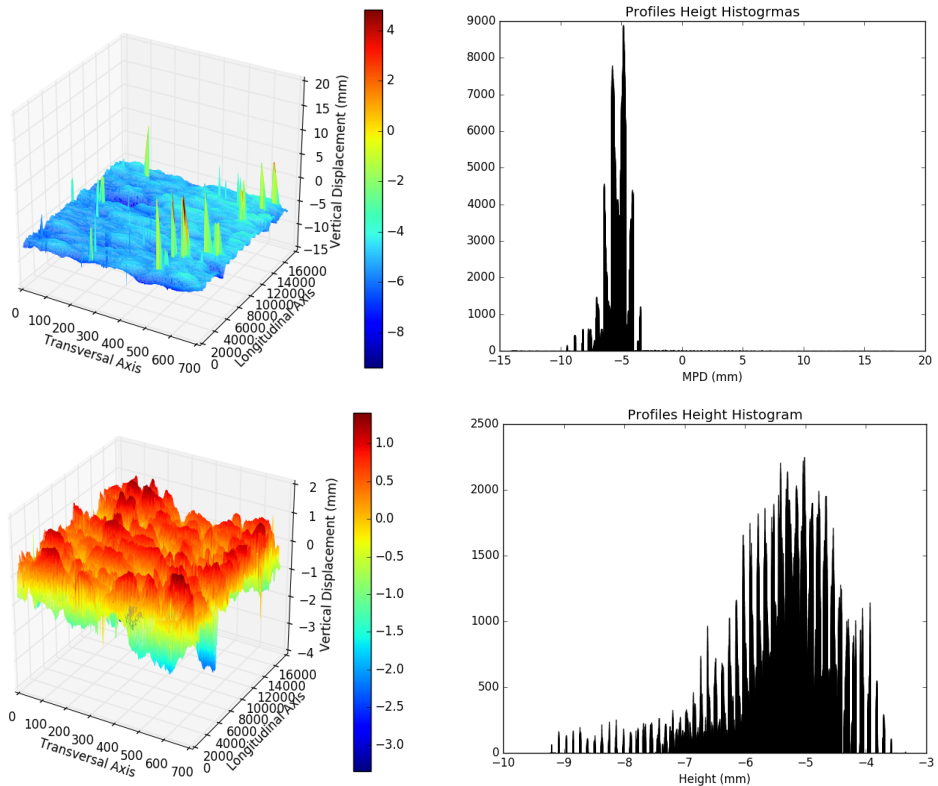


Figure 3.8: Example of reflective pavement surface (a) 3D plot of original profiles, (b) histogram of original profiles, (c) 3D plot of processed profiles, and (b) histogram of processed profiles.

Filtering Macro- and Micro-Texture Profiles

In this study, pavement texture profiles were collected using the LLS. Fourier Transform (FT) was used to convert the signal/data (texture profiles) from the space domain to the texture frequency (or wavelength) domain and to analyze the separate effect of each texture component. The FT transforms the texture profiles into a sum of sinusoidal waves. The output consists of the amplitudes corresponding to each texture frequency. This information can be displayed in a Power Spectral Density (PSD) plot, in which the square of the amplitude is plotted against its corresponding frequency. It can be interpreted as the power or “energy” of a signal (in this case texture) in a specific frequency or

wavelength. Due to the discrete nature of the scans produced by the LLS, the Discrete Fourier Transform (FT) was used in this study.

The data obtained by the LLS correspond to relative heights, as explained previously. The relative height distance is transformed to profile height by normalizing with respect to the best-fit line of each profile, this process is called “detrending”. Thus, the profiles are normalized with respect to an average height set equal to zero. After this process, the data are first transformed to the frequency domain using Discrete FT and then filtered using a Butterworth linear filter. The Butterworth filter was designed to be as close as possible to the ideal filter. The Python code for these filters is presented in Appendix A. A low-pass filter was used to isolate macro-texture wavelengths; while, a band-pass filter was used to isolate micro-texture wavelengths:

- Macro-Texture component: low-pass filter

In this filter, all the frequencies above 2,000 cycles/m (wavelength lower than 0.5 mm) are rejected to isolate only the effect of macro-texture, as shown in Figure 3.9 (a). The cut-off frequency used is 3,000 cycles/m. It was chosen slightly above the desired frequency to avoid the attenuation of the frequency range of interest. The filter was designed using different orders. Order 5 was selected since it is the closest to the ideal filter. This filter is applied in the frequency domain. Figure 3.9 (b) shows the average PSD of the profiles (700 profiles in total) before and after using the filter. As shown, the wavelengths lower than 0.5 mm are attenuated in the filtered profile.

- Micro-texture first decade component: band-pass filter

In this filter, all the frequencies between 2,000 and 20,000 cycles/m (wavelength from 0.05 to 0.5 mm) are allowed to “pass.” Frequencies out of this range are rejected, as

shown in Figure 3.9 (c). The low-cut and high-cut were selected such as the desired frequency range of interest was not attenuated at the limit values, the selected range was 1,500 and 20,000 cycles/m, respectively. A filter of order 5 was used. Figure 3.9 (d) shows the application of the filter in the frequency domain.

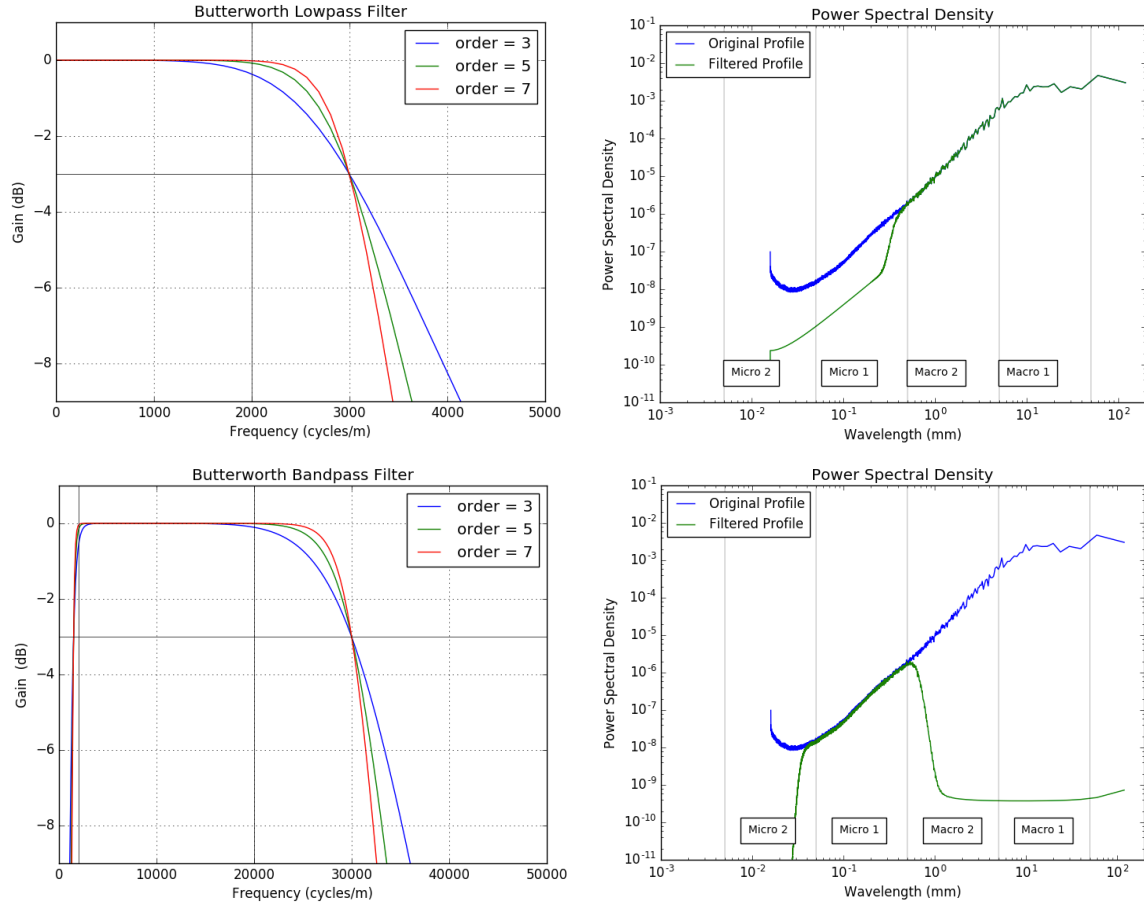


Figure 3.9: (a) Macro-texture low-pass filter, (b) average PSD of macro-texture filtered profiles, (c) micro-texture band-pass filter, and (d) average PSD of micro-texture filtered profiles.

After the filters are applied in the frequency domain, an inverse Fourier transform is applied to transform back to the space domain. The original profile is now decomposed

into two different components: macro-texture and micro-texture (first decade). Figure 3.10 shows the filtered profiles along with the original profile.

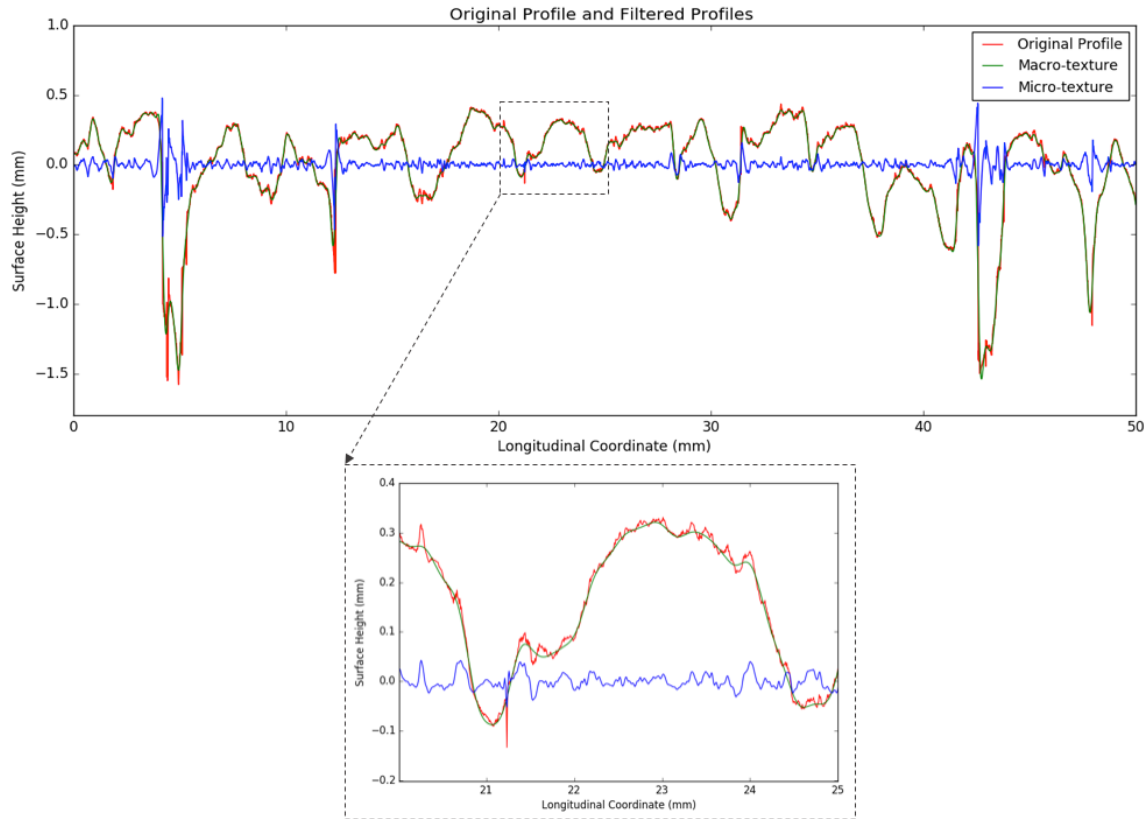


Figure 3.10: Original profile and filtered profiles.

The macro-texture component only includes the lower frequencies. All the high frequencies are in the micro-texture component. The advantage of this is that, since a low-pass filter is applied, it clears much of the noise remaining in the macro-texture component after the processing of the erroneous data. However, for the micro-texture components, this noise becomes highly notable. An additional processing was performed to the micro-texture profiles to account only for the micro-texture signal that represents the actual

pavement surface. It was found that micro-texture tends to present noisy signal in valleys area, even after the processing (Figure 3.11 a). Filtering amplitudes higher or lower than two height standard deviations showed that these alterations could be cleared. The filtered amplitudes were trimmed out from the profile, and the analysis was performed only with the segments of continuous profiles that do not include this high amplitude values. Figure 3.11 (b) shows the processed micro-texture profile.

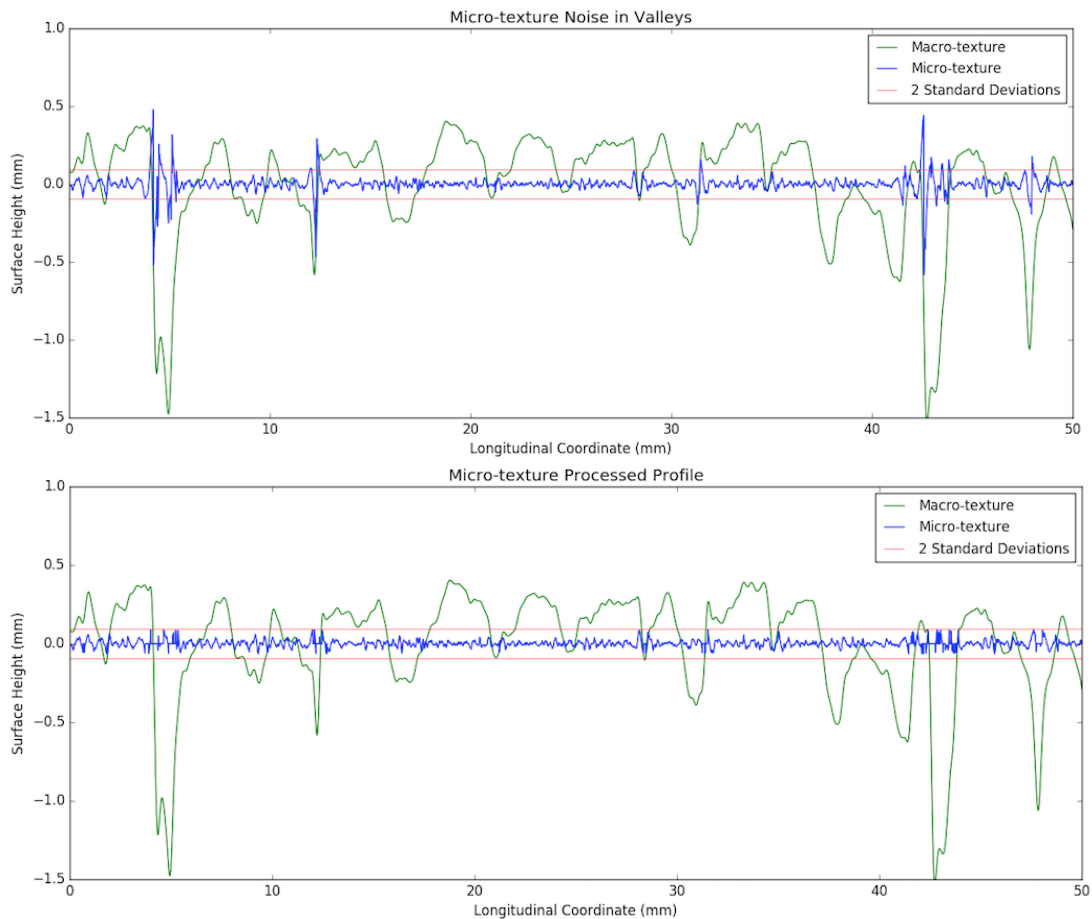


Figure 3.11: (a) Micro-texture noise in valleys, and (b) Micro-texture processed profile

Characterization of Pavement Texture

The macro-texture and micro-texture profiles are characterized using spatial parameters. For this study, the spatial parameters presented in Table 2.2 were obtained for both texture components. The parameters are reported as the mean and the median of the calculation of the parameters for all the segments obtained from the profiles. However, the analysis was based on the median values since the literature review suggested that this statistic is a better predictor for friction. The segments analyzed for the macro-texture have a baseline of 100 mm. While, the segment analyzed for micro-texture has a baseline of 1.0 mm, based on the literature review. Additionally, for the micro-texture, only the tire/pavement contact area is used. This contact or “active” area is estimated as the portion of the surface above the mean height of the profiles. Since the profiles were normalized with respect to the average height, the active area corresponds to the positive heights, as shown in Figure 3.12. The final profiles analyzed are shown in Figure 3.13.

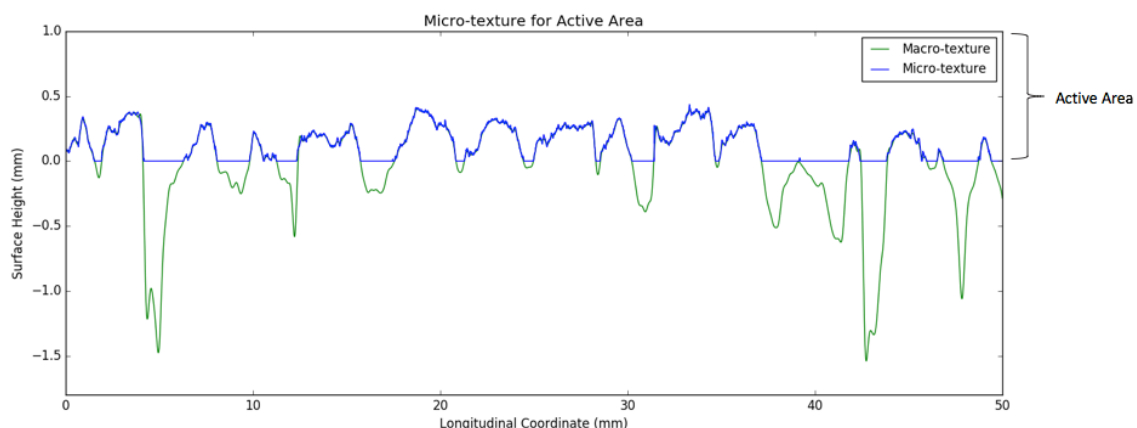


Figure 3.12: Micro-texture for the active area.

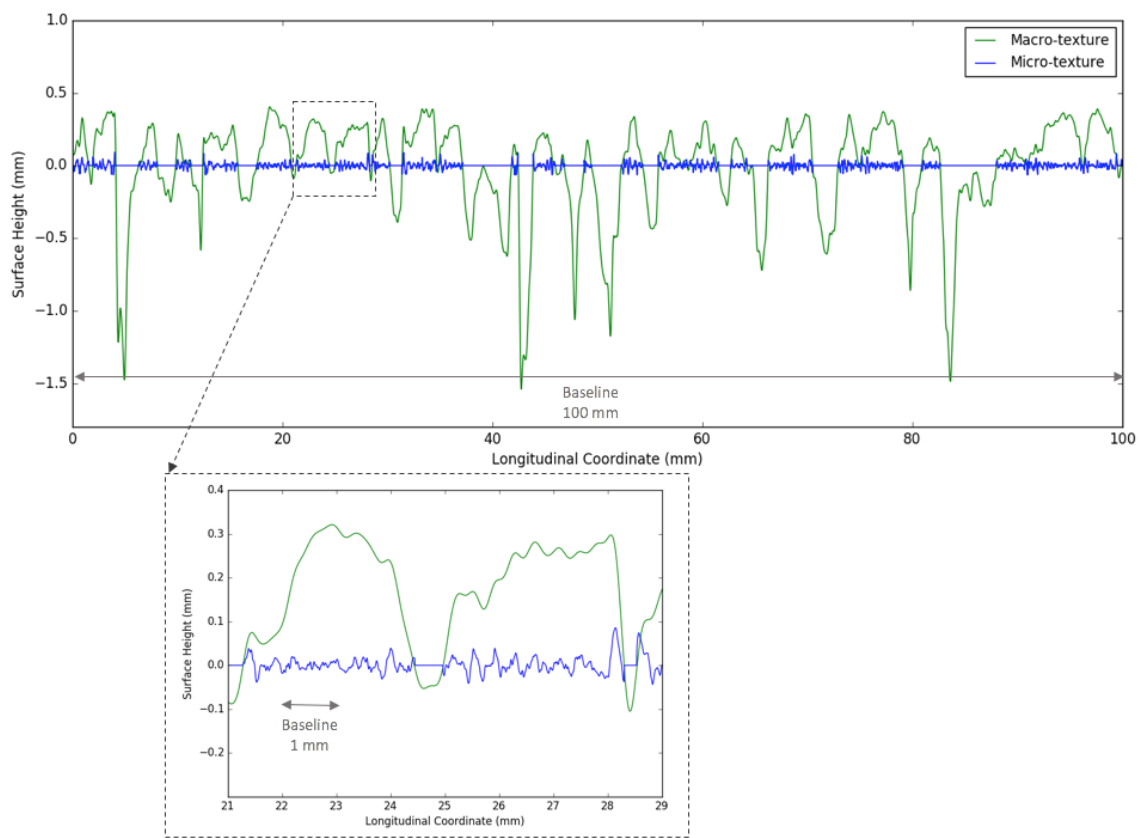


Figure 3.13: Final profiles.

Chapter 4: Friction and Texture Data Collection

This chapter covers the friction and texture data collection phase. This phase consisted of field measurements of friction and texture using a variety of test methods. The test sections included a broad range of friction coefficients and texture characteristics. The friction characterization tests included the British Pendulum test (BPT), the Dynamic Friction test (DFT), and the Micro GripTester. While, the texture characterization tests included the Sand Patch test, the Circular Track Meter (CTM) and the Line Laser Scanner (LLS), developed at the University of Texas at Austin.

The chapter consists of three sections. The first section provides a description of the experiment design and the experimental variables. The second section describes the characteristics of the test sections and the sample size. Finally, the third section describes the data collection procedure.

EXPERIMENT DESIGN

The experimental design considered different variables to account for a representative sample of the distinct possible friction and texture combinations. This design included surfaces with low and high friction coefficient values, as well as surfaces with a mixture of low and high micro- and macro- texture, as presented in Figure 4.1. The main experimental variables considered are listed below:

- Pavement type:
 - Flexible (asphalt) pavements
 - Surface treatments
 - Rigid (concrete) pavements
- Hot-mix asphalt (HMA) type:
 - Dense-graded
 - Open-graded

- Gap-graded
- Surface Treatment:
 - Chip Seal
 - Slurry Seal
 - Fog Seal
- Facility type:
 - Interstate highways (IH)
 - State highways (SH)
 - United State highways (US)
 - Farm to market (FM)

The variables included represented different material types, surface finishing, traffic level, and usage. Therefore, the experiment design covered a broad range of friction coefficients and surface texture.

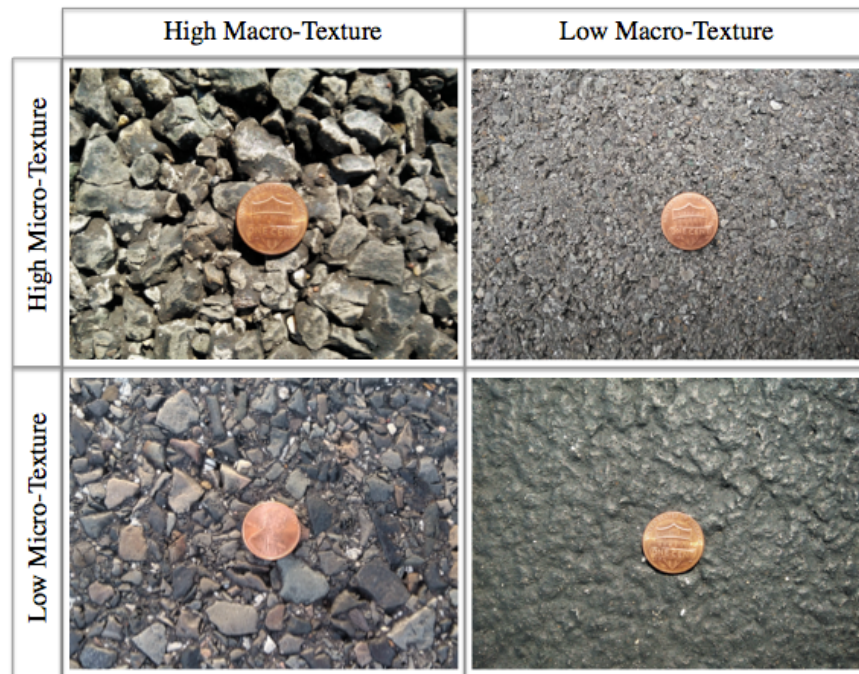


Figure 4.1: Surface combination of macro- and micro-texture.

TEST SECTIONS

The survey was performed on a total of nine in-service flexible pavements around Texas. Additionally, the study evaluated different surfaces at two parking areas in the Austin area, to account for a broader variety of surfaces. The flexible pavement sections correspond to various Texas Department of Transportation (TxDOT) districts: Atlanta, Austin, Brownwood, Bryan, Fort Worth, Houston, San Antonio, and Waco. The parking lots evaluated are located at the Pickle Research Center (PRC) of the University of Texas at Austin, and at the TxDOT Austin District Offices. Figure 4.2 shows the test sections location.

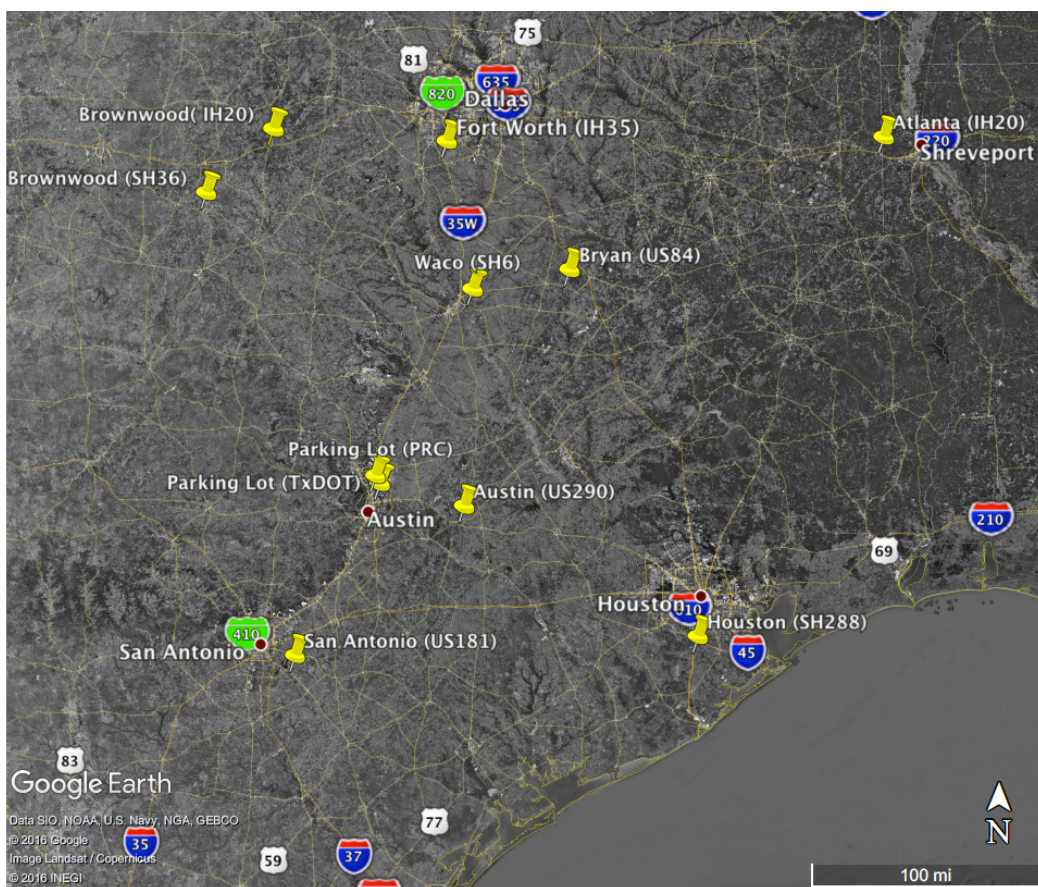


Figure 4.2: Location of test sections.

It was possible to select a total of thirty-six different surfaces from the tested sections, including twenty-nine flexible pavement surfaces and seven concrete sidewalks. Table 4.1 shows a list of the test sections, a description of the location, the surface type, and the number of samples.

The samples collected in the field sections correspond to measures of the right wheel path and the center of the outside lane. These measures were treated as two distinct samples because the studied sections presented significant differences in the trafficked and un-trafficked surfaces areas. As expected, the right wheel path showed more traffic damage in terms of rutting and raveling than the center of the lane.

Table 4.1: Test sections.

Field Section					
District	County	Highway	Direction	Description	Samples
Atlanta	Harrison	IH20	Eastbound	Stone Matrix Asphalt Type C (SMA-C)	2
Austin	Bastrop	US290	Eastbound	Porous Friction Course (PFC)	2
Brownwood	Eastland	IH20	Westbound	Dense-Graded Type D	2
Brownwood	Eastland	SH36	Westbound	Dense-Graded Type C	2
Bryan	Freestone	US84	Eastbound	Dense-Graded Type C	2
Fort Worth	Johnson	IH35	Southbound	Dense-Graded Type D	2
Houston	Brazoria	SH288	Southbound	Porous Friction Course (PFC)	2
San Antonio	Wilson	US181	Southbound	Novachip	2
Waco	McLean	SH6	Westbound	Porous Friction Course (PFC)	4
Parking Lots Sections					
District	County	Location		Description	Samples
Austin	Travis	Pickle Research Center (PRC), University of Texas at Austin		Dense-Graded Type D	2
				Dense-Graded Type F	2
				Fog Seal	1
				Concrete Sidewalk	3
	Austin	Texas Department of Transportation (TxDOT) Offices, North I-35		Dense-Graded Type C	2
				Thin Overlay Mix (TOM)	2
				Concrete Sidewalk	4

The flexible pavement sections include a variety of types of pavements and mixes. Table 4.2 summarize the sample size per surface type. Hot-mix asphalt (HMA) pavements are classified based on the aggregate gradation as dense-graded, open-graded and gap-graded. Additionally, they can be classified depending on its maximum aggregate size as type: A, B, C, D, and F. Where “A” corresponds to coarse mixes (high maximum aggregate size), and “F” to fine mixes (low maximum aggregate size) (TxDOT, 2014).

Table 4.2: Summary of samples per surface type.

Type		Samples		
Flexible Pavement	Hot Mix Asphalt (HMA)	Dense-Graded Type C	6	29
		Dense-Graded Type D	6	
		Dense-Graded Type F	2	
		Porous Friction Course (PFC)	8	
		Novachip	2	
		Stone Matrix Asphalt Type C (SMA-C)	2	
		Thin Overlay Mix (TOM)	2	
	Surface Treatment	Fog Seal	1	36
Concrete		Concrete Sidewalk	7	

A dense-graded mix has a continuously graded aggregate; its gradation curve does not present any abrupt slope change (see Figure 4.3). Dense-graded mixes have low void content and are considered to be impermeable. An open-graded mix is produced with a relative uniformed-sized aggregate with an absence of intermediate-sized particle, which allow a high void content. Therefore, open-graded, unlike dense-graded, are permeable. Examples of open graded mixes are Porous Fiction Course (PFC) mixes and Novachip mixes (see Figure 4.3).

Gap-graded mixes use an aggregate gradation with particles ranging from coarse to fine with some intermediate sizes missing or present in small amounts. The gradation curve

may have a “flat” region denoting the absence of a particle size or a steep slope denoting small quantities of these intermediate aggregate sizes. Stone-matrix asphalt (SMA) will be missing most intermediate sizes but have a relatively high proportion of fines (see Figure 4.3).

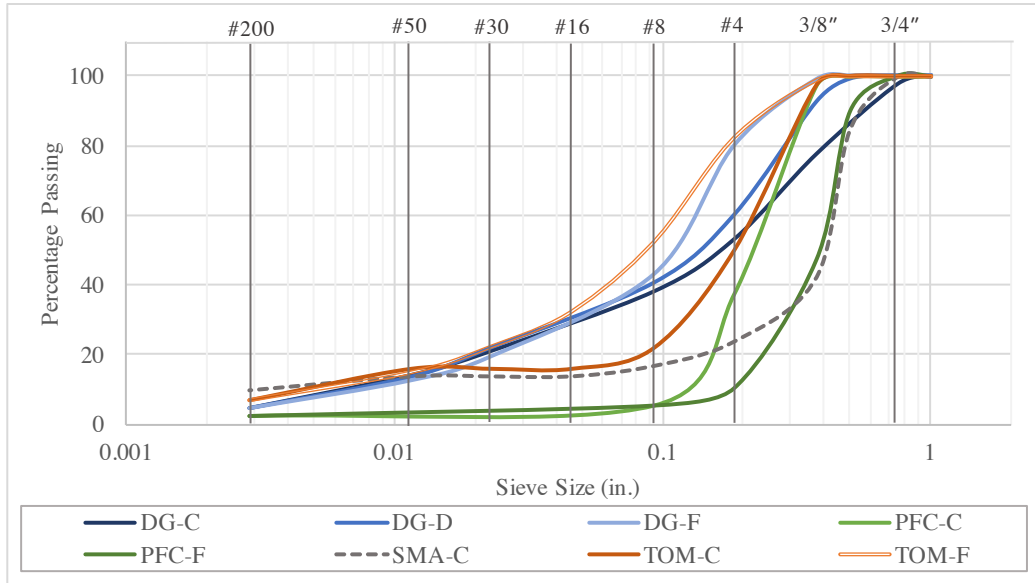


Figure 4.3: Typical gradation curves per asphalt surface type (based on TxDOT, 2014).

The *Standard Specifications for Construction and Maintenance of Highways, Streets, and Bridges* of the Texas Department of Transportation TxDOT (2014) includes a characterization for all the mixtures used in Texas. Based on these specifications, Table 4.3 presents a brief description of each type of asphalt pavement included in this study.

Table 4.3: Asphalt surface type description

	Dense-Graded Mixes - Item 341
	Produced with well or continuously graded aggregate. The minimum lift thickness is 2 in. (Type C), 1.5 in. (Type D), and 2.5 in. (Type F).
	Permeable Friction Course (PFC) - Item 342
	Composed of a compacted permeable mixture of aggregate, asphalt binder, and additives mixed hot in a mixing plant.
	Thin Bonded Friction Course (TBFC) or Novachip - Item 348
Hot Mix Asphalt (HMA)	Composed of a warm spray-applied polymer modified emulsion membrane followed with a compacted mixture of aggregate, asphalt binder, and additives mixed hot in a mixing plant.
	Stone Matrix Asphalt (SMA) - Item 346
	Composed of compacted mixture of aggregate, asphalt binder, and additives mixed hot in a mixing plant. SMA Type C has a minimum lift thickness of 2.25 in.
	Thin Overlay Mix (TOM) - Item 347
	Thin overlays are composed of a compacted mixture of aggregate and asphalt binder mixed hot in a mixing plant. A thin overlay mixture (TOM) is produced with a minimum lift thickness of 1/2 in. (Type F), and 3/4 in. (Type C).
Surface Treatment	Surface treatments are applied to restore texture and weatherproofing (including protection from oxidation), but do not contribute to improvement in ride or increased structural capacity.
	Fog Seal - Item 315
	Application of an emulsified asphalt and water mixture as an aggregate loss preventative or surface seal.

Definitions based on the *Standard Specifications for Construction and Maintenance of Highways, Streets, and Bridges* of the Texas Department of Transportation TxDOT, 2014.

DATA COLLECTION PROCEDURE

The data collection consisted of measurements of texture and friction to characterize each surface. The tests used to characterize friction are the BPT, DFT and the Micro GripTester. While for characterizing texture, the methods used include the sand patch test, the CTM, and the LLS. Table 4.4 summarizes the tests applied and the parameters obtained.

Table 4.4: Texture and friction tests and parameters.

Texture			
Test	Parameter		Texture Component
Sand Patch Test	Mean Texture Depth	MTD	Macro-Texture
Circular Track Meter (CTM)	Mean Profile Depth	MPD _{CTM}	Macro-Texture
	Root Mean Square	RMS _{CTM}	
Line Laser Scanner (LLS)	Mean Profile Depth	MPD _{LLS}	Macro-Texture
	Root Mean Square	RMS _{LLS}	
	Average Height	R _a	
	Maximum Height	R _z	
	Skewness	R _{sk}	
	Kurtosis	R _{ku}	
	Two Points Slope Variance	SV _{2pts}	
	Six Points Slope Variance	SV _{6pts}	Micro-Texture
	Mean Profile Depth	MPD _μ	
	Root Mean Square	RMS _μ	
	Average Height	R _a _μ	
	Maximum Height	R _z _μ	
	Skewness	R _{sk} _μ	
	Kurtosis	R _{ku} _μ	
	Two Points Slope Variance	SV _{2pts} _μ	
	Six Points Slope Variance	SV _{6pts} _μ	
Friction			
Test	Parameter		Speed (km/h)
British Pendulum Test (BPT)	British Pendulum Number	BPN	10
Micro GripTester	Grip Number	GN	2.5
Dynamic Friction Test (DFT)	Dynamic Friction Test Number	DFTN	10 to 80

The data collection in the field section consisted of measures of the right wheel path and the center of the outer lane. Three different measures were collected in each case, with a separation of approximately 15 m (Figure 4.4). The results reported consisted in the average of the three replicates. The data collection at the parking lots sections included one measure of the surface.

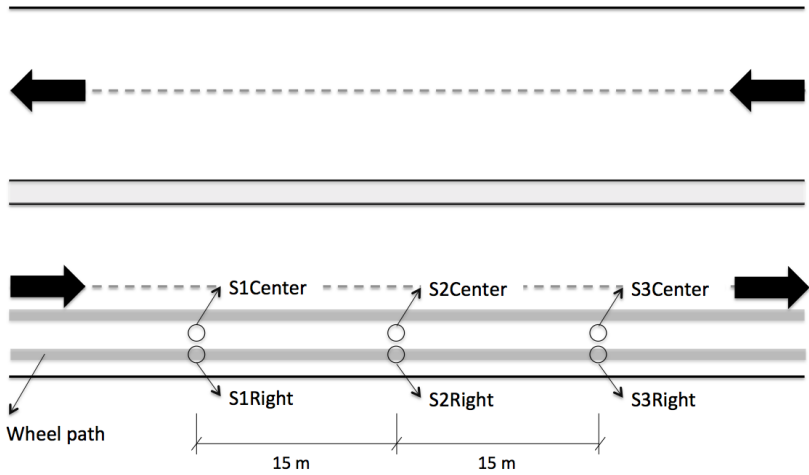


Figure 4.4: Field test sampling method.

The data collection process comprised different steps. The sequence is described below:

- 1) The first step included an inspection of the surface to select a dry and homogeneous surface, avoiding localized distresses and failures such as patches, cracks and joints.
- 2) After that, the surface was thoroughly cleaned using a soft-bristled brush to remove residue, debris or loose aggregate from the surface.
- 3) Then, CTM test was performed following the standard ASTM E2157.
- 4) Next, the LLS measurements were made in the same area covered by the CTM. The LLS was located in the sectors A and E of the CTM circumference, corresponding to the traffic direction (Figure 4.5). The results reported by the LLS consisted on the average of the two measures (sector A and E).
- 5) The DFT (ASTM E1911) was then performed in the same area of the CTM measure, as recommended by the standard.
- 6) The BPT (ASTM 303) and the Sand Patch (ASTM E965) test were done in the area adjacent to the CTM and DFT spot, to keep the measurements in homogenous areas.

7) Finally, the Micro GripTester was run in the traffic direction, over a longitudinal distance of 30 m, including the selected sampling spot.

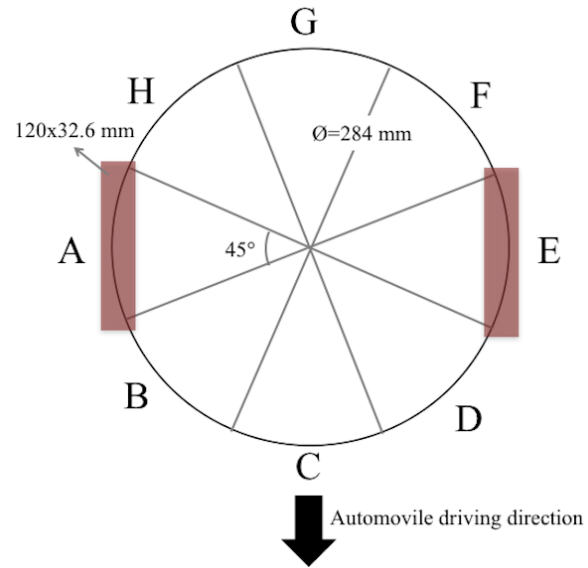


Figure 4.5: Location of the Line Laser Scanner (LLS).

Appendix B presents the individual sample description including a value of friction (BPN), texture (MPD from the CTM), location, and a picture of the surface.

Chapter 5: Analysis of Friction and Texture Measurements

This chapter presents the analysis of the results obtained for friction and texture measurements. It consists of three sections. The first section presents results of the distinct friction tests. The second section shows results for texture test methods including the Line Laser Scanner (LSS). The third section includes the analysis of the friction as a function of texture.

FRICITION

Three different friction tests were performed in this study: the British Pendulum Test (BPT), the Dynamic Friction Test (DFT), and the Micro GripTester. These methods use different principles. The BPT and the DFT used the slider principle, while the Micro GripTester uses the longitudinal friction coefficient (LFC) principle. The main difference between these tests is the speed at which the friction measurement is taken. The DFT test has a speed of 10 km/h (Henry, 2000), and the Micro GripTester has a speed of 2.5 km/h; while the DFT captures friction information in a speed range from 10 km/h to 80 km/h.

It is well known that the friction coefficient decreases as the speed increases. However, the results obtained from the DFT were not so consistent with this principle. Some sections showed an increase of friction with increasing speed, as illustrated in Figure 5.1. The figure indicates that the porous friction course (PFC) sample have a directly proportional relation between speed and friction. In contrast, the thin overlay mix (TOM) and the dense-graded Type C (DG-C) presented an inversely proportional relation. Furthermore, the relationship of increasing friction with texture was not found in all the PFC samples.

The results obtained from the DFT can be used to represent the surface friction at different speeds. Three speeds were selected to describe the DFT number (DFTN): 20

(DFT20), 40 (DFT40), and 60 km/h (DFT60). These parameters were estimated as the average DFTN of the selected speed and a range of DFTN values within ± 5 km/h. For instance, DFT20 is obtained as the average of DFTN values from a range of speed of 15 km/h to 25 km/h. Using the average value instead of the punctual value allows a more robust analysis and increased confidence in the obtained results.

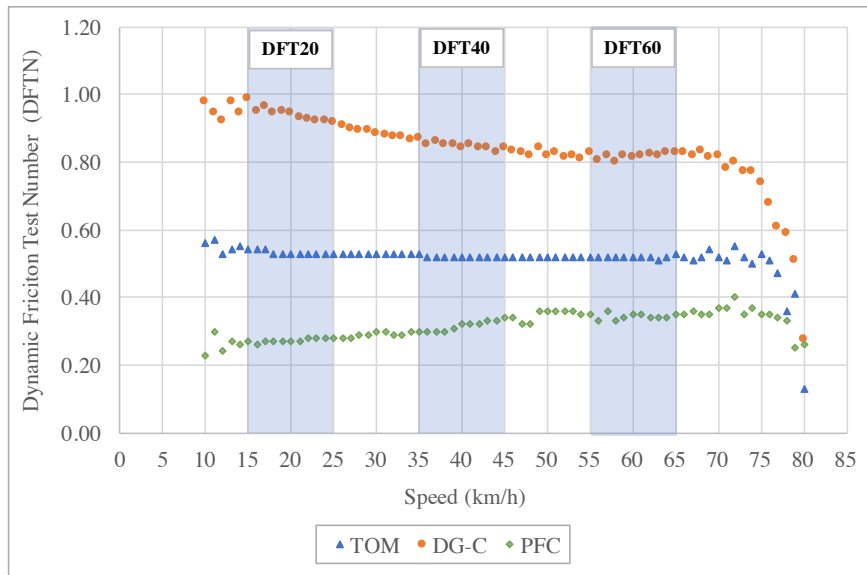


Figure 5.1: Dynamic Friction Test (DFT) results.

The BPT results were compared with the DFT results. Figure 5.2 shows charts of the relation of the BPT number (BPN) with the DFT20, DFT40, and DFT60, respectively, for the thirty-six samples studied. The graphs includes a simple linear regression (SLR) line (an approximate linear relationship between Y and X values) and the coefficient of determination (R^2). The R^2 is interpreted as the proportion of observed changes in Y values (BPN in this case) that can be explained by changes in the X values. The graphs show the higher R^2 with the relation of BPN and DFT60, and the lowest R^2 with the relation of BPN and DFT20. This means that high-speed DFTN values correlate better with the BPN than

low-speed DFTN values. This result is contrary to the expected relationship since BPT is performed at low speed (10 km/h). However, in general, BPT results presented high correlation with DFT results, with the lowest R^2 of 69 % and the highest of 82%.

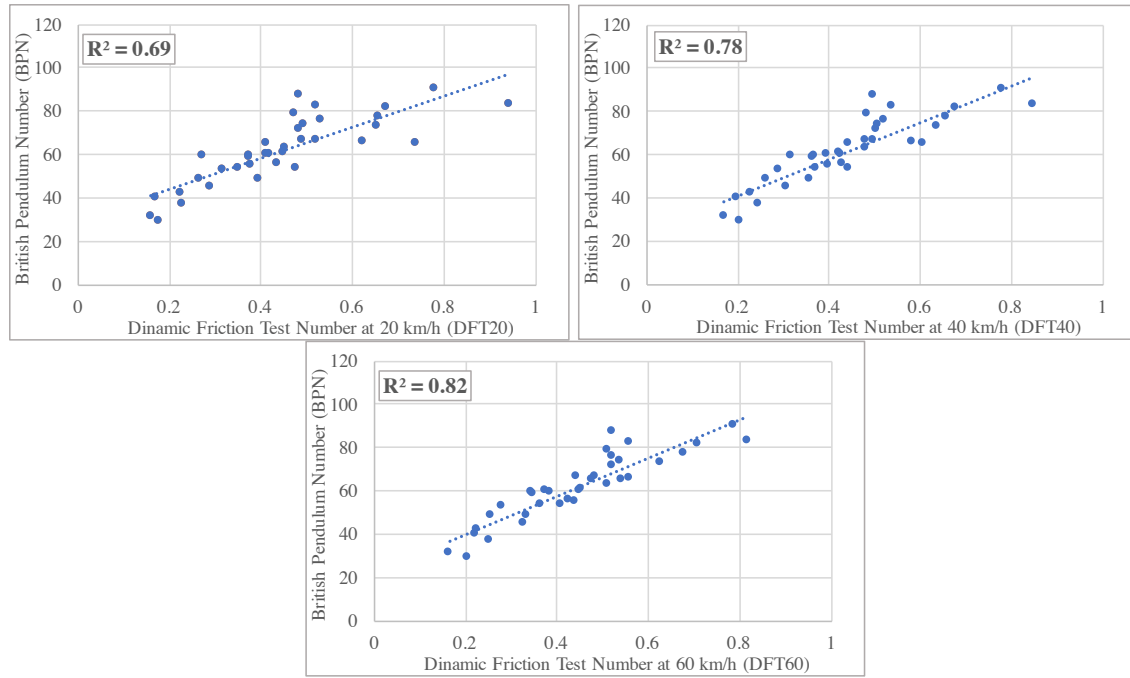


Figure 5.2: British Pendulum Test (BPT) and Dynamic Friction Test (DFT) results.

The Micro GripTester is a continuous friction measuring equipment, therefore, the results consisted of a series of friction measures, expressed as Grip Numbers (GN), along the distance evaluated. The GN for each sample was obtained as the average of the GN measures along the evaluated distance.

The Micro GripTester results were compared with the DFT results. Figure 5.3 presents graphs of the relation between GN and DFT20, DFT40, and DFT60, respectively. Based on the R^2 , GN has the greater correlation with DFT60, and the lowest with DFT20. This means that GN correlates better with DFNs as the DFT test-speed increases. This

result is similar to the correlation found between BPN and DFTN. The Micro GripTester is performed at a low speed (2.5 km/h), for this reason, a better correlation with low-speed DFTNs was expected. In general, the coefficient of correlations found between GN and DFTNs are high, 69 % the smallest, and 79 % the highest.

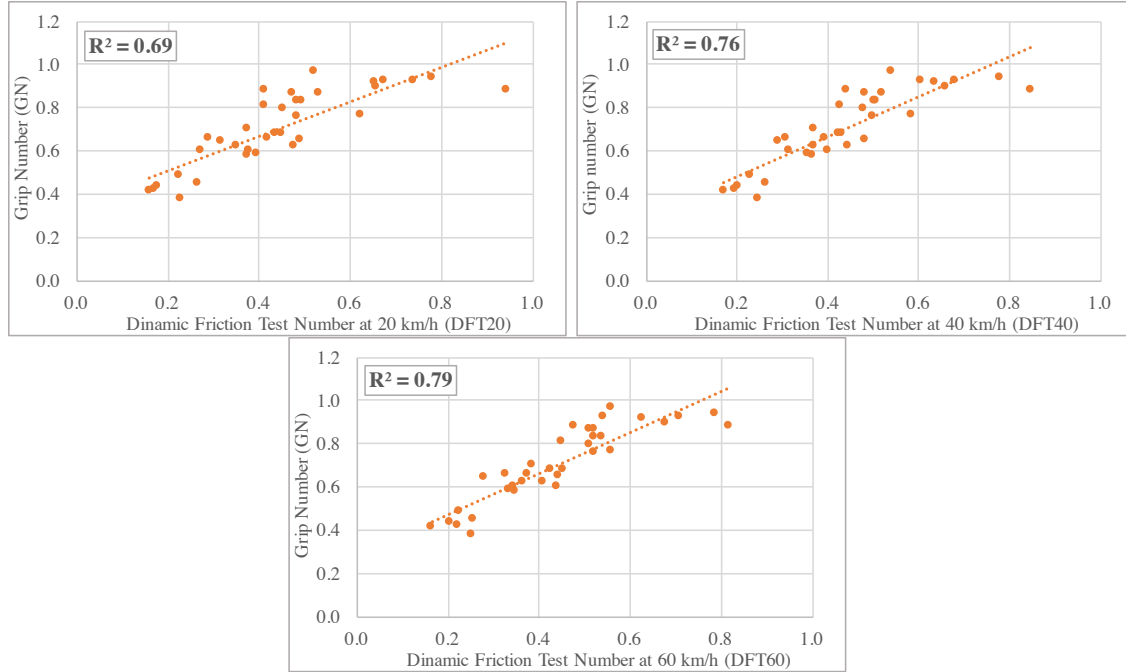


Figure 5.3: Micro GripTester and Dynamic Friction Test (DFT) results.

The Micro GripTester results were also compared directly with the BPT. The R^2 between GN and BPT is 79%, see Figure 5.4. This result is comparable to the R^2 found between GN and DFT60 (79%) and can be considered as an indicator of high correlation between GN and BPN.

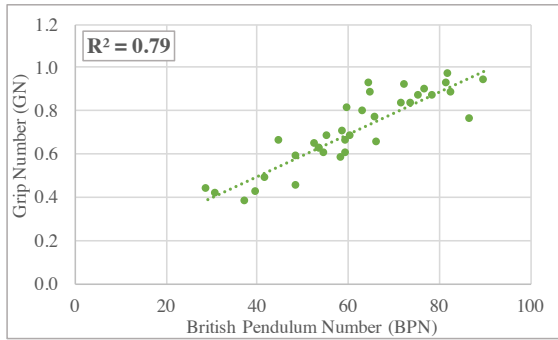


Figure 5.4: Micro GripTester and British Pendulum Test (BPT) results.

TEXTURE

Three test methods were used to characterize texture: the Sand Patch test, the Circular Track Meter (CTM), and the LLS. Several different parameters that characterize the texture are obtained using these techniques (Table 4.4). The Mean Texture Depth (MTD) is obtained using the sand patch test. The CTM provides values of Mean Profile Depth (MPD), and the root mean square (RMS) for the macro-texture component. The LSS also provides values of MPD and RMS for macro-texture, additionally, it provides values of MPD and RMS for the micro-texture component. The LSS also provides the average height (R_a), maximum height (R_z), skewness (R_{sk}), kurtosis (R_{ku}), and slope variance two points (SV_{2pts}), and six points (SV_{6pts}), for both macro- and micro-texture components (Table 4.4).

Sand Patch Test and Circular Track Meter (CTM)

The results of MPD from the CTM were compared with the MTD from the Sand Patch test. The MTD is obtained based on a volumetric technique as it uses a surface (3D) covered by sand, while, the MPD is obtained based on linear profiles (2D). However, these parameters showed high correlation. Figure 5.5 presents MTD as a function of MPD. The R^2 is 94% which is considered high. The regression equation is also provided in the graph.

This equation can be used to estimate texture depth (ETD), which is the MTD obtained from the MPD relation.

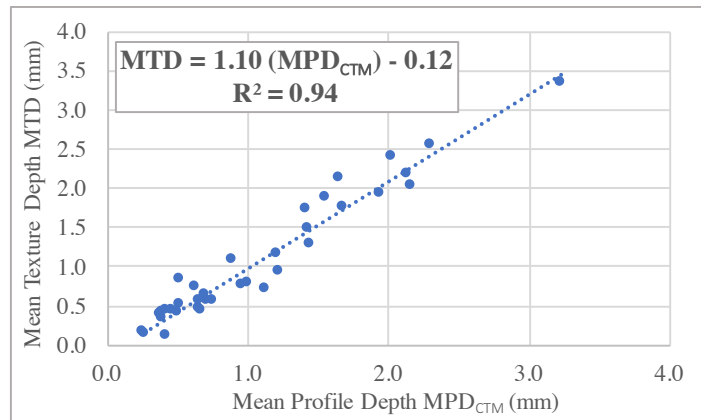


Figure 5.5: Mean texture depth (MTD) as a function of the mean profile depth (MPD_{CTM}).

The CTM estimates the MPD (and the RMS) based on the average MPD (or RMS) value of the eight segments that compose the CTM circumference (Figure 2.6 b). The standard deviation of the MPD and RMS values are obtained to quantify the variability. The standard deviation is a measure of the dispersion of a set of data from its mean: the higher the dispersion, the higher the standard deviation. Figure 5.6 shows the graphs of standard deviation as a function of MPD (a) and RMS (b) values. Based on the figure, higher standard deviations are found for MPD values above 1.5 mm (dashed line limit). Additionally, the RMS values greater than 0.75 mm present high standard deviations. Thus, the results show that high values of MPD and RMS (measured with the CTM) present greater variability than low values.

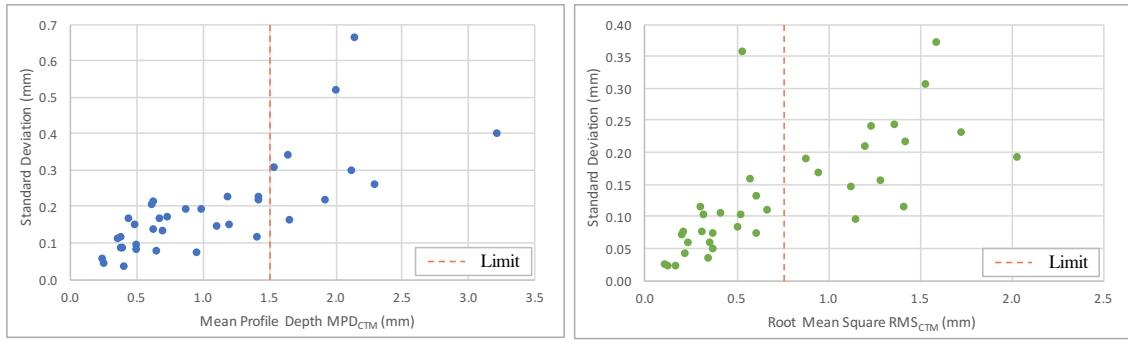


Figure 5.6: (a) Standard deviation of the mean profile depth (MPD_{CTM}), and (b) standard deviation of the root mean square (RMS_{CTM})

Line Laser Scanner (LLS)

The LLS results for the MPD and RMS (macro-texture) are compared with the MPD and RMS results obtained from the CTM. Figure 5.7 presents the MPD_{LLS} as a function of MPD_{CTM} (a) and RMS_{LLS} as a function of RMS_{CTM} (b). The figure shows that the MPDs have an R^2 of 96%, and the RMSs of 95%. These coefficients of determination are considered high, meaning that the results from the LLS at a macro-texture level are highly correlated with the CTM results.

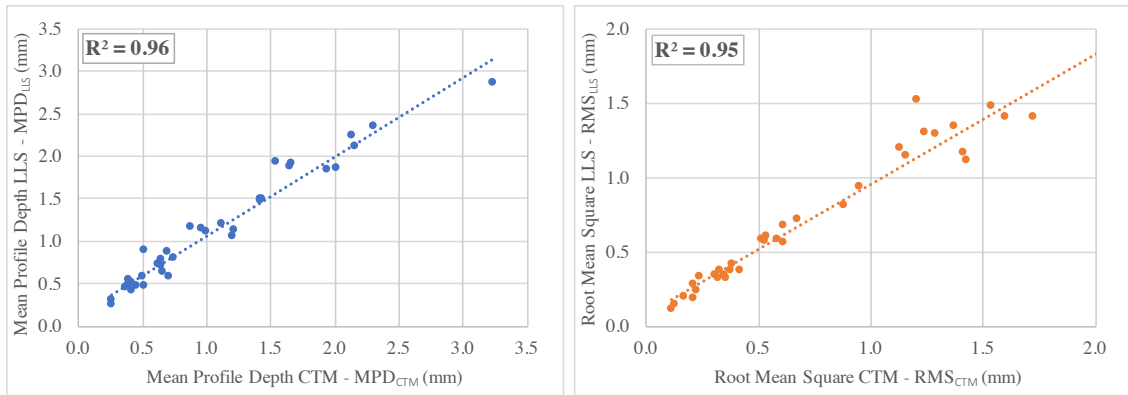


Figure 5.7: (a) Mean profile depth (MPD) from the CTM and from the LLS, and (b) root mean square (RMS) from the CTM and from the LLS.

FRICITION AS A FUNCTION OF TEXTURE

The friction information collected was modeled as a function of texture parameters. The texture characterization used for the modeling purpose was based on the LSS results. Several parameters were considered for both macro- and micro-texture components using this method.

The friction results from the BPT were modeled as a function of the texture parameter MPD macro-texture (MPD_{LSS}) and MPD micro-texture ($MPD\mu$). Figure 5.8 presents shows the friction and macro-texture relationship. Figure 5.8 (a) shows the simple linear regression (SLR) line and the corresponding R^2 . It can be noted that the SLR model indicates a low correlation between BPT and MPD_{LSS} , with an R^2 of 5% and a negative slope. The negative slope implies that macro-texture has a negative influence on friction, i.e. the greater the macro-texture, the lower the friction. Based on the theory and previous research efforts described in the literature review, it is widely recognized that the surface texture exerts a positive effect on friction. This fact suggests that, when pooling all data, SLR analysis is not appropriate to model friction as a function of texture data only. Figure 5.8 (b) presents the information including the description per every surface type evaluated. This categorization allows the determination of positive tendencies between BPN and MPD_{LSS} when accounting for the pavement type.

Figure 5.9 presents the relationship between friction and micro-texture. Figure 5.9 (a) shows the SLR line and the R^2 , while Figure 5.9 (b) presents the information including the surface type. The R^2 found is close to zero. Similar to the friction and macro-texture relationship, when pooling all data, the SLR analysis was not appropriate to model friction and micro-texture either. However, the disaggregation per surface type shows positive relations.

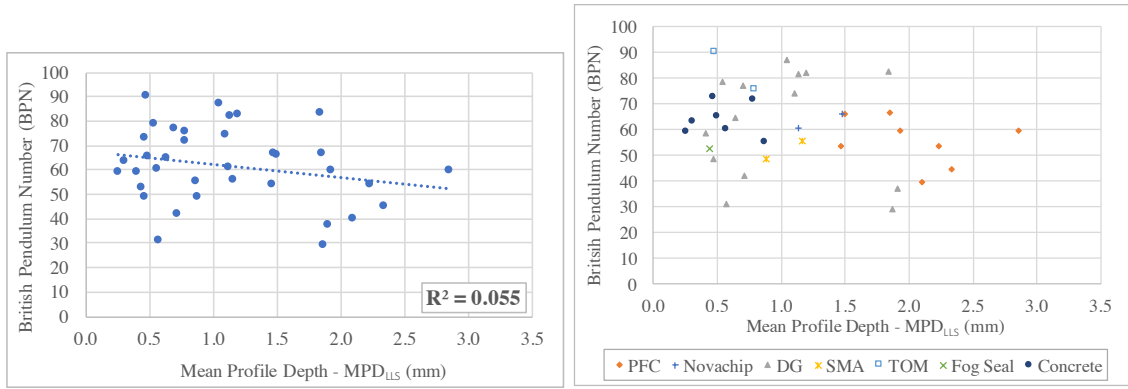


Figure 5.8: (a) British pendulum number (BPN) as a function of the mean profile depth (MPD_{LLS}), and its (b) description per surface type.

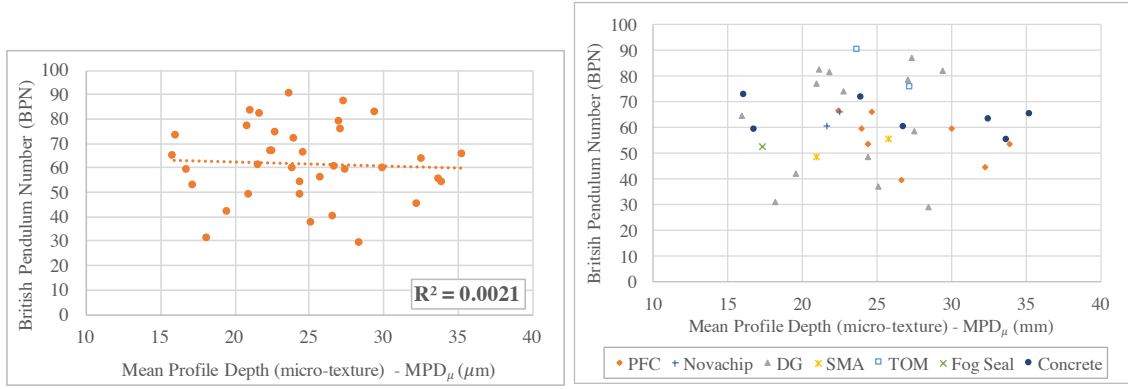


Figure 5.9: (a) British pendulum number (BPN) as a function of the mean profile depth for the micro-texture component (MPD_μ), and its (b) description per surface type.

The previous discussion showed that SLR analysis cannot be used for the purpose of modeling friction based on the available texture data. A better relation is “visually” found when accounting for the surface type. This fact suggests that it is necessary to include an additional dimension for the analysis. For this reason, a panel data analysis was proposed. A panel (or longitudinal) data refers to multi-dimensional data including information of multiple phenomena. The panel data analysis incorporates the use of multiple regression analysis (MRA), which allows the inclusion of the surface type information in the friction model.

The various tested sections were grouped using the information showed in Figures 5.8 (b) and 5.9 (b). The concrete sidewalk data were not used in this part of the analysis because there was no further information about the surface. Additionally, the TOM and fog seal samples were not incorporated either due to the low number of samples available. Thus, the analysis focused only on the different types of hot-mix asphalt (HMA) collected (refer to Chapter 4 for a detailed description of the HMA types).

The different HMA types were grouped based on the observed tendency between the BPN and MPD_{LLS} . Figure 5.10 (a) shows the chart of BPN as a function of MPD_{LLS} . The dashed line represents an “arbitrary” limit separating HMA types with a similar positive relation. Two different clusters were observed for the PFC data. The PFC pavements tend to present a variety of surface differences depending on the type of asphalt used, age, weather, maintenance, among other factors. The two observed PFC clusters were separated as PFC_1 and PFC_2 , since they presented different behavior, although there is no further information about the characteristics of the surfaces, two types of PFC mixtures are used in Texas, one contains rubber and the other does not. The Novachip mix is included with the PFC_2 group since it is considered a porous friction course.

The dense-graded mixes were separated into two groups based on the maximum aggregate size. The first group contains the finer mixes Type D and F (finer), the second group is the coarse mix Type C (coarser). This group consisted of two samples with values away from the dense-graded cluster group, see Figure 5.10 (a) marked as “Brownwood SH36”. The values were considered as outliers and were not included in the analysis. The final sample size used was 24. There are five different HMA groups:

- Type 1: Porous Friction Course 2 (PFC_2) and Novachip
- Type 2: Stone matrix asphalt type C (SMA-C)

- Type 3: Dense-graded type C (DG-C)
- Type 4: Dense-graded types D and F (DG-D&F)
- Type 5: Porous Friction Course 1 (PFC₁)

The correlation between BPN and MPD_{LLS} for the identified groups is presented in Figure 5.10 (b). The separation of the groups allowed greater coefficients of determination and the slopes obtained for the groups are all positive, indicating a positive relation between friction and texture.

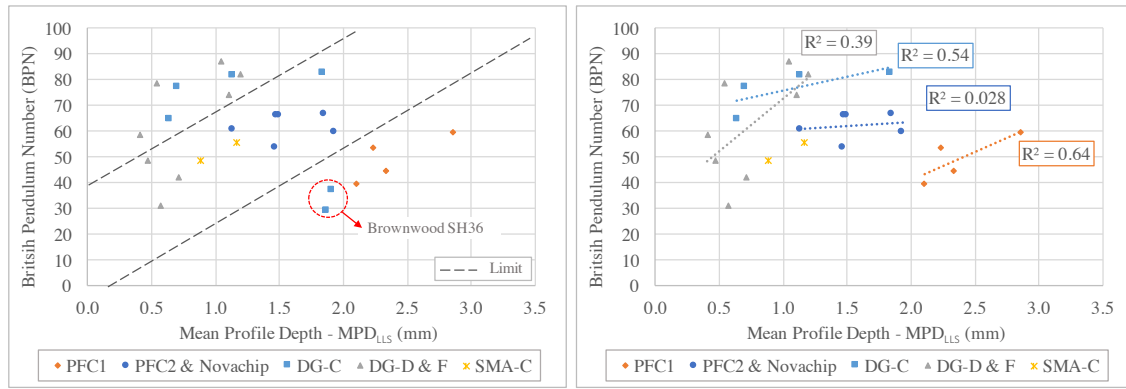


Figure 5.10: BPN as a function of MPD_{LLS} per flexible pavement type (a) limits, and (b) proposed pavement types groups.

The friction and micro-texture relation was also studied using the proposed groups. Figure 5.11 (a) shows the “arbitrary” limit separating HMA types and the outlier value for “Brownwood SH36” found previously. Additionally, Figure 5.11 (b) shows the correlation between BPN and MPD μ per group. The figure shows the same tendency found for the friction and macro-texture when separating by the HMA types. Therefore, the analysis was based on the texture data and the five HMA groups selected.

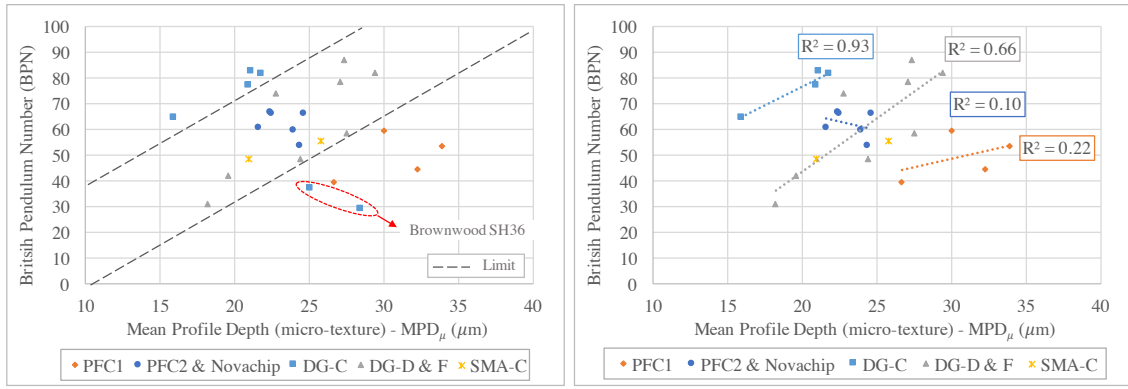


Figure 5.11: BPN as a function of $\text{MPD}\mu$ per flexible pavement type (a) limits, and (b) proposed pavement types groups.

The proposed analysis includes the used MRA to model friction using texture information and HMA types. The HMA types are categorical (or qualitative) variables. Thus, they are incorporated into the models using a dummy or indicator variable whose possible values are 0 and 1. The variable takes a value of one when the sample belongs to the proposed HMA group, and a value of zero otherwise.

Three friction models were proposed using texture and HMA types, as shown in Equations 5.1, 5.2 and 5.3. These models were considered as first-order with no interaction models, which are the most straightforward generalization of the SLR. The slope is constant for all the HMA types, and the types are represented as parallel lines. Although, it is important to mention that Figures 5.10 (b) and 5.11 (b) showed that the slopes were different. The constant slope was a reasonable assumption of the suggested models.

The Model 1 considers only the macro-texture and HMA-type information for the independent variables X 's. Therefore, the result of the coefficient β_{Macro} indicates the influence of the macro-texture over the friction measure, represented by the dependent variable $Y_{Friction}$. Similarly, for the Model 2, the β_{Micro} specifies the impact of the micro-texture over the friction test. The Model 3 includes the values for both macro- and micro-

texture. In this case, the model denotes the effect over the friction measure prediction when incorporating the information of the two texture components studied.

The coefficient values of the dummy HMA-type variables indicate the difference between the friction of the evaluated type with respect to the friction of type 5, when using a fixed texture-parameter value. Figure 5.12 shows a representation of the Model 1 and Model 2 that illustrates the previous statement. The model 3 is not represented graphically because it has an additional dimension.

Model 1:

$$Y_{Friction} = \beta_0 + \beta_{Macro}X_{Macro} + \beta_1X_{Type\ 1} + \beta_2X_{Type\ 2} + \beta_3X_{Type\ 3} + \beta_4X_{Type\ 4} \quad (5.1)$$

Model 2:

$$Y_{Friction} = \beta_0 + \beta_{Micro}X_{Micro} + X_{Type\ 1} + \beta_2X_{Type\ 2} + \beta_3X_{Type\ 3} + \beta_4X_{Type\ 4} \quad (5.2)$$

Model 3:

$$Y_{Friction} = \beta_0 + \beta_{Macro}X_{Macro} + \beta_{Micro}X_{Micro} + \beta_2X_{Type\ 1} + \beta_2X_{Type\ 2} + \beta_3X_{Type\ 3} + \beta_4X_{Type\ 4} \quad (5.3)$$

Where,

$Y_{Friction}$ = friction measure obtained using a test method

β_0 = intersect of the model for HMA type 5 with the friction axis

β_{Macro} = influence of the macro-texture parameter in the friction measure

X_{Macro} = parameter X for the macro-texture component

β_{Micro} = influence of the micro-texture parameter in the friction measure

X_{Micro} = parameter X for the micro-texture component

β_1 = difference in friction between the HMA type 1 and the type 5

$X_{Type\ 1}$ = dummy variable for HMA type 1

β_2 = difference in friction between the HMA type 2 and the type 5

$X_{Type\ 2}$ = dummy variable for HMA type 2

β_3 = difference in friction between the HMA type 3 and the type 5

$X_{Type\ 3}$ = dummy variable for HMA type 3

β_4 = difference in friction between the HMA type 4 and the type 5

$X_{Type\ 4}$ = dummy variable for HMA type 4

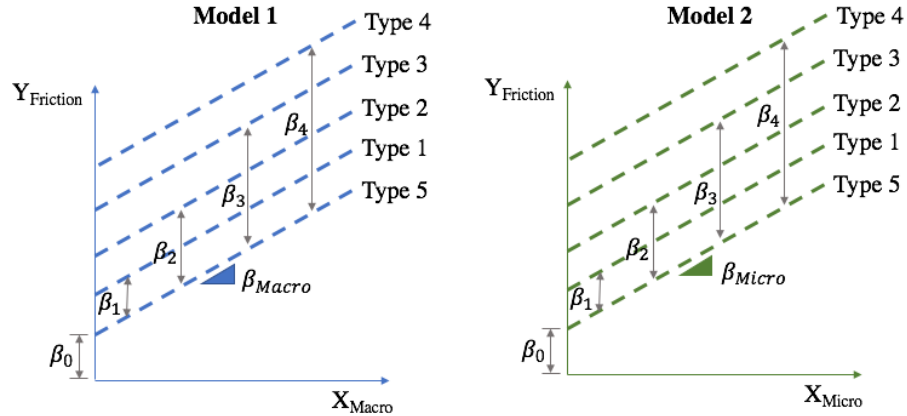


Figure 5.12: Representation of the (a) Model 1, and (b) Model 2.

A total of 120 models were studied. The three models are applied using the five friction measures obtained from the tests methods as the dependent variable:

- British Pendulum number (BPN)
- Grip number (GN)
- Dynamic Friction Test number at 20 km/h (DFT20), 40 km/h (DFT40), and 60 km/h (DFT60).

Additionally, the texture measures include the results obtained from the LLS for both macro-texture (X_{Macro}), and micro-texture (X_{Micro}). The texture information contained in the models corresponds to the eight parameters obtained from the LLS for each texture component:

- Mean profile depth (MPD)
- Root mean square (RMS)
- Average height (R_a)
- Maximum height (R_z)
- Skewness (R_{sk})

- Kurtosis (R_{ku})
- Slope variance two points (SV_{2pts}), and six points (SV_{6pts}).

The models were obtained using Microsoft Excel 2016. A two-tailed hypothesis test was used to determine if the independent variables included in the models (texture and HMA type) had a statistically significant influence on friction. The confidence level selected was 95%, i.e. a significance level, $\alpha = 0.05$.

The null hypothesis (H_0) established that the coefficient (β_i) was equal to zero, meaning that the corresponding independent variable did not have any impact on the friction. The alternative hypothesis (H_a) is that the coefficient is distinct from zero, which means that the variable did have a statistically significant influence on friction. The null hypothesis needs to be rejected to be able to conclude that the coefficients are different than zero and that the corresponding independent variable has a statistically significant influence on the friction with a confidence level of 95%.

$$H_0: \beta_i = 0 \quad (5.4)$$

$$H_a: \beta_i \neq 0 \quad (5.5)$$

Where,

i =Macro, Micro, Type 1, Type 2, Type 3, and Type 4

Information about the t-static and p-value for each coefficient value were analyzed for the hypothesis testing. These two indicators determine whether to reject or not the null hypothesis. The t-statistic is a ratio of the departure of an estimated parameter from its notional value and its standard error. The p-value (or observed significance level) represents the probability, assuming that the null hypothesis is true, of obtaining a value of the t-statistic at least as contradictory to the null hypothesis as the value calculated from the available sample.

The p-value is used to make the final decision of rejecting or not the null hypothesis. It is compared with the significance level (α), which is the probability of rejecting the null

hypothesis when true (type I error). The p-values must be lower than $\alpha = 0.05$ to reject the null hypothesis.

The SLR models use the coefficient of determination (R^2), as a comparison measure of which model has a greater correlation between Y and X values, since it measures how close the data are to the fitted regression line. However, the R^2 is not an appropriate parameter to compare MRA models, because its value increases every time an additional predictor is added to the model. The coefficient of multiple determination (R_{adj}^2) adjusts the R^2 for the number of predictor variables in the model. Thus, this indicator is more appropriate to compared models with a different number of independent variables. For this reason, the R_{adj}^2 was obtained for the models analyzed in this study.

The first parameter studied is the MPD. Table 5.1 shows the results for the t-statistic and p-value for the models' coefficients, and the R_{adj}^2 for the friction models. The shaded t-statistic and p-values represent the conditions of failing to reject the null hypothesis. The results using BPN as the predictor variable show that Model 1 suggests that macro-texture has a statistical influence on friction, based on the t-statistic and p-value for β_{Macro} . Similarly, Model 2 suggests that micro-texture has an influence on friction. The results for Model 3 show that both macro- and micro-texture affect friction and that by including both components to the model, the R_{adj}^2 increased compared to Models 1 and 2, where only the individual effects were incorporated. The same results are found for the friction parameters obtained from the DFT (DFT20, DFT40, and DFT60). The greater R_{adj}^2 obtained is 83%, corresponded to Model 3 when using DFT40 as the dependent variable.

The results from the GN from Table 5.1 show that using macro-texture information (Model 1), the null hypothesis cannot be rejected for all the variables included. Therefore, the model suggests that the friction cannot be predicted using macro-texture information

for the Micro GripTester. However, the Model 2 shows that the micro-texture has an effect on GN. The results show that the friction prediction is not improved by incorporating both macro- and micro-texture information since the Model 3 presents a similar R_{adj}^2 than Model 2. Therefore, the Model 2 is the most appropriate for the Micro GripTester. The results can be related to the speed of the test (2.5 km/h). The micro-texture influence is greater at low speeds and the macro-texture at high speeds. It is possible that the test is not capturing macro-texture influence due to the low speed.

Table 5.1: Friction Models Using Mean Profile Depth (MPD) as a Texture Parameter

Y_{Friction}			Texture Parameter: <i>Mean Texture Depth (MPD)</i> *					
			β_{Macro}	β_{Micro}	β_1	β_2	β_3	β_4
British Pendulum Number (BPN)	Model 1	t-stat	2.53		2.86	1.97	3.97	3.09
		p-value	0.021		0.010	0.064	0.001	0.006
		R_{adj}^2			0.357			
	Model 2	t-stat		4.40	4.36	2.57	5.87	4.38
		p-value		0.000	0.000	0.019	0.000	0.000
		R_{adj}^2			0.579			
	Model 3	t-stat	2.14	4.00	5.23	3.53	6.61	4.65
		p-value	0.047	0.001	0.000	0.003	0.000	0.000
		R_{adj}^2			0.649			
Grip Number (GN)	Model 1	t-stat	1.68		1.94	1.55	3.48	2.02
		p-value	0.111		0.069	0.139	0.003	0.059
		R_{adj}^2			0.339			
	Model 2	t-stat		3.47	3.21	2.34	5.36	3.17
		p-value		0.003	0.005	0.032	0.000	0.006
		R_{adj}^2			0.549			
	Model 3	t-stat	1.01	2.99	3.32	2.48	5.11	2.74
		p-value	0.326	0.009	0.004	0.025	0.000	0.014
		R_{adj}^2			0.549			
Dynamic Friction Tests at 20 km/h (DFT20)	Model 1	t-stat	2.61		4.47	3.09	6.55	3.14
		p-value	0.018		0.000	0.006	0.000	0.006
		R_{adj}^2			0.728			
	Model 2	t-stat		3.48	5.30	3.47	7.78	3.62
		p-value		0.003	0.000	0.003	0.000	0.002
		R_{adj}^2			0.776			
	Model 3	t-stat	3.03	2.14	6.17	4.33	8.40	4.15
		p-value	0.008	0.047	0.000	0.000	0.000	0.001
		R_{adj}^2			0.813			
Dynamic Friction Tests at 40 km/h (DFT40)	Model 1	t-stat	2.89		4.11	2.91	6.20	3.26
		p-value	0.010		0.001	0.009	0.000	0.004
		R_{adj}^2			0.682			
	Model 2	t-stat		4.40	5.51	3.54	8.19	4.06
		p-value		0.000	0.000	0.002	0.000	0.001
		R_{adj}^2			0.775			
	Model 3	t-stat	2.62	4.10	6.86	4.84	9.43	4.96
		p-value	0.018	0.001	0.000	0.000	0.000	0.000
		R_{adj}^2			0.830			
Dynamic Friction Tests at 60 km/h (DFT60)	Model 1	t-stat	2.80		3.45	2.52	5.54	3.04
		p-value	0.012		0.003	0.021	0.000	0.007
		R_{adj}^2			0.613			
	Model 2	t-stat		4.35	4.79	3.05	7.45	3.77
		p-value		0.000	0.000	0.007	0.000	0.001
		R_{adj}^2			0.729			
	Model 3	t-stat	2.48	4.01	5.97	4.26	8.52	4.61
		p-value	0.024	0.001	0.000	0.001	0.000	0.000
		R_{adj}^2			0.790			

Notes:

* $X_{\text{Macro}} = \text{MPD}_{\text{LLS}}$ (mm) and $X_{\text{Micro}} = \text{MPD}_{\mu}$ (μm) | t-stat < 1.96 | p-value > 0.05

The results shown in Table 5.1 for the MPD parameter were also obtained for the other seven parameters considered. The tables are shown in Appendix C. Table 5.2 summarized the main findings for the eight parameters studied. The columns show the coefficients β_{Macro} and the β_{Micro} for each of the parameters, and the rows show its t-statistic, p-value, and the R_{adj}^2 for the three proposed models, using the five different friction measures as the dependent variable. The shaded t-statistic and p-values represent the conditions of failing to reject the null hypothesis. It is possible to compare the models when using different parameters to characterize texture by using Table 5.2.

Table 5.2 shows that the macro-texture parameters that present a significant impact on friction (Model 1) are: MPD, R_z , R_{sk} and R_{ku} . The micro-texture parameters that show influence on friction (Model 2) are MPD, R_z , R_a , $SV_{2\text{pts}}$, and $SV_{6\text{pts}}$. Additionally, it can be observed that besides the MPD, only the parameter R_z captures the effect of including both macro- and micro-texture on the friction prediction (Model 3) for DFT40 and DFT60 (high-speed). It is important to mention that the MPD and the R_z were obtained with a similar methodology. The R_z is the highest peak of a 100-mm baseline, while the MPD is the average of the highest peaks of two sub-segments of 50 mm within the 100 mm baseline. Therefore, is likely that these two parameters present similar results. Although, based on the results, the MPD appeared to be the better texture characterization parameter to model friction.

Based on hypothesis testing, the most appropriate friction models as a function of macro-texture (Model 1), micro-texture (Model 2) and both macro- and micro-texture (Model 3) are shown in Table 5.3. The table shows the values for the coefficient for each independent variable and the R_{adj}^2 obtained for the respective model.

Table 5.2: Friction models for different texture parameters.

Y _{Friction}	Model	MPD		RMS		R _a		R _z		R _{sk}		R _{ku}		SV _{2pts}		SV _{6pts}			
		β_{Macro}	β_{Micro}	β_{Macro}	β_{Micro}	β_{Macro}	β_{Micro}	β_{Macro}	β_{Micro}	β_{Macro}	β_{Micro}	β_{Macro}	β_{Micro}	β_{Macro}	β_{Micro}	β_{Macro}	β_{Micro}		
		t-stat	2.53	p-value	0.021	R _{adj} ²	0.357	RMS	0.232	R _a	0.255	R _z	0.338	R _{sk}	0.456	R _{ku}	0.643	SV _{2pts}	0.262
BPN	1	t-stat	2.53		1.56		1.76		2.39		3.30		-5.10		1.81		1.85		
		p-value	0.021		0.136		0.096		0.028		0.004		0.000		0.087		0.081		
		R _{adj} ²	0.357		0.232		0.255		0.338		0.456		0.643		0.262		0.267		
	2	t-stat		4.40		4.54		4.57		4.47		0.67		0.55		3.34		3.56	
		p-value		0.000		0.000		0.000		0.000		0.514		0.591		0.004		0.002	
		R _{adj} ²	0.579		0.593		0.596		0.587		0.149		0.142		0.578		0.488		
	3	t-stat	2.14	4.00	1.26	4.26	1.51	4.31	1.91	4.01	3.17	0.53	-4.89	-0.09	-0.07	2.51	0.17	2.72	
		p-value	0.047	0.001	0.223	0.001	0.148	0.000	0.073	0.001	0.006	0.600	0.000	0.929	0.949	0.023	0.865	0.015	
		R _{adj} ²	0.649		0.606		0.623		0.640		0.434		0.622		0.429		0.458		
GN	1	t-stat	1.68		0.69		0.81		1.59		3.02		-3.82		1.78		1.61		
		p-value	0.111		0.498		0.431		0.131		0.008		0.001		0.092		0.126		
		R _{adj} ²	0.339		0.250		0.257		0.329		0.498		0.586		0.350		0.331		
	2	t-stat		3.47		3.64		3.65		3.50		0.85		0.31		3.03		3.24	
		p-value		0.003		0.002		0.002		0.003		0.408		0.763		0.008		0.005	
		R _{adj} ²	0.549		0.567		0.567		0.552		0.260		0.233		0.499		0.524		
	3	t-stat	1.01	2.99	0.09	3.42	0.22	3.40	0.86	3.01	2.92	0.81	-3.72	-0.33	0.08	2.18	0.02	2.55	
		p-value	0.326	0.009	0.933	0.004	0.829	0.004	0.403	0.008	0.010	0.427	0.002	0.742	0.940	0.045	0.983	0.022	
		R _{adj} ²	0.549		0.540		0.542		0.545		0.488		0.682		0.468		0.494		
DFT20	1	t-stat	2.61		1.61		1.72		2.52		2.78		-3.32		2.60		2.61		
		p-value	0.018		0.126		0.103		0.022		0.012		0.004		0.018		0.018		
		R _{adj} ²	0.728		0.672		0.678		0.723		0.737		0.768		0.727		0.728		
	2	t-stat		3.48		3.50		3.56		3.42		0.79		0.48		3.51		3.46	
		p-value		0.003		0.003		0.002		0.003		0.443		0.276		0.003		0.003	
		R _{adj} ²	0.776		0.777		0.780		0.772		0.716		0.708		0.777		0.775		
	3	t-stat	3.03	2.14	1.28	3.23	1.40	3.28	2.00	2.93	2.66	0.67	-3.23	-0.26	0.77	2.13	1.06	2.22	
		p-value	0.008	0.047	0.218	0.005	0.179	0.004	0.062	0.009	0.016	0.511	0.005	0.797	0.451	0.048	0.306	0.041	
		R _{adj} ²	0.813		0.785		0.791		0.805		0.729		0.755		0.772		0.776		

Note: t-stat < 1.96 | p-value > 0.05

Table 5.2: Friction models for different texture parameters (Cont.).

Y _{Friction}	Model	MPD		RMS		R _a		R _z		R _{sk}		R _{ku}		SV _{2pts}		SV _{6pts}		
		β_{Macro}	β_{Micro}	β_{Macro}	β_{Micro}	β_{Macro}	β_{Micro}	β_{Macro}	β_{Micro}	β_{Macro}	β_{Micro}	β_{Macro}	β_{Micro}	β_{Macro}	β_{Micro}	β_{Macro}	β_{Micro}	
DFT40	1	t-stat	2.89	1.78	0.092	1.89	0.074	2.75	0.013	2.79	0.012	-3.88	0.001	2.78	0.012	2.82	0.011	
		p-value	0.010															
		R _{adj} ²	0.682	0.604		0.696		0.671		0.675		0.746		0.673		0.677		
	2	t-stat	4.40	4.52	4.57	4.44	0.000	0.000	0.000	0.000	0.392	0.514	0.67	0.88	0.00	3.79	0.001	
		p-value																
		R _{adj} ²	0.775	0.782		0.784		0.778		0.553		0.545		0.736		0.741		
	3	t-stat	2.62	4.10	1.57	4.28	1.71	4.34	2.38	4.06	2.68	0.78	-3.67	0.18	0.88	2.24	1.18	2.43
		p-value	0.018	0.001	0.135	0.001	0.106	0.000	0.030	0.001	0.016	0.448	0.002	0.863	0.394	0.039	0.253	0.026
		R _{adj} ²	0.830	0.798		0.805		0.823		0.667		0.731		0.733		0.746		
DFT60	1	t-stat	2.80	1.71	0.082	1.84	0.082	2.63	0.017	2.78	0.012	-4.19	0.001	0.02	0.040	2.63	0.017	
		p-value	0.012															
		R _{adj} ²	0.613	0.523		0.533		0.599		0.612		0.719		0.586		0.599		
	2	t-stat	4.35	4.50	0.000	4.53	0.000	4.44	0.000	0.86	0.399	0.73	0.477	3.37	0.003	3.51	0.002	
		p-value																
		R _{adj} ²	0.729	0.739		0.741		0.735		0.467		0.461		0.660		0.671		
	3	t-stat	2.48	4.01	1.47	4.25	1.63	4.29	2.22	4.02	2.67	0.76	-3.97	0.23	0.70	2.07	1.06	2.25
		p-value	0.024	0.001	0.159	0.001	0.122	0.000	0.040	0.001	0.016	0.456	0.001	0.820	0.495	0.054	0.304	0.038
		R _{adj} ²	0.790	0.755		0.763		0.782		0.603		0.703		0.650		0.673		

Note: | t-stat | < 1.96 | p-value > 0.05 |

Table 5.3: Proposed friction models as a function of texture and HMA-type.

Y _{Friction}		X _{Texture or HMA-Type}	Texture Parameter: Mean Texture Depth (MPD)*						
			β_0	β_{Macro}	β_{Micro}	β_1	β_2	β_3	β_4
British Pendulum Number (BPN)	Model 1	Coefficient	2.3	19.8		29.0	29.5	52.9	45.5
		R_{adj}^2	0.357						
	Model 2	Coefficient	-47.6		3.2	36.2	25.7	61.2	32.7
		R_{adj}^2	0.579						
Grip Number (GN)	Model 3	Coefficient	-65.4	12.9	2.7	43.7	40.1	73.5	51.1
		R_{adj}^2	0.649						
	Model 2	Coefficient	-0.307		0.029	0.310	0.269	0.641	0.272
		R_{adj}^2	0.549						
Dynamic Friction Tests at 20 km/h (DFT20)	Model 1	Coefficient	-0.117	0.163		0.360	0.367	0.694	0.368
		R_{adj}^2	0.728						
	Model 2	Coefficient	-0.415		0.022	0.393	0.310	0.723	0.242
		R_{adj}^2	0.776						
	Model 3	Coefficient	-0.574	0.019	0.116	0.460	0.439	0.833	0.406
		R_{adj}^2	0.813						
Dynamic Friction Tests at 40 km/h (DFT40)	Model 1	Coefficient	-0.109	0.171		0.314	0.328	0.623	0.362
		R_{adj}^2	0.682						
	Model 2	Coefficient	-0.464		0.025	0.358	0.277	0.668	0.238
		R_{adj}^2	0.775						
	Model 3	Coefficient	-0.626	0.118	0.021	0.426	0.409	0.780	0.405
		R_{adj}^2	0.830						
Dynamic Friction Tests at 60 km/h (DFT60)	Model 1	Coefficient	-0.114	0.180		0.288	0.309	0.606	0.368
		R_{adj}^2	0.613						
	Model 2	Coefficient	-0.502		0.027	0.337	0.259	0.659	0.240
		R_{adj}^2	0.729						
	Model 3	Coefficient	-0.671	0.123	0.023	0.409	0.397	0.776	0.415
		R_{adj}^2	0.790						

Note: * $X_{Macro} = MPD_{LLS}$ (mm) and $X_{Micro} = MPD_\mu$ (μ m)

Chapter 6: Summary, Conclusions and Recommendations

This chapter presents a summary of the work performed, the most important findings and conclusion, and a series of recommendations for future work.

SUMMARY

Highway surface skid resistance has a significant influence on the number of wet weather accidents. For this reason, monitoring and managing skid resistance properties is crucial to reduce the number of highway accidents and fatalities. Current methodologies to measure road friction present several disadvantages that make them impractical for field data collection over large highway networks. Thus, it is important to study different ways to estimate surface friction characteristics based on other properties that are easier to measure. It is widely recognized that surface texture is the primary pavement property controlling skid resistance. Therefore, the main objective of this study was to analyze surface texture characteristics and to observe their influence on friction. A Line Laser Scanner (LLS) was implemented to characterize road texture.

Through the literature review, presented in Chapter 2, it was possible to assess the theoretical basis for pavement texture and friction characterization and to analyze recent research findings. Highway surface texture is divided into different components (mega-, macro-, and micro-texture) that allow a better study of its characteristics and functions. The present study focused on both macro- and micro-texture.

Currently, texture characterization is concentrated on the analysis of the macro-texture. There are different test methods and widely used parameters that describe macro-texture. However, to date there are not standard methodologies to describe micro-texture for pavement applications.

A methodological framework to collect texture information using the LLS was implemented to characterize both macro- and micro-texture. The LLS characteristics were described in Chapter 3. The LLS consists of a line laser head and a linear translator system to control its displacement. The LLS captures height information of up to 800 profiles in 15 seconds, which can be further processed and analyzed to provide a description of the texture. Each profile consists of up to 15,000 data points. The LSS repeatability allows covering the whole macro-texture wavelength range and the first decade of micro-texture. A series of guidelines were provided for processing invalid and erroneous data obtained from the LLS. Finally, the use of linear filters was proposed to separate the texture profiles' wavelengths into macro- and micro-texture components.

The macro-texture characterization was based on a baseline of 100 mm, while a baseline of 1.0 mm was used for micro-texture based on findings from previous research at the University of Texas at Austin. The micro-texture characterization was applied only to the active area, which was defined as the tire/pavement interaction area. The final profiles were characterized using different parameters. The median value of the parameters obtained for all the baseline-segments was used to the analysis.

Field measurements of friction and texture were collected around Texas using different tests methods. The test sections included a broad range of friction coefficients and texture characteristics. The friction characterization tests included the British Pendulum test (BPT), the Dynamic Friction test (DFT), and the Micro GripTester. While, the texture characterization tests included the Sand Patch test, the Circular Track Meter (CTM) and the LLS. The total sample size collected was 36, including different surface types such as hot-mix asphalt (HMA), surface treatment, and concrete sidewalk. A broad description of the surfaces and the data collection process is provided in Chapter 4.

The results of the friction measurements were contrasted within the different test methods. Additionally, the macro-texture results from the LLS were compared to macro-texture results obtained from the CTM. The relation of friction as a function of texture was also analyzed. A multiple regression analysis was proposed to model friction as a function of texture including the data from the HMA sections. Three different models were proposed. Model 1 included only macro-texture information. Model 2 included only micro-texture. Model 3 incorporated information of both texture components. A total of 120 models were evaluated using two-tailed hypothesis testing to observe the statistical significance of the variables included and to compare the different parameters used to describe the texture. The details can be found in Chapter 5. Finally, models as a function of texture and HMA-type were proposed to the different friction measures.

IMPORTANT FINDINGS CONCLUSIONS

The major findings and conclusions from this study are summarized next:

- The Line Laser Scanner (LLS) can be effectively used to describe macro-texture and the first decade of micro-texture. It is more precise than the CTM and more efficient than the LTS.
- Friction measures obtained using the BPT were significantly affected by macro- and by micro-texture. The BPT is a robust and reliable test method.
- Friction measures obtained using the DFT at 20 (DFT20), 40 (DFT40) and 60 km/h (DFT60) were significantly affected by macro- and by micro-texture. It was found that, for the sections tested, DFT friction does not necessarily decrease with speed.
- Friction measurements obtained using the BPT and DFT showed higher correlation with models using only micro-texture information than with models using only macro-texture information.

- The prediction of friction measures obtained using the BPT and the DFT significantly improved when including information of both macro- and micro-texture into the model. Therefore, a measure of micro-texture should be included into friction models based on texture.
- Friction measurements obtained using the Micro GripTester were significantly affected by the micro-texture but not by the macro-texture. Thus, including information of both macro- and micro-texture into the model did not show improvement in the prediction of friction.
- It is important to include the surface type information when modeling friction. Better correlations were found between friction and texture when including the surface type information into the model. That is, there is not a unique relationship between texture and friction. The relationship between texture and friction is strong but it is different for each type of surface.
- The mean profile depth (MPD) was the most significant parameter for macro- and for micro-texture to explain the distinct friction measures.
- The macro-texture parameters that have significant explanatory power for friction were MPD, R_z , skewness (R_{sk}) and kurtosis (R_{ku}).
- The micro-texture parameters that had a significant effect on friction were MPD, R_z , average height (R_a), and slope variance two points (SV_{2pts}) and six points (SV_{6pts}).
- The MPD and the Rz are the only parameters that showed significance impact on friction for both macro- and micro-texture.

RECOMMENDATIONS

During this research study friction measurements obtained with different devoices were used. However, the devices and methods are mostly low-speed tests using rubber sliders. Further analyses of the relation between friction and texture using full-scale test tires and higher speeds, such as the Locked Wheel test and the GripTester, are recommended.

The LLS provides information that can be applied for a further texture characterization. A wider exploration of both spatial parameters and its relationship with friction is also recommended.

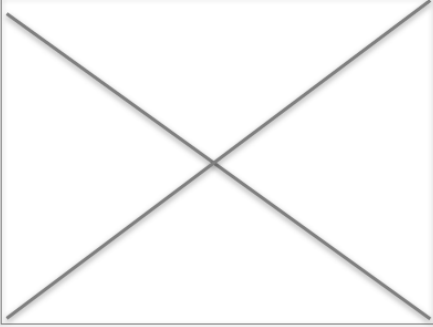
The evaluation of friction and the influence of macro- and micro-texture should be further investigated by evaluating a wider range of surface types.

Appendices

APPENDIX A. BUTTERWORTH FILTERS PYTHON CODE

```
1 # -*- coding: utf-8 -*-
2 """
3 @author: nataliazuniga
4 """
5
6 import numpy as np
7 from scipy import signal
8 from scipy.signal import butter, filtfilt
9
10
11 #%% Load Data form 0.008 mm
12
13 data=np.loadtxt(open("Data01_z8mms.csv","rb"),delimiter=",")
14 z=np.array(data).astype('float')
15
16
17 #%% Information of Data
18
19 r=np.shape(z)[0]; c=np.shape(z)[1] # Rows and Columns
20 dx=0.008 # distance between points in mm
21 fs=1000/dx # Sampling Frequency in m^-1
22 N=15000 # Length of the signal is 15,000 profiles
23
24
25 #%% Filter just for macro-texture
26
27 cutoff=3000 # Eliminate wavelength lower than 0.33 mm
28 order=5
29
30 def butter_lowpass(cutoff, fs, order=order):
31     nyq = 0.5 * fs
32     normalCutoff = cutoff / nyq
33     b, a = butter(order, normalCutoff, btype='low')
34     return b, a
35
36 def butter_lowpass_filter(data, cutoff, fs, order=order):
37     b, a = butter_lowpass(cutoff, fs, order=order)
38     y = filtfilt(b, a, data)
39     return y
40
41 # Filter application
42 x=np.linspace(0,120,num=15000)
43
44 A1=np.zeros((N,c))
45 for i in range(c):
46     A1[:,i] = butter_lowpass_filter(signal.detrend(z[:,i]), cutoff, fs, order=order)
47
48
49 #%% Band Pass Filter
50
51 lowcut=1500 # Eliminate wavelength higher than 0.66 mm
52 highcut=30000 # Eliminate wavelength lower than 0.033 mm
53
54 # Filter
55
56 def butter_bandpass(lowcut, highcut, fs, order=5):
57     nyq = 0.5 * fs
58     low = lowcut / nyq
59     high = highcut / nyq
60     b, a = butter(order, [low, high], btype='band')
61     return b, a
62
63
64 def butter_bandpass_filter(data, lowcut, highcut, fs, order=5):
65     b, a = butter_bandpass(lowcut, highcut, fs, order=order)
66     y = filtfilt(b, a, data)
67     return y
68
69 # Filter application
70
71 B1=np.zeros((N,c))
72 for i in range(c):
73     B1[:,i] = butter_bandpass_filter(signal.detrend(z[:,i]), lowcut, highcut, fs, order=5)
74
```

APPENDIX B. SAMPLES DESCRIPTION

	Surface S01 Location: Waco (SH6) <i>Wheel Path</i> Type: Porous Friction Course (PFC) MPD: 2.16 mm BPN: 40		Surface S02 Location: Waco (SH6) <i>Center</i> Type: Porous Friction Course (PFC) MPD: 3.23 mm BPN: 60
	Surface S03 Location: Waco (SH6) <i>Wheel Path</i> Type: Porous Friction Course (PFC) [new] MPD: 1.55 mm BPN: 60		Surface S04 Location: Waco (SH6) <i>Center</i> Type: Porous Friction Course (PFC) [new] MPD: 2.01 mm BPN: 67
	Surface S05 Location: Houston (SH288) <i>Wheel Path</i> Type: Porous Friction Course (PFC) MPD: 2.14 mm BPN: 54		Surface S06 Location: Houston (SH288) <i>Center</i> Type: Porous Friction Course (PFC) MPD: 2.30 mm BPN: 45
	Surface S07 Location: Austin (US290) <i>Wheel Path</i> Type: Porous Friction Course (PFC) MPD: 1.43 mm BPN: 54		Surface S08 Location: Austin (US290) <i>Center</i> Type: Porous Friction Course (PFC) MPD: 1.42 mm BPN: 66

	Surface S09 Location: San Antonio (US181) <i>Wheel Path</i> Type: Novachip MPD: 1.22 mm BPN: 61		Surface S10 Location: San Antonio (US181) <i>Center</i> Type: Novachip MPD: 1.44 mm BPN: 66
	Surface S11 Location: Bryan (US84) <i>Wheel Path</i> Type: Dense-Graded Type C MPD: 0.66 mm BPN: 65		Surface S12 Location: Bryan (US84) <i>Center</i> Type: Dense-Graded Type C MPD: 1.94 mm BPN: 83
	Surface S13 Location: Brownwood (SH36) <i>Wheel Path</i> Type: Dense-Graded Type C MPD: 1.65 mm BPN: 29		Surface S14 Location: Brownwood (SH36) <i>Center</i> Type: Dense-Graded Type C MPD: 1.67 mm BPN: 37
	Surface S15 Location: Brownwood (IH20) <i>Wheel Path</i> Type: Dense-Graded Type D MPD: 0.71 mm BPN: 31		Surface S16 Location: Brownwood (IH20) <i>Center</i> Type: Dense-Graded Type D MPD: 0.63 mm BPN: 42

	Surface S17 Location: Fort Worth <i>Wheel Path</i> Type: Dense-Graded Type D MPD: 0.51 mm BPN: 49		Surface S18 Location: Fort Worth <i>Center</i> Type: Dense-Graded Type D MPD: 0.42 mm BPN: 59
	Surface S19 Location: Atlanta <i>Wheel Path</i> Type: Stone Matrix Asphalt Type-C MPD: 0.52 mm BPN: 49		Surface S20 Location: Atlanta <i>Center</i> Type: Stone Matrix Asphalt Type-C MPD: 0.88 mm BPN: 56
	Surface S21 Location: PRC Parking Lot Type: Dense-Graded Type C MPD: 1.20 mm BPN: 87		Surface S22 Location: PRC Parking Lot Type: Dense-Graded Type C MPD: 1.12 mm BPN: 82
	Surface S23 Location: PRC Parking Lot Type: Dense-Graded Type F MPD: 0.40 mm BPN: 79		Surface S24 Location: PRC Parking Lot Type: Dense-Graded Type F MPD: 1.00 mm BPN: 74

	<p>Surface S25</p> <p>Location: PRC Parking Lot</p> <p>Type: Fog Seal</p> <p>MPD: 0.37 mm BPN: 53</p>		<p>Surface S26</p> <p>Location: TxDOT Parking Lot</p> <p>Type: Dense-Graded Type C</p> <p>MPD: 0.65 mm BPN: 77</p>
	<p>Surface S27</p> <p>Location: TxDOT Parking Lot</p> <p>Type: Dense Graded Type C</p> <p>MPD: 0.96 mm BPN: 82</p>		<p>Surface S28</p> <p>Location: TxDOT Parking Lot</p> <p>Type: Thin Overlay Mix (TOM)</p> <p>MPD: 0.39 mm BPN: 90</p>
	<p>Surface S29</p> <p>Location: TxDOT Parking Lot</p> <p>Type: Thin Overlay Mix (TOM)</p> <p>MPD: 0.75 mm BPN: 76</p>		<p>Surface S30</p> <p>Location: PRC Parking Lot</p> <p>Type: Concrete sidewalk</p> <p>MPD: 0.46 mm BPN: 73</p>
	<p>Surface S31</p> <p>Location: PRC Parking Lot</p> <p>Type: Concrete sidewalk</p> <p>MPD: 0.27 mm BPN: 63</p>		<p>Surface S32</p> <p>Location: PRC Parking Lot</p> <p>Type: Concrete sidewalk</p> <p>MPD: 0.41 mm BPN: 65</p>

	<p>Surface S33</p> <p>Location: TxDOT Parking Lot</p> <p>Type: Concrete sidewalk</p> <p>MPD: 0.26 mm BPN: 59</p>		<p>Surface S34</p> <p>Location: TxDOT Parking Lot</p> <p>Type: Concrete sidewalk</p> <p>MPD: 0.69 mm BPN: 55</p>
	<p>Surface S35</p> <p>Location: TxDOT Parking Lot</p> <p>Type: Concrete sidewalk</p> <p>MPD: 0.64 mm BPN: 72</p>		<p>Surface S36</p> <p>Location: TxDOT Parking Lot</p> <p>Type: Concrete sidewalk</p> <p>MPD: 0.50 mm BPN: 60</p>

APPENDIX C. FRICTION MODELS USING DIFFERENT TEXTURE PARAMETERS

Y _{Friction}		Texture Parameter: Root Mean Square (RMS)*						
		β_{Macro}	β_{Micro}	β_1	β_2	β_3	β_4	
British Pendulum Number (BPN)	Model 1	t-stat	1.56		1.99	1.25	3.01	2.16
		p-value	0.136		0.063	0.228	0.008	0.044
		R_{adj}^2			0.232			
	Model 2	t-stat		4.54	4.54	2.83	6.02	4.62
		p-value		0.000	0.000	0.011	0.000	0.000
		R_{adj}^2			0.593			
	Model 3	t-stat	1.26	4.26	4.78	3.09	5.72	3.94
		p-value	0.223	0.001	0.000	0.007	0.000	0.001
		R_{adj}^2			0.606			
Grip Number (GN)	Model 1	t-stat	0.69		1.24	0.82	2.52	1.13
		p-value	0.498		0.231	0.424	0.022	0.276
		R_{adj}^2			0.250			
	Model 2	t-stat		3.64	3.40	2.58	5.54	3.41
		p-value		0.002	0.003	0.020	0.000	0.003
		R_{adj}^2			0.567			
	Model 3	t-stat	0.09	3.42	3.23	2.09	4.42	2.13
		p-value	0.933	0.004	0.005	0.052	0.000	0.050
		R_{adj}^2			0.540			
Dynamic Friction Tests at 20 km/h (DFT20)	Model 1	t-stat	1.61		3.68	2.26	5.24	2.19
		p-value	0.126		0.002	0.036	0.000	0.042
		R_{adj}^2			0.672			
	Model 2	t-stat		3.50	5.33	3.58	7.82	3.74
		p-value		0.003	0.000	0.002	0.000	0.002
		R_{adj}^2			0.777			
	Model 3	t-stat	1.28	3.23	5.57	3.72	7.23	3.38
		p-value	0.218	0.005	0.000	0.002	0.000	0.004
		R_{adj}^2			0.785			
Dynamic Friction Tests at 40 km/h (DFT40)	Model 1	t-stat	1.78		3.13	2.02	4.83	2.22
		p-value	0.092		0.006	0.058	0.000	0.040
		R_{adj}^2			0.604			
	Model 2	t-stat		4.52	5.66	3.78	8.35	4.30
		p-value		0.000	0.000	0.001	0.000	0.000
		R_{adj}^2			0.782			
	Model 3	t-stat	1.57	4.28	6.08	4.12	7.99	4.03
		p-value	0.135	0.001	0.000	0.001	0.000	0.001
		R_{adj}^2			0.798			
Dynamic Friction Tests at 60 km/h (DFT60)	Model 1	t-stat	1.71		2.48	1.68	4.29	2.04
		p-value	0.104		0.023	0.110	0.000	0.056
		R_{adj}^2			0.523			
	Model 2	t-stat		4.50	4.97	3.31	7.64	4.04
		p-value		0.000	0.000	0.004	0.000	0.001
		R_{adj}^2			0.739			
	Model 3	t-stat	1.47	4.25	5.32	3.65	7.28	3.77
		p-value	0.159	0.001	0.000	0.002	0.000	0.002
		R_{adj}^2			0.755			

*Note: $X_{\text{Macro}} = \text{RMS}_{\text{LLS}}$ (mm) and $X_{\text{Micro}} = \text{RMS}\mu$ (μm)

Y _{Friction}			Texture Parameter: Average Height (R_a)*					
			β_{Macro}	β_{Micro}	β_1	β_2	β_3	β_4
British Pendulum Number (BPN)	Model 1	t-stat	1.76		2.11	1.37	3.24	2.36
		p-value	0.096		0.049	0.186	0.005	0.030
		R_{adj}^2			0.255			
	Model 2	t-stat		4.57	4.57	2.83	6.05	4.64
		p-value		0.000	0.000	0.011	0.000	0.000
		R_{adj}^2			0.596			
	Model 3	t-stat	1.51	4.31	4.94	3.27	6.11	4.29
		p-value	0.148	0.000	0.000	0.004	0.000	0.000
		R_{adj}^2			0.623			
Grip Number (GN)	Model 1	t-stat	0.81		1.30	0.90	2.71	1.24
		p-value	0.431		0.210	0.382	0.015	0.231
		R_{adj}^2			0.257			
	Model 2	t-stat		3.65	3.41	2.57	5.55	3.41
		p-value		0.002	0.003	0.020	0.000	0.003
		R_{adj}^2			0.567			
	Model 3	t-stat	0.22	3.40	3.26	2.18	4.68	2.32
		p-value	0.829	0.004	0.005	0.045	0.000	0.034
		R_{adj}^2			0.542			
Dynamic Friction Tests at 20 km/h (DFT20)	Model 1	t-stat	1.72		3.76	2.35	5.55	2.31
		p-value	0.103		0.001	0.030	0.000	0.033
		R_{adj}^2			0.678			
	Model 2	t-stat		3.56	5.39	3.62	7.89	3.78
		p-value		0.002	0.000	0.002	0.000	0.001
		R_{adj}^2			0.780			
	Model 3	t-stat	1.40	3.28	5.71	3.86	7.61	3.60
		p-value	0.179	0.004	0.000	0.001	0.000	0.002
		R_{adj}^2			0.791			
Dynamic Friction Tests at 40 km/h (DFT40)	Model 1	t-stat	1.89		3.22	2.10	5.10	2.33
		p-value	0.074		0.005	0.050	0.000	0.032
		R_{adj}^2			0.696			
	Model 2	t-stat		4.57	5.70	3.79	8.41	4.33
		p-value		0.000	0.000	0.001	0.000	0.000
		R_{adj}^2			0.784			
	Model 3	t-stat	1.71	4.34	6.23	4.25	8.40	4.27
		p-value	0.106	0.000	0.000	0.001	0.000	0.001
		R_{adj}^2			0.805			
Dynamic Friction Tests at 60 km/h (DFT60)	Model 1	t-stat	1.84		2.58	1.76	4.53	2.16
		p-value	0.082		0.019	0.095	0.000	0.044
		R_{adj}^2			0.533			
	Model 2	t-stat		4.53	5.00	3.31	7.68	4.06
		p-value		0.000	0.000	0.004	0.000	0.001
		R_{adj}^2			0.741			
	Model 3	t-stat	1.63	4.29	5.46	3.78	7.66	4.01
		p-value	0.122	0.000	0.000	0.002	0.000	0.001
		R_{adj}^2			0.763			

*Note: $X_{Macro} = R_a$ (mm) and $X_{Micro} = R_a \mu$ (μm)

Y _{Friction}			Texture Parameter: Maximum Height (R_z)*					
			β_{Macro}	β_{Micro}	β_1	β_2	β_3	β_4
British Pendulum Number (BPN)	Model 1	t-stat	2.39		2.78	1.92	3.79	2.94
		p-value	0.028		0.012	0.070	0.001	0.009
		R_{adj}^2			0.338			
	Model 2	t-stat		4.47	4.47	2.75	5.95	4.48
		p-value		0.000	0.000	0.013	0.000	0.000
		R_{adj}^2			0.587			
	Model 3	t-stat	1.91	4.01	5.13	3.50	6.36	4.40
		p-value	0.073	0.001	0.000	0.003	0.000	0.000
		R_{adj}^2			0.640			
Grip Number (GN)	Model 1	t-stat	1.59		1.89	1.51	3.32	1.93
		p-value	0.131		0.076	0.149	0.004	0.070
		R_{adj}^2			0.329			
	Model 2	t-stat		3.50	3.27	2.46	5.39	3.23
		p-value		0.003	0.005	0.025	0.000	0.005
		R_{adj}^2			0.552			
	Model 3	t-stat	0.86	3.01	3.25	2.45	4.91	2.58
		p-value	0.403	0.008	0.005	0.026	0.000	0.020
		R_{adj}^2			0.545			
Dynamic Friction Tests at 20 km/h (DFT20)	Model 1	t-stat	2.52		4.36	3.03	6.26	3.04
		p-value	0.022		0.000	0.007	0.000	0.007
		R_{adj}^2			0.723			
	Model 2	t-stat		3.42	5.24	3.50	7.69	3.61
		p-value		0.003	0.000	0.003	0.000	0.002
		R_{adj}^2			0.772			
	Model 3	t-stat	2.00	2.93	5.95	4.21	8.01	3.93
		p-value	0.062	0.009	0.000	0.001	0.000	0.001
		R_{adj}^2			0.805			
Dynamic Friction Tests at 40 km/h (DFT40)	Model 1	t-stat	2.75		3.99	2.83	5.90	3.12
		p-value	0.013		0.001	0.011	0.000	0.006
		R_{adj}^2			0.671			
	Model 2	t-stat		4.44	5.57	3.68	8.24	4.14
		p-value		0.000	0.000	0.002	0.000	0.001
		R_{adj}^2			0.778			
	Model 3	t-stat	2.38	4.06	6.65	4.72	9.00	4.68
		p-value	0.030	0.001	0.000	0.000	0.000	0.000
		R_{adj}^2			0.823			
Dynamic Friction Tests at 60 km/h (DFT60)	Model 1	t-stat	2.63		3.34	2.44	5.25	2.89
		p-value	0.017		0.004	0.025	0.000	0.010
		R_{adj}^2			0.599			
	Model 2	t-stat		4.44	4.90	3.23	7.55	3.89
		p-value		0.000	0.000	0.005	0.000	0.001
		R_{adj}^2			0.735			
	Model 3	t-stat	2.22	4.02	5.83	4.18	8.16	4.34
		p-value	0.040	0.001	0.000	0.001	0.000	0.000
		R_{adj}^2			0.782			

*Note: $X_{Macro} = R_z$ (mm) and $X_{Micro} = R_z \mu$ (μm)

Y_{Friction}			Texture Parameter: Skewness (R_{sk})*					
			β_{Macro}	β_{Micro}	β_1	β_2	β_3	β_4
British Pendulum Number (BPN)	Model 1	t-stat	3.30		2.82	0.68	2.77	2.84
		p-value	0.004		0.011	0.506	0.013	0.011
		R_{adj}^2			0.456			
	Model 2	t-stat		0.67	1.43	0.22	2.69	1.23
		p-value		0.514	0.170	0.826	0.015	0.236
		R_{adj}^2			0.149			
	Model 3	t-stat	3.17	0.53	2.76	0.67	2.69	2.42
		p-value	0.006	0.600	0.013	0.514	0.015	0.027
		R_{adj}^2			0.434			
Grip Number (GN)	Model 1	t-stat	3.02		2.30	0.95	3.33	2.16
		p-value	0.008		0.034	0.356	0.004	0.046
		R_{adj}^2			0.498			
	Model 2	t-stat		0.85	1.13	0.48	3.19	0.71
		p-value		0.408	0.275	0.634	0.005	0.485
		R_{adj}^2			0.260			
	Model 3	t-stat	2.92	0.81	2.32	0.94	3.25	1.71
		p-value	0.010	0.427	0.034	0.359	0.005	0.106
		R_{adj}^2			0.488			
Dynamic Friction Tests at 20 km/h (DFT20)	Model 1	t-stat	2.78		4.45	2.12	6.57	2.55
		p-value	0.012		0.000	0.048	0.000	0.020
		R_{adj}^2			0.737			
	Model 2	t-stat		0.79	3.18	1.53	6.07	1.17
		p-value		0.443	0.005	0.144	0.000	0.259
		R_{adj}^2			0.716			
	Model 3	t-stat	2.66	0.67	4.39	2.09	6.44	2.11
		p-value	0.016	0.511	0.000	0.052	0.000	0.050
		R_{adj}^2			0.729			
Dynamic Friction Tests at 40 km/h (DFT40)	Model 1	t-stat	2.79		3.71	1.54	5.52	2.27
		p-value	0.012		0.002	0.140	0.000	0.036
		R_{adj}^2			0.675			
	Model 2	t-stat		0.88	2.52	1.04	5.16	0.90
		p-value		0.392	0.022	0.313	0.000	0.380
		R_{adj}^2			0.553			
	Model 3	t-stat	2.68	0.78	3.68	1.53	5.42	1.83
		p-value	0.016	0.448	0.002	0.145	0.000	0.085
		R_{adj}^2			0.667			
Dynamic Friction Tests at 60 km/h (DFT60)	Model 1	t-stat	2.78		3.02	1.09	4.68	2.02
		p-value	0.012		0.007	0.288	0.000	0.059
		R_{adj}^2			0.612			
	Model 2	t-stat		0.86	1.89	0.65	4.44	0.70
		p-value		0.399	0.076	0.522	0.000	0.493
		R_{adj}^2			0.467			
	Model 3	t-stat	2.67	0.76	2.99	1.08	4.59	1.60
		p-value	0.016	0.456	0.008	0.293	0.000	0.127
		R_{adj}^2			0.603			

*Note: $X_{\text{Macro}} = R_{sk}$ and $X_{\text{Micro}} = R_{sk} \mu$

Y _{Friction}			Texture Parameter: Kurtosis (R_{ku})*					
			β_{Macro}	β_{Micro}	β_1	β_2	β_3	β_4
British Pendulum Number (BPN)	Model 1	t-stat	-5.10		3.40	1.38	4.05	4.21
		p-value	0.000		0.003	0.183	0.001	0.001
		R_{adj}^2			0.643			
	Model 2	t-stat		0.55	1.49	0.49	2.41	1.55
		p-value		0.591	0.153	0.628	0.027	0.137
		R_{adj}^2			0.142			
Grip Number (GN)	Model 3	t-stat	-4.89	-0.09	2.96	1.06	2.86	3.39
		p-value	0.000	0.929	0.009	0.305	0.011	0.003
		R_{adj}^2			0.622			
	Model 1	t-stat	-3.82		2.40	1.42	4.20	2.83
		p-value	0.001		0.028	0.175	0.001	0.012
		R_{adj}^2			0.586			
Dynamic Friction Tests at 20 km/h (DFT20)	Model 2	t-stat		0.31	1.06	0.55	2.59	1.02
		p-value		0.763	0.303	0.587	0.019	0.321
		R_{adj}^2			0.233			
	Model 3	t-stat	-3.72	-0.33	2.03	0.94	2.80	2.14
		p-value	0.002	0.742	0.060	0.359	0.013	0.048
		R_{adj}^2			0.682			
Dynamic Friction Tests at 40 km/h (DFT40)	Model 1	t-stat	-3.32		4.66	2.55	7.53	3.06
		p-value	0.004		0.000	0.020	0.000	0.007
		R_{adj}^2			0.768			
	Model 2	t-stat		0.48	0.08	0.12	0.11	0.09
		p-value		0.276	2.875	1.369	4.706	1.360
		R_{adj}^2			0.708			
Dynamic Friction Tests at 60 km/h (DFT60)	Model 3	t-stat	-3.23	-0.26	3.99	1.89	5.26	2.37
		p-value	0.005	0.797	0.001	0.075	0.000	0.030
		R_{adj}^2			0.755			
	Model 1	t-stat	-3.88		4.18	2.14	6.79	3.08
		p-value	0.001		0.001	0.046	0.000	0.006
		R_{adj}^2			0.746			
Dynamic Friction Tests at 40 km/h (DFT40)	Model 2	t-stat		0.67	2.49	1.21	4.32	1.41
		p-value		0.514	0.023	0.241	0.000	0.176
		R_{adj}^2			0.545			
	Model 3	t-stat	-3.67	0.18	3.75	1.81	5.02	2.62
		p-value	0.002	0.863	0.002	0.088	0.000	0.018
		R_{adj}^2			0.731			
Dynamic Friction Tests at 60 km/h (DFT60)	Model 1	t-stat	-4.19		3.54	1.74	6.04	2.99
		p-value	0.001		0.002	0.100	0.000	0.008
		R_{adj}^2			0.719			
	Model 2	t-stat		0.73	1.96	0.94	3.83	1.28
		p-value		0.477	0.065	0.359	0.001	0.218
		R_{adj}^2			0.461			
Dynamic Friction Tests at 60 km/h (DFT60)	Model 3	t-stat	-3.97	0.23	3.22	1.52	4.52	2.57
		p-value	0.001	0.820	0.005	0.146	0.000	0.020
		R_{adj}^2			0.703			

*Note: $X_{Macro} = R_{ku}$ and $X_{Micro} = R_{ku} \mu$

Y _{Friction}			Texture Parameter: Slope Variance Two Points (SV_{2pts})*					
			β_{Macro}	β_{Micro}	β_1	β_2	β_3	β_4
British Pendulum Number (BPN)	Model 1	t-stat	1.81		2.35	1.62	3.00	2.35
		p-value	0.087		0.030	0.123	0.008	0.030
		R_{adj}^2			0.262			
	Model 2	t-stat		3.34	3.42	1.59	4.75	3.61
		p-value		0.004	0.003	0.129	0.000	0.002
		R_{adj}^2			0.578			
	Model 3	t-stat	-0.07	2.51	2.81	0.85	3.55	1.81
		p-value	0.949	0.023	0.012	0.406	0.002	0.089
		R_{adj}^2			0.429			
Grip Number (GN)	Model 1	t-stat	1.78		2.06	1.75	3.23	2.10
		p-value	0.092		0.055	0.098	0.005	0.051
		R_{adj}^2			0.350			
	Model 2	t-stat		3.03	2.81	1.74	4.82	2.92
		p-value		0.008	0.012	0.099	0.000	0.009
		R_{adj}^2			0.499			
	Model 3	t-stat	0.08	2.18	2.39	1.05	3.69	1.57
		p-value	0.940	0.045	0.029	0.307	0.002	0.136
		R_{adj}^2			0.468			
Dynamic Friction Tests at 20 km/h (DFT20)	Model 1	t-stat	2.60		4.38	3.13	5.67	3.10
		p-value	0.018		0.000	0.006	0.000	0.006
		R_{adj}^2			0.727			
	Model 2	t-stat		3.51	5.32	3.18	7.57	3.72
		p-value		0.003	0.000	0.005	0.000	0.002
		R_{adj}^2			0.777			
	Model 3	t-stat	0.77	2.13	4.91	2.47	6.31	2.61
		p-value	0.451	0.048	0.000	0.024	0.000	0.018
		R_{adj}^2			0.772			
Dynamic Friction Tests at 40 km/h (DFT40)	Model 1	t-stat	2.78		4.01	2.96	5.37	3.15
		p-value	0.012		0.001	0.008	0.000	0.006
		R_{adj}^2			0.673			
	Model 2	t-stat		0.00	0.00	0.01	0.00	0.00
		p-value		0.837	0.183	0.049	0.480	0.101
		R_{adj}^2			0.736			
	Model 3	t-stat	0.88	2.24	4.55	2.29	6.06	2.66
		p-value	0.394	0.039	0.000	0.035	0.000	0.017
		R_{adj}^2			0.733			
Dynamic Friction Tests at 60 km/h (DFT60)	Model 1	t-stat	0.02		0.00	0.02	0.00	0.01
		p-value	0.040		0.110	0.054	0.383	0.095
		R_{adj}^2			0.586			
	Model 2	t-stat		3.37	3.87	2.09	6.12	3.15
		p-value		0.003	0.001	0.051	0.000	0.006
		R_{adj}^2			0.660			
	Model 3	t-stat	0.70	2.07	3.63	1.77	5.13	2.24
		p-value	0.495	0.054	0.002	0.094	0.000	0.039
		R_{adj}^2			0.650			

*Note: $X_{Macro} = SV_{2pts}$ and $X_{Micro} = SV_{2pts} \mu$

Y _{Friction}			Texture Parameter: Slope Variance Six Points (SV_{6pts})*					
			β_{Macro}	β_{Micro}	β_1	β_2	β_3	β_4
British Pendulum Number (BPN)	Model 1	t-stat	1.85		2.39	1.69	2.93	2.33
		p-value	0.081		0.028	0.109	0.009	0.032
		R_{adj}^2			0.267			
	Model 2	t-stat		3.56	3.52	1.52	5.00	3.62
		p-value		0.002	0.002	0.145	0.000	0.002
		R_{adj}^2			0.488			
	Model 3	t-stat	0.17	2.72	2.81	0.93	3.32	1.60
		p-value	0.865	0.015	0.012	0.363	0.004	0.128
		R_{adj}^2			0.458			
Grip Number (GN)	Model 1	t-stat	1.61		1.94	1.63	2.91	1.91
		p-value	0.126		0.069	0.122	0.010	0.073
		R_{adj}^2			0.331			
	Model 2	t-stat		3.24	2.90	1.70	5.10	2.91
		p-value		0.005	0.010	0.107	0.000	0.010
		R_{adj}^2			0.524			
	Model 3	t-stat	0.02	2.55	2.23	0.90	3.26	1.17
		p-value	0.983	0.022	0.040	0.383	0.005	0.259
		R_{adj}^2			0.494			
Dynamic Friction Tests at 20 km/h (DFT20)	Model 1	t-stat	2.61		4.34	3.14	5.38	3.07
		p-value	0.018		0.000	0.006	0.000	0.007
		R_{adj}^2			0.728			
	Model 2	t-stat		3.46	5.26	3.03	7.69	3.53
		p-value		0.003	0.000	0.007	0.000	0.002
		R_{adj}^2			0.775			
	Model 3	t-stat	1.06	2.22	4.81	2.51	5.87	2.41
		p-value	0.306	0.041	0.000	0.022	0.000	0.028
		R_{adj}^2			0.776			
Dynamic Friction Tests at 40 km/h (DFT40)	Model 1	t-stat	2.82		4.04	3.03	5.18	3.18
		p-value	0.011		0.001	0.007	0.000	0.005
		R_{adj}^2			0.677			
	Model 2	t-stat		3.79	4.84	2.61	7.34	3.49
		p-value		0.001	0.000	0.018	0.000	0.003
		R_{adj}^2			0.741			
	Model 3	t-stat	1.18	2.43	4.59	2.40	5.77	2.52
		p-value	0.253	0.026	0.000	0.028	0.000	0.022
		R_{adj}^2			0.746			
Dynamic Friction Tests at 60 km/h (DFT60)	Model 1	t-stat	2.63		3.38	2.62	4.59	2.89
		p-value	0.017		0.003	0.017	0.000	0.010
		R_{adj}^2			0.599			
	Model 2	t-stat		3.51	3.94	2.01	6.39	3.06
		p-value		0.002	0.001	0.059	0.000	0.007
		R_{adj}^2			0.671			
	Model 3	t-stat	1.06	2.25	3.77	1.97	5.01	2.22
		p-value	0.304	0.038	0.002	0.065	0.000	0.040
		R_{adj}^2			0.673			

*Note: $X_{Macro} = SV_{6pts}$ and $X_{Micro} = SV_{6pts} \mu$

References

- American Association of State Highway and Transportation Officials (AASHTO). (2008). AASHTO Guide for Pavement Friction, first ed., Washington DC.
- AMES Engineering (2010). Laser Texture Scanner User Manual. Iowa.
- ASTM E 274 (2015). Standard Test Method for Skid Resistance of Paved Surfaces Using a Full-Scale Tire. American Society for Testing and Materials (ASTM).
- ASTM E 501 (2015). Standard Specification for Standard Rib Tire for Pavement Skid-Resistance Tests. American Society for Testing and Materials (ASTM).
- ASTM E 524 (2015). Standard Specification for Standard Smooth Tire for Pavement Skid-Resistance Tests. American Society for Testing and Materials (ASTM).
- ASTM E 670 (2015). Standard Test Method for Testing Side Force Friction on Paved Surfaces Using the Mu-Meter. American Society for Testing and Materials (ASTM).
- ASTM E1845 (2009). Standard Practice for Calculating Pavement Macrotexture Mean Profile Depth. American Society for Testing and Materials (ASTM).
- ASTM E1911 (2009). Standard Test Method for Measuring Paved Surface Frictional Properties Using the Dynamic Friction Tester. American Society for Testing and Materials (ASTM).
- ASTM E1960 (2015). Standard Practice for Calculating International Friction Index of a Pavement Surface. American Society for Testing and Materials (ASTM).
- ASTM E2157 (2015). Standard Test Method for Measuring Pavement Macrotexture Properties Using the Circular Track Meter. American Society for Testing and Materials (ASTM).
- ASTM E2380 (2015). Standard Test Method for Measuring Pavement Texture Drainage Using an Outflow Meter. American Society for Testing and Materials (ASTM).
- ASTM E303 (1998). Standard Test Method for Measuring Surface Frictional Properties Using the British Pendulum Tester. American Society for Testing and Materials (ASTM).
- ASTM E867 (2012). Standard Terminology Relating to Vehicle-Pavement Systems. American Society for Testing and Materials (ASTM).
- ASTM E965 (2006). Standard Test Method for Measuring Pavement Macrotexture Depth Using a Volumetric Technique. American Society for Testing and Materials (ASTM).

- Descornet, G., Schmidt, B., Boulet, M., Gothie, M. Do, M. T., Fafie, J., and Viner, H. (2006). HERMES Project (Harmonization of European Routine and research Measuring Equipment for Skid Resistance).
- Flintsch, G.W., McGhee K.K., Izeppi, K.L., and Najafi, S. (2012). The Little Book of Tire Pavement Friction.
- Gunaratne, M. Bandara, J. Mendzorian, J. Chawla, M., and Ulrich, P. (2000). Correlation of Tire Wear and Friction to Texture of Concrete Pavements. *J. Mater. Civ. Eng.*, 10.1061/(ASCE)0899-1561(2000)12:1(46), 46-54.
- Haider, M., Conter, M., Wehr, R., Sandberg, U., and Ledee, F. A. (2014). Project ROSANNE: rolling resistance, skid resistance, and noise emission measurement standards for road surfaces. In Internoise 2014 (p. 6p).
- Hall, J.W., K.L. Smith, J.C. Wambold, T.J. Yager and Z. Rado (2009). Guide for Pavement Friction. NCHRP Web-Only Document 108. National Cooperative Highway Research Program, Washington, D.C.
- Henry, J.J. (2000). Evaluation of Pavement Friction Characteristics. NCHRP Synthesis 291. National Cooperative Highway Research Program, Washington, D.C.
- ISO/TS 13473-4 (2008). Characterization of pavement texture by use of surface profiles - - Part 4: Spectral analysis of surface profiles. International Organization for Standardization ISO.
- Jayawickrama P.W., and Madhira, P. (2008). Review of TxDOT WWARP Aggregate Classification System. Report No. FHWA/TX-08/0-1707-8.
- Keyence (2015). High-speed 2d/3d Laser Scanner LJ-V700 Series. Specification Manual.
- Kogbara, R.B., Masad E.A., Kassem, E. Sparpas A.T. Anupam, K. (2016). A state of art review of parameters influencing measurements and modeling of skid resistance of asphalt pavements. *Construction and Building Materials* 114 602–617.
- Li, Q., Guangwei, Y., Wang, K.C., Zhan, Y, and Wang, C. (2017) Novel Macro- and Micro-Texture Indicators for Pavement Friction Using High-Resolution 3D Surface Data. *Transportation Research Board 96th Annual Meeting*, Paper 17-05098.
- Li, S., Noureldin, S., and Zhu, K. (2010). Safety Enhancement of the INDOT Network Pavement Friction Testing Program: Macrotecture and Microtexture Testing Using Laser Sensors. *Joint Transportation Research Program FHWA/IN/JTRP-2010/25*. Purdue University. West Lafayette, Indiana.
- Li, S., Noureldin, S., and Zhu, K. (2011). Characterization of Microtextures on Typical Pavement Surfaces: A Pilot Study. *Transportation Research Board 90th Annual Meeting*, Paper 11-1457.

- Madeiros, M.S., Underwood, B.S., Catoren, C., Rupnow, T. Rowls, M. (2016) 3D Measurement of Pavement Macrotexture Using Digital Stereoscopic Vision. Transportation Research Board 95th Annual Meeting, Paper 16-5504.
- Masad, E. (2005). Aggregate Imaging System (AIMS): Basics and Applications. Texas: Texas Transportation Institute. FHWA/TX-05/5-1707-01-1.
- McGhee, K.K., and Flintsch, G.W. (2003). High-speed Texture Measurement of Pavements. Final Report VTRC 3-R9. Virginia Transportation Research Council. Charlottesville, Virginia.
- Miao, Y., Song, P., and Gong, X. (2014) Fractal and Multifractal Characteristics of 3D Asphalt Pavement Macrotexture. *J. Mater. Civ. Eng.*, 10.1061/(ASCE) MT.1943-5533.0000912, 04014033.
- Miller, T., Swiertz, D., Tashman, L. Tabatabae, N. Bahia, H. (2012). Characterization of Asphalt Pavement Surface Texture. In *Transportation Research Record: Journal of the Transportation Research Board*, No. 2295, Transportation Research Board of the National Academies, Washington, D.C., pp. 19–26.
- Panaguoli O.K., and Kokkalis, A. G. (1997). Skid Resistance and fractal pavement surface. *Chaos, Solitons & Fractals* Volume 9, Issue 3, March 1998, Pages 493-505.
- PIARC, (1983). PIARC Technical Committee on Surface Characteristics: Technical Committee Report on Surface Characteristics to the XVII World Road Congress, Sydney, Australia.
- PIARC, (1987). PIARC Technical Committee on Surface Characteristics: Technical Committee Report No 1 to the XVIII World Road Congress, Brussels, Belgium.
- Rajaei, S., Chatti, K., and Dargazany, R. (2017). A review: Pavement Surface Microtexture and its contribution to Surface Friction. Transportation Research Board 96th Annual Meeting, Paper 17-06773.
- Scharnigg, K., Schwalbe, G., and Haider, M. (2011). TYROSAFE (Tyre and Road Surface Optimization for Skid Resistance and Further Effects). In International Surface Friction Conference, 3rd, 2011.
- Sandberg, U., and Descornet, G. (1980). Road surface influence on tyre/road noise - parts i and ii. Proceedings of Inter-Noise 80, Miami, Florida, pages 259–272.
- Sandburg, U. (1998). Influence of Road Surface Texture on Traffic Characteristics Related to Environment, Economy, and Safety: A State-of-the-Art Study Regarding Measures and Measuring Methods, VTI Report 53A-1997, Swedish National Road Administration, Borlange, Sweden.
- Sayers, M.W., Gillespie, T.D., and Paterson, D.O. (1986). Guidelines for Conducting and Calibrating Road Roughness Measurements. Work Bank Technical Paper Number 46. The World Bank, Washington, D.C.

- Serigos, P.A., Smit, A., and Prozzi, J. A. (2014). Incorporating Surface Micro-texture in the Prediction of Skid Resistance of Flexible Pavements. In Transportation Research Record: Journal of the Transportation Research Board, No. 2457, Transportation Research Board of the National Academies, Washington, D.C., pp. 105–113.
- Texas Department of Transportation (TxDOT) (2014). Standard Specifications for Construction and Maintenance of Highways, Streets, and Bridges.
- Thomas, L. (2008) Grip Tester MK2 D-Type Maintenance Manual. Findaly, Irvine Limited. Midlothian, Scotland.
- Thor Labs (2016). 150 mm Linear Translation Stage with Integrated Controller, Stepper Motor. Specification Manual.
- Ueckermann, A., Wang, D. (2014). Towards Contactless Skid Resistance Measurements. RWTH Aachen University, Institute of Highway Engineering.
- Villani, M.M., Scarpas, A., Bondt, A., Khedoe, R. and Artamendi I. (2014). Application of fractal analysis for measuring the effects of rubber polishing on the friction of asphalt concrete mixtures. Wear, Volume 320, 15 December 2014, Pages 179–188.
- Wambold, J. C., Antle, C. E., Henry, J. J., Rado, Z., Descornet, G., Sandberg, U., Gothié, M. and Huschek S. (1995). International PIARC Experiment to Compare and Harmonize Skid Resistance and Texture Measurements (Paris: PIARC) Publication number 01.04.T.
- Wambold, J. C., and Henry, J. J. (2002). NASA Wallops Tire/Runway Friction Workshops: 1993-2002 (No. TP 14190E).
- Woodward (2010). Correlation of microGT (μ GT) with British Pendulum using TRL Rubber. Highway Engineering Research Group HERG Report 0468. University of Ulster. County Antrim, Northern Ireland.